COLOUR CHARACTERIZATION AND SPECIFICATION FOR LIQUID CRYSTAL DISPLAYS (LCDS) AND ORGANIC LIGHT EMITTING DIODE (OLED) DISPLAYS

WU JIALU

PhD

The Hong Kong Polytechnic University

2023

The Hong Kong Polytechnic University

Building Environment and Energy Engineering

Colour Characterization and Specification for Liquid Crystal Displays (LCDs) and Organic Light Emitting Diode (OLED) Displays

WU Jialu

A thesis submitted in partial fulfilment of the requirements for the degree of Doctor of Philosophy

December 2022

CERTIFICATE OF ORIGINALITY

I hereby declare that this thesis is my own work and that, to the best of my knowledge and belief, it reproduces no materials previously published or written, nor material that has been accepted for the award of any other degree or diploma, except where due acknowledgement has been made in the text.

_____ (Signed)

WU JIALU (Name of student)

Abstract

As a procedure to present images in appropriate quality and accurate colours, display calibration was explored since the invention of the electronic display in the nineteenth century. Its aim is to accurately reproduce colours on the display corresponding to real-world vision or another display. Overall, the procedure involves two stages: colour characterization and colour specification. The first stage involves characterizing the colours presented on displays in the International Commission on Illumination (CIE) colorimetry system based on the input digital count values to evaluate the colours perceived by the human visual system. Thereafter, the values in the CIE colorimetry system were specified in a hypothetical display colour space that is independent of the devices. Thus, the displays were calibrated to produce colours according to the values defined in the hypothetical colour spaces.

However, the conventional models of colour characterization were developed assuming channel independence and channel-chromaticity constancy according to the property of the conventional cathode ray tube (CRT) displays. Those models failed to characterize the newly developed organic light emitting diode (OLED) display and a component of the liquid crystal display (LCD), which did not satisfy channel independence. Although various models have been developed to resolve the issue of channel dependency for these displays, extensive measurements are required to achieve high accuracy for such models.

Other problems with the display calibration involves colour mismatch, which refer to the phenomenon that colours with the same values defined in the hypothetical colour spaces appear as different colours to human observers, or colours observed the same colour appearances but having different values defined in the hypothetical colour spaces. This phenomenon illustrated that the CIE colorimetry system may not explain the colour perception of the human visual system in

certain conditions, because the values in the hypothetical colour spaces were calculated based on those defined in the CIE colorimetry system. Moreover, the variations of densities of optical pigments in human eyes varied across individuals, which caused the phenomenon of observer metamerism—a pair of stimuli with a matched colour appearance to one observer exhibits a different appearance to another observer. Thus, the use of one standard observer to represent the colour vision of normal observers may cause failure of characterization for certain observers.

Taking considerations of those problems, in Study 1, this dissertation proposed a display colour characterization model to correct the influences of channel dependency and can be used to accurately characterize OLED displays. We propose a 3D piecewise model, wherein dividing the display RGB space into 27 subspaces and characterizes the interactions between two and three channels based on the measurements of the tristimulus values of 64 RGB combinations of digital count values. The average colour difference in terms of ΔE_{ab} in the CIELAB colour space (Section 2.2.4) of 41 test colours between the model predictions and the measurements was around 0.92, in comparison to the average of 10.47 by the widely used model assuming channel independence (i. e., the GOG model as described in Section 2.5.1), across nine OLED displays. As a result, the proposed model performed great improvement compared to the conventional model in the characterization of OLED displays.

In Study 2, two colour matching experiments were reported to explore the performance of the CIE colorimetry system on the characterization of the colours presented on various displays. In the experiments, human observers matched the colour appearance of six colour stimuli produced by four smartphone displays, including one LCD and three OLED displays, to those produced by a reference smartphone OLED display. The matching and reference stimuli had a field of view (FOV) around 4.77° for the first part of Study 2 and 20.2° for the second part of Study 2. The performance

of the four CMFs, however, were not significantly changed with the increase of the FOV. The experimental results indicated the failure of the applicability of the CIE colorimetry system in characterization of the colours between LCD and OLED displays, corresponding to the colour perception of the human visual system.

In Study 3, a corrected method of colour mismatch between LCD and OLED displays was proposed. A colour matching experiment was carried out in Study 3. The experiment results indicated the similar performance of the CIE colorimetry system in characterization of the colours between displays, but more serious degrees of colour mismatch and observer metamerism compared with the results derived in Study 2. The colour matching data collected from the experiment were used for correcting the colour mismatch. The results indicated the effectiveness performance of the correction, through which the degree of colour mismatch between LCD and OLED displays was significantly reduced.

In summary, this dissertation aids in understanding the procedure of display calibration applied to various display technologies. The present findings will serve as references to achieve accurate display calibration—both in the processes of the colour characterization and colour specification—for new types of displays such as OLED displays.

Publications

Journal:

[1] J. Wu, M. Wei, Y. Fu, et al., “Color Mismatch and Observer Metamerism between Conventional Liquid Crystal Displays and Organic Light Emitting Diode Displays,” *Optics Express*, 29(8), pp.12292-12306, 2021.

[2] J. Wu and M. Wei, Y, “Color Mismatch and Observer Metamerism between Conventional Liquid Crystal Displays and Organic Light Emitting Diode Displays, Part II: Adjacent Stimuli with a Larger Field of View,” *Optics Express* 29(25), pp.41731-41744, 2021.

[3] J. Wu, M. Wei, Y. Yang, W, et al., “Color Characterization Model for OLED Displays with Crosstalk Effects,” *Color Research & Application*, (Under review).

Conference:

[4] J. Wu, J. Yang, M. Wei, et al., “Characterization of Color Differences for Color Palettes,” *Proceeding of 28th IS&T Color and Imaging Conference. Society for Imaging Science and Technology*, pp.232-236, 2020.

Acknowledgments

First of all, I would like to give my heartfelt thanks to my supervisor, Professor Minchen Wei. His profound knowledge and plentiful experience have encouraged me during my period of my Ph.D. study. Under his guidance, I have developed my capacities of academic researches. He provides me the opportunity to deeply investigate the science of colour.

I also want to deliver my sincere gratitude to my fellow colleagues for their selfless help and encouragement in our daily life. They helped me identify the limitations of my work and provided me many useful suggestions. The experience of working with them is really memorable.

Finally, I would be remiss in not mentioning my family, especially my parents, for their unconditional support. Without their tremendous understanding and encouragement, it would be impossible for me to complete my study.

Table of Contents

List of Figures

List of Tables

Chapter 1 Introduction

1.1 Research Background

Electronic displays are widely used in daily life and industrial applications. Generally, they include output devices used on television sets, computer monitors, and smartphones to present visual information transmitted in the format of electrical signals. Display calibration is the process used to produce accurate colours on a display, which should visually correspond with colours in the real world as well as those on other devices.

In presenting a colour image, the digital count values stored in the digital image are converted into electrical signals to drive the optical components in the display structure. The panel design of a typical display follows the characteristic of the human visual system, through which colour perception is initially processed according to the responses to light of three distinct wavelengths. The display panel includes millions of pixels that can emit light in three primary colours—red, green, and blue—corresponding to the sensitivity responses of the human visual system. In human eyes, three types of photoreceptors contribute to the visual response in the retina, i.e., cones, rods, and intrinsically photosensitive retina ganglion cells (ipRGCs). The colour vision is generated through a mix of responses from three types of cones on the retina, which exhibit peak sensitivities toward light in the short, middle, and long wavelengths.

Display calibration aims to present accurate colours on a display corresponding to the perception of the human visual system. The procedure involves two stages: colour characterization and colour specification. The relationship between the digital count values (Section 2.4.1) and the values representing the responses of the human visual system was constructed in the display colour characterization. Those responses were quantified according to the International Commission on Illumination (CIE) colorimetry system (Section 2.2). Thereafter, the response values were

specified in a standard display colour space that is independent of devices. Following this procedure and considering the values in the standard colour spaces, the displays can be calibrated to produce accurate colours.

1.2 Problem and Objective

Since the development of electronic display technology in the late 19th century, several explorations on display calibration have been conducted to achieve higher accuracy colours on the displays to improve the image quality for users. However, several researchers reported failures in display calibration, especially in the calibrations of the newly developed OLED and a component of the LCD displays. In other words, the colour characterization models developed for conventional CRT displays cannot accurately predict the colour calibration values for new types of displays (OLED and LCD displays) based on the CIE colorimetry system. In addition, the colours with same values in the CIE colorimetry system on various displays exhibited multiple colour appearances by human observers. This phenomenon illustrated that the CIE colorimetry system may not represent the colour responses of the human visual system in certain conditions. The colours on various displays exhibited the same appearances by one human observer were reported different appearances by another human observer, which was also cannot be explained through the CIE colorimetry system.

This dissertation aims to explore more accurate models for the calibration of LCD and OLED displays and explore the performance of the CIE colorimetry system on the representation of colour perception of the human visual system. The results will aid in achieving accurate display calibration for new types of displays, both in the processes of colour characterization and colour specification.

1.3 Dissertation Structure

The dissertation is organized as follows.

The relevant literature on the colour perception of human observers, characterization of colours by the CIE colorimetry system, and the development of display technologies and calibration are reviewed in Chapter 2.

The research gaps and questions in the relevant studies performed in this dissertation, are described in Chapter 3.

Based on the input digital count values, a new model of colour characterization that can accurately predict the values of colours in the CIE colorimetry system were applied on the OLED displays, as discussed in Chapter 4.

In Chapter 5 and Chapter 6, two psychophysical experiments were conducted involving human observers to identify the colour appearances on various displays. The results quantified the performance of the CIE colorimetry system in characterizing the colour differences between the LCD and OLED displays or multiple OLED displays. The two studies were conducted for small (4.8°) and large (20.2°) fields of view (FOV), respectively, to explore and compare the results under various FOVs with the other experimental variables remaining constant.

In Chapter 7, a psychophysical experiment was conducted to collect the colour matching data to produce a method for correcting the colour mismatch between LCD and OLED displays when the displays were characterized using the CIE 1931 2° CMFs.

The present findings of all studies and contributions are summarized in Chapter 8.

Chapter 2 Literature Review

2.1 Perception of Colour

Colour perception is the result of the information processing of the human visual system for physical light stimuli from the external environment [1]. In principle, physical light is defined as electromagnetic radiation that can be absorbed by the photopigments in human eyes to generate electrical signals that can be processed by the brain to generate colour perception. The radiation in the wavelength range of 300–800 nm is known as the visible spectrum, within which various wavelengths of light cause distinct colour perception.

2.1.1 Theories of Colour Vision

The research on colour perception originated in the philosophical studies on subjectivism in Ancient Greece. Prior to the scientific explanation of colour conception proposed by Newton in the 17th century [1], the general knowledge considered colour as a property of objects, i.e., a special subjective experience that depends on the perceivers [2]. In 1672, Newton [1] conducted the famous prism experiment to explore the physical property of colour. Through refraction in a glass prism, the incident sunlight dispersed into bands of monochromatic light that formed a spectrum on a white wall in a dark room. Based on this phenomenon, the wave property of light was discovered, and concurrently, colours were defined as the intrinsic properties of light according to its dominant wavelength. Consequently, human observers can perceive the colours of objects owing to the reflection of light with dominant wavelengths.

Expect for the physical property of colour, Newton illustrated his argument regarding colour vision in *Opticks* [3]. He claimed that colour perception is produced based on certain types of disposition of light acting on the sensations of human observers, which is similar to the previous explanation of subjective experience.

For two centuries thereafter, Newton’s theory on colour vision facilitated the development of psychological research on the human visual system. In 1802, Young [4] proposed a hypothesis suggesting that the retina of human eyes is sensitive to three frequency vibrations of light, corresponding to red, yellow, and blue, which were called principal colours. However, the principal colours were later revised as red, green, and violet. In 1860, Helmholtz [5] summarized the trichromatic theory based on the results of the psychophysical experiment conducted by Maxwell [6] in 1857, which verified Young's hypothesis. Maxwell conducted the world’s first colour matching experiment by mixing three colour stimuli to match the colour appearance of achromatic colours. The results suggested that the perception of any colour can be generated by mixing the three primary colours (originally called principal colours) of light—red, green, and blue—in a particular ratio. In addition, the concept of “coterminal response curves” was first proposed by Maxwell, which described the sensitivity of the retina to the three primary colours of light within the visual spectrum. The hypothesis diagram of the curves plotted by Helmholtz is presented in Figure 2-1 [5].

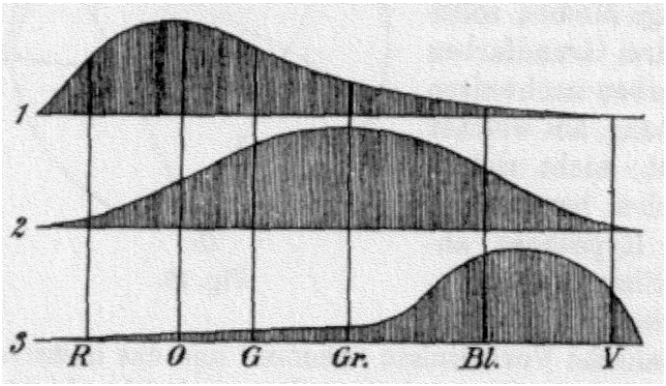

Figure 2-1 “Coterminal response curves” of retina hypothesized by Helmholtz [5].

However, another group of researchers objected to the trichromatic theory. Hering [7] proposed a four-colour opponent theory based on the phenomenon that colour cannot be simultaneously

perceived as yellowish and blueish or greenish and reddish, which cannot be explained by the trichromatic theory. He suggested three types of receptive visual substances on the retina responsible for perceiving two pairs of opponent colours (yellow–blue and red–green) and a pair of achromatism black and white.

After long-term exploration and argument on these two theories, researchers finally achieved consensus on the colour vision theory in the latter half of the 19th century. The evidence from physiological studies validated the existence of both mechanisms but in sequential occurrence. Ultimately, the theory was summarized as "zone theory" [8] that forms the basis of the modern colour vision theory.

Following the framework of "zone theory," the responses of the three opponent signals as functions of wavelength were linearly transformed from those of the trichromatic signals on the human visual system [9-11], which was consistent with the results measured by Jameson and Hurvich [12] in 1955 through psychophysical experiments (Figure 2-2). In their experiment, they recorded the intensities of the pairs of opponent colours that can neutralize each other. The discoveries of physiological research corroborated the zone theory. In 1967, Tomita et al. [13] uncovered three types of cones (L-, M-, and S-cones) in the retina of a carp, which were correspondingly sensitive to the three primary colours in long-, middle-, and short wavelengths. In 1958, DeValois et al. [14] discovered four types of colour-sensitive cells and two types of achromatic cells in the lateral geniculate nucleus of monkeys.

Generally, the stage processing based on the framework of "zone theory" is believed by modern researchers because it explains all phenomena of colour perception that cannot be explained singularly through trichromatic or opponent-colour theories.

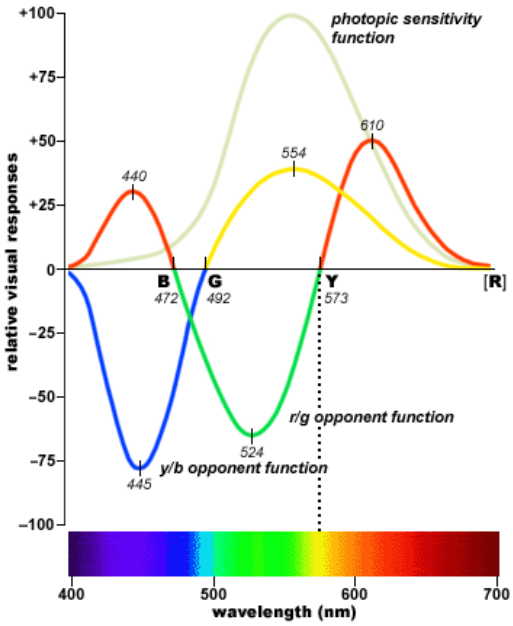

Figure 2-2 Responses of the three opponent signals of red–green, yellow–blue, and white–black from Hurvich & Jameson (1955) [12].

2.1.2 Human Visual System

In human eyes, three types of photoreceptors contribute to the visual response in the retina, i.e., cones, rods, and ipRGCs. In addition, two types of optical media—lens and macula—are present at the front of the retina and influence the colour perception of human observers, as depicted in Figure 2-3. According to the principle of photochemical activation [15], light can affect matter only if it is absorbed by it. Pigments in the photoreceptors and optical media influencing the human visual system were discovered because of their coloured appearance. Before reaching the retina, certain wavelengths of the light entering the human eyes from the cornea would be partially absorbed by the pigments in the lens and macula. Accordingly, colour perception is affected by the optical density of the lens and macular pigments.

The lens is a nearly transparent structure suspended behind the iris of the eye. Its dominant function involves accommodation, which is achieved by altering its shape *via* contraction and diastole of

the ciliary muscles. The alteration of the lens shape creates a range of refractive index that enables observers to focus on nearby and distant scenes. Initially, the research on lens focused on the emergence of the yellowish colour at the centre of the lens of aged individuals, even in case of aged animals. Numerous researchers discovered that the density of the yellowish pigments in the lens increases with aging [16-20]. The lens pigments primarily absorbed the light in the short-wavelength range to protect human eyes from the hazard of blue light, as the density as a function of wavelength illustrated in Figure 2-4.

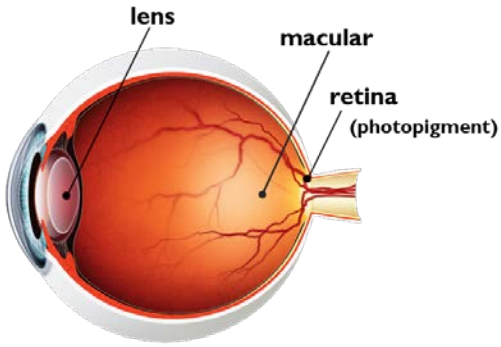

Figure 2-3 Illustrations of cross-section of human eye.

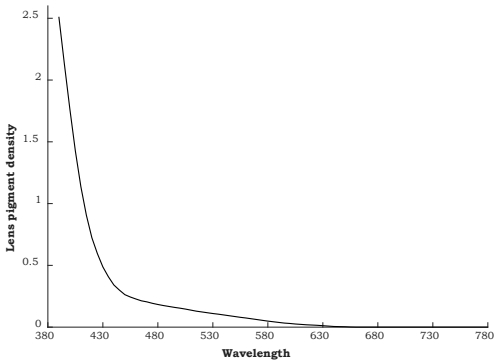

Figure 2-4 Relationships of lens pigment density and wavelength of stimuli for a 32-year-old observer proposed by Stockman and Sharpe in 2000 [56].

Before the absorption by the photopigments in the cones and rods, the focused light reaches the centre of the retina, where the light is partially absorbed by the pigments in the macula. In

particular, the macula is the circular region located at the centre of the retina at the rear end of the eyeball. The researchers in this field discovered that the macular pigments are concentrated on the front of the retina at approximately 2° of FOV, and their density gradually decreases as the FOV increases. The peak density of macular pigments was observed at a stimuli wavelength of 460 nm. Thus, as a function of wavelength, the macular pigment density for 2° and 10° FOV is plotted in Figure 2-5 .

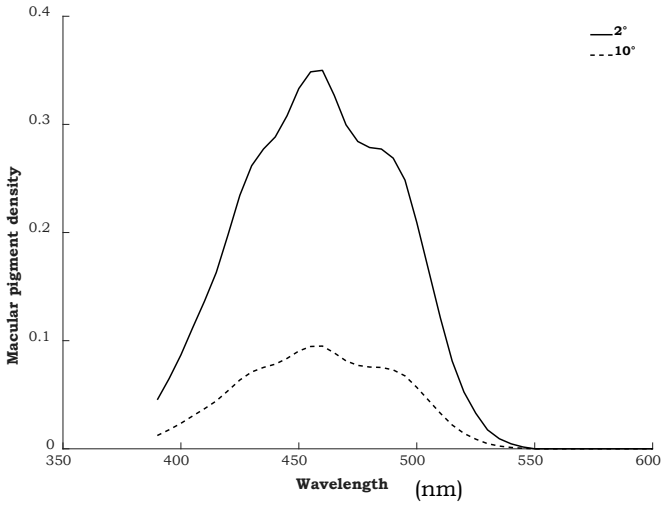

Figure 2-5 Macular pigment density for 2° and 10° FOV proposed by Stockman and Sharpe in 2000 [56].

The structures located inside the human eye prior to the retina are called pre-retinal ocular media that absorbs a significant portion of the radiation incident on the eye. The transmissivity portion is achieved and absorbed by the photopigments in the rod and cone cells on the retina to form the perception of brightness and colour. The rod and cone cells were first observed by Schulze [21] in 1866 in an anatomical study of the retina. His observations suggested the more prevalent distribution of rods exist on the retina than the cones, but notably, only cones were present on the *fovea centralis*—the centre of the retina.

In a physiological study in 1878, Kühne [22] discovered the light sensitivity of the pigments in rods. A pigment named “rhodopsin” was detected in the rods that are bleached under daylight and become purple in the dark. Thereafter, Kühne measured the sensitivity responses of rhodopsin toward the visible spectrum, the results were consistent with the scotopic light-sensitivity curve obtained using flicker-photometry [23] as indicated by the dashed curve in Figure 2-6. However, the peak wavelength of the sensitivity response curve measured under daylight shifted toward a longer wavelength direction, as denoted by the solid curve in Figure 2-6. Based on certain studies on the behaviour of animals with only rods or cones and the phenomenon that colours can be perceived only under daylight, scientists theorized that cones are responsible for colour vision as well as photopic vision [24].

Until 1964, the photopigments in the three types of cones sensitive to light in short-, middle-, and long-wavelength ranges could not be observed under the microscope, and Brown and Wald used microspectrophotometry to report its discovery [25]. The absorption spectra of various photopigments in the three cones are presented in Figure 2-7. As the receptors of the three dominant wavelengths of visible light, cones absorb the light transmitted through the pre-retinal ocular media and convert them into electric signals. This is described by the first stage of the model of colour vision theory based on the framework of zone theory. After being received by the visual cortex of the brain, the signals were processed into three pairs of opposite signals recognized by human observers.

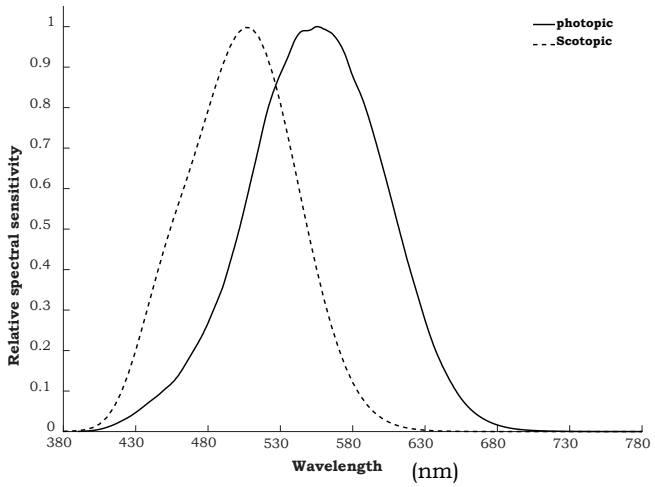

Figure 2-6 CIE 1951 scotopic luminosity and CIE 2° 1924 photopic luminosity functions [31].

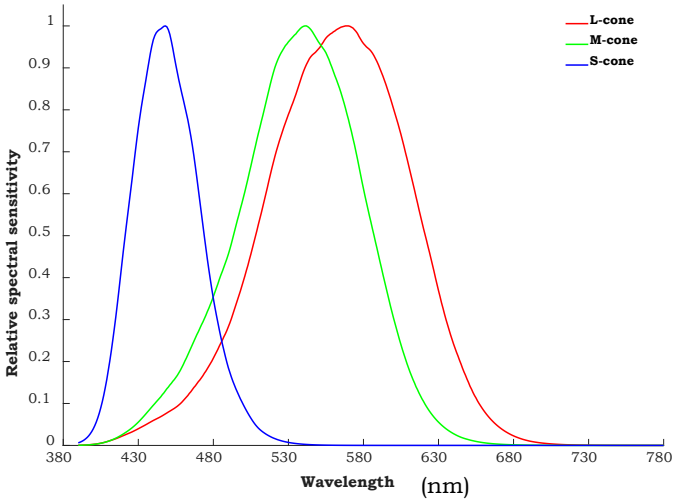

Figure 2-7 Relative spectral sensitivity of L-, M-, and S-cones for lights in various wavelengths measured by Stockman and Sharpe in 2000 [56].

In addition to rods and cones, ipRGCs form a type of light-sensitive cell in the retina of human eyes, which was initially regarded as the controller of circadian rhythms [26] and pupillary light reflex [27]. However, certain recent studies reported its contribution to colour vision [28,29]. The sensitivity response curve of ipRGC is plotted in Figure 2-8 [30].

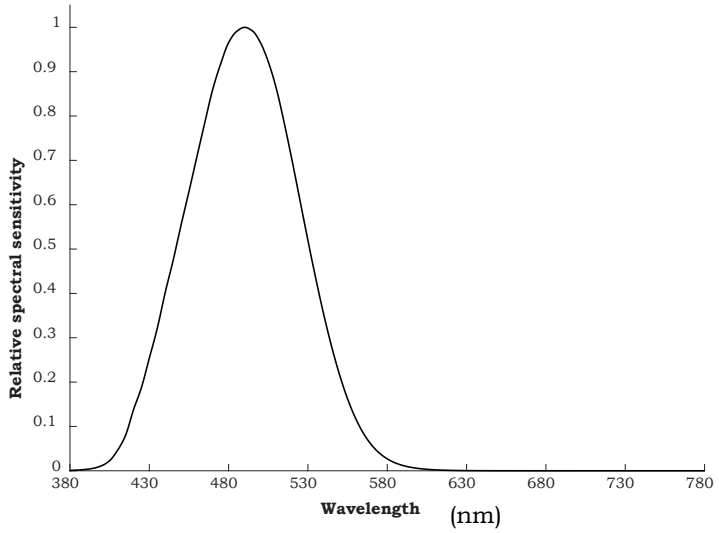

Figure 2-8 Relative spectral sensitivity of ipRGCs for lights in various wavelengths measured by Enezi et al. [30].

2.2 CIE Colorimetry System and Standard CMFs

2.2.1 Colour Mixing and Grassmann's Law

The colorimetry system was first developed by Newton based on his discovery in the prism experiment. Upon mixing a red and yellow monochromatic light in a particular ratio, an orange colour with the same colour appearance as one of the bands of monochromatic light was observed. He presented all the colours in a circular system, as illustrated in Figure 2-9. The monochromatic light bands are located at the circumference of the circle, and white is located at the centre. Any colour on the circle is perceived to correspond to a mixture of two monochromatic lights in a certain ratio.

Inspired by Newton's colorimetry system, in 1853, Grassmann [31] quantized colours in a three-dimensional system with three attributes: brightness, hue, and saturation, as depicted in Figure 2-10. Any colour can be presented as a vector in the coordinate system constructed by these three attributes.

According to the method for calculating vectors, Grassmann deduced his laws regarding colour theory, among which the additive colour mixture law formed the theoretical basis of the trichromatic colour theory in the CIE colorimetry system described in the following section. The law of additive colour mixture can be mathematically explained using Equations (1)–(3). In a three-dimensional system, a colour generated by mixing two colours C_1 and C_2 characterized by the vector [a,b,c] and [d,e,f] exhibit the same colour appearance as the colour C_3 characterized by the vector [$a+d$,$b+e$,$c+f$].

$$C_1 = aA_1 + bA_2 + cA_3 \tag{1}$$

$$C_2 = dA_1 + eA_2 + fA_3 \tag{2}$$

$$C_3 = C_1 + C_2 = (a+d)A_1 + (b+e)A_2 + (c+f)A_3 \tag{3}$$

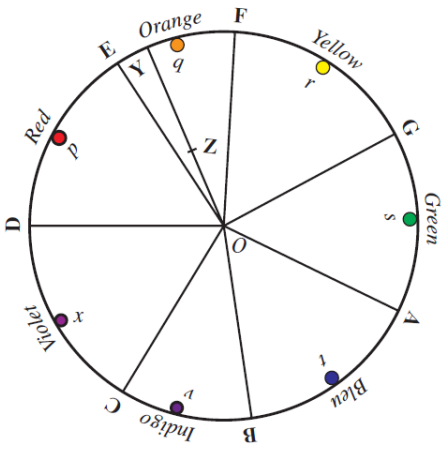

Figure 2-9 Schematic of Newton's colour circle system.

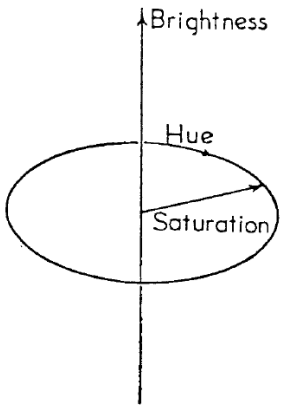

Figure 2-10 Schematic of Grassmann's three-dimensional system.

Limitations of Grassmann's law

The applicability of Grassmann's laws were verified only for the macular regions of the retina (FOV < 4°) [32,33] and a luminance < 23 cd/m^2 [33]. In Maxwell's [6] colour matching experiments, all the observers detected the colour mismatch when viewing the two matched fields through a red filter. Furthermore, Grassmann's law failed in similar experiments [34,35].

Thereafter, Thornton [36,38] systematically and comprehensively demonstrated the colour mismatch between two stimuli for the same chromaticities reported by observers. He conducted colour matching experiments under a FOV of 10° using three sets of primaries to match the monochromatic lights. Upon characterizing the results using CIE 1964 10° colour matching functions (CMFs; Section 2.2.2), the usage of multiple primaries caused several degrees of variations in chromaticities between the visually matched colours. The minimum colour difference was obtained from the experiment using primaries in "prime-colour" (PC) regions (with dominant wavelengths of 452, 533, and 607 nm), which correspond to the primaries experimentally adopted by the CIE to propose the CIE 1931 2° and 10° CMFs. The remaining two sets of primaries used in the Thornton's experiments were referred to as "anti-prime" (AP) regions (with dominant

wavelengths of 497, 579, and 653 nm), which produced the maximum error, and “non-prime” (NP) regions (dominant wavelengths of 477, 558, and 638 nm).

In addition, the colour mismatch was reported by observers when viewing the stimuli with the same chromaticity characterized using the individual CMFs of this observer. The largest error occurred in the experiments using the primaries in the AP regions, and the chromaticities of stimuli displayed higher consistency between the visually matched colours generated using the primaries in the PC region. This result further suggested that the colour mismatch was caused not only by the variations between the individual observers and the CIE standard observer, but also by the failure of Grassmann’s law of additive colour mixture.

Recently, Li et al. [39,40] performed colour matching experiments by selecting eight sets of primaries according to the PC and AP regions proposed by Thornton. As characterized in the CIE 1976 *u’v’* chromaticity diagram based on the CIE 1931 2° CMFs, the chromaticities of the colours matched by human observers are presented in Figure 2-11. Large degree of chromaticities variations were also observed between the colours with matched appearances. The smallest chromaticities variations are presented in the results of the experiment conducted using the primaries with dominant wavelengths in Thornton’s PC regions.

Although the laws were not valid for the typical viewing condition in case of observing displays in daily life, the model colorimetry theory is formed based on them and widely applied to practical production.

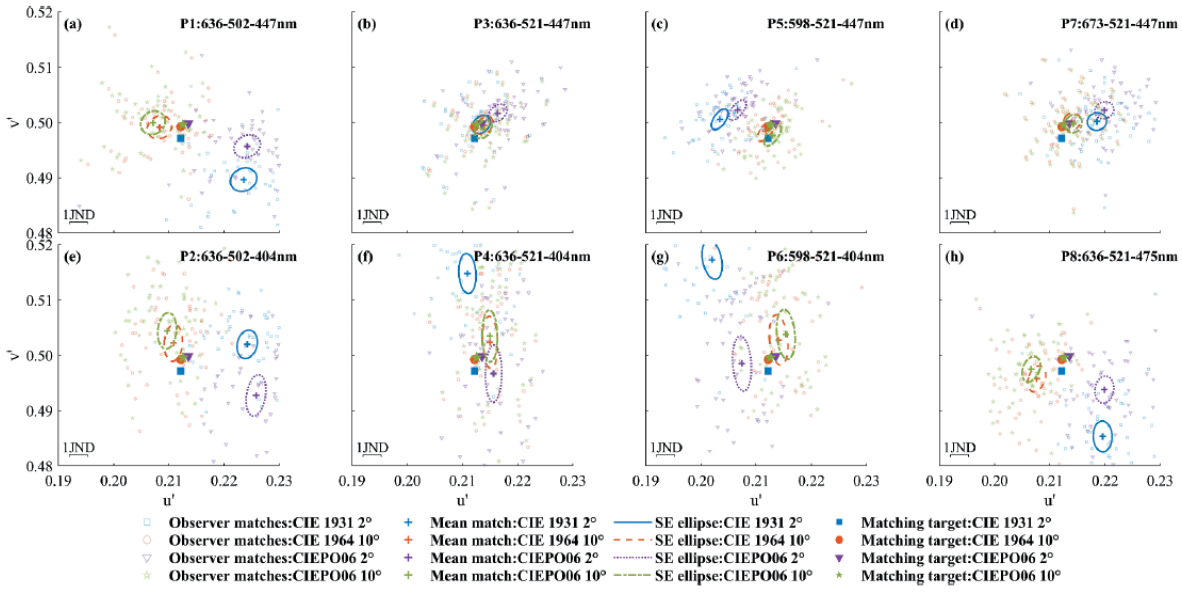

Figure 2-11 Mean CIE 1976 *u'v'* chromaticity of matched colours (coloured crosses) and their SE ellipses (*n* = 54 observers) for various primary sets and multiple CMF sets in the study of Li et al. [39].

2.2.2 CIE Standard Colour Matching Functions

CIE 1931 and CIE 1964

After the development of the trichromatic theory, the contents of the three primaries (red, green, and blue) were adopted as three attributes [*r*,*g*,*b*] to quantify a colour. This system is still used in the model colorimetry system. According to the definition by CIE, any colour can be mathematically represented by the integral of the contents of the three primaries of monochromatic light forming the spectra in the visible wavelength range, as described in Equations (4)–(6). $\bar{r}(\lambda)$, $\bar{g}(\lambda)$, and $\bar{b}(\lambda)$ denote the contents of the three primaries for monochromatic light in the wavelength λ; $S(\lambda)$ represents the spectral power distribution (SPD) of the colour stimulus; *R*, *G*, and *B* are evaluated as the primary contents of the colour. This definition was developed based on Grassmann's law of additive colour mixture. In the system adopted by CIE, $\bar{r}(\lambda)$, $\bar{g}(\lambda)$, and $\bar{b}(\lambda)$ are defined as CMFs in terms of wavelength. The first set of CMFs was measured by Maxwell [6]

through the colour matching experiments using an experimental apparatus of his invention. In particular, two primaries and the monochromatic light to be characterized were mixed in specific ratios to match the appearance of white light for human observers.

$$R = \int S(\lambda) \cdot \bar{r}(\lambda)\, d\lambda \tag{4}$$

$$G = \int S(\lambda) \cdot \bar{g}(\lambda)\, d\lambda \tag{5}$$

$$B = \int S(\lambda) \cdot \bar{b}(\lambda)\, d\lambda \tag{6}$$

In the last hundred years, CIE recommended four sets of standard CMFs for the average observer, among which the earliest standard developed in 1931 [41] is still widely used in several fields such as the calibration of electronic displays.

In 1931 [41], CIE recommended a set of CMFs for 2° FOV, which is based on the original data collected by Wright's [42] and Guild's [43] colour matching experiments with ten and seven observers, respectively. In their experiments, the intensities of three primaries mixing in half of a 2° FOV were adjusted to match the colour appearance of the monochromatic lights to be characterized in the other half. Although the dominant wavelengths of the three primaries in the two experiments varied from each other, the CMFs collected by Guild were transformed into the primaries employed by Wright (dominant wavelengths of primaries are 460, 530, and 650 nm) using Guild's method [44].

The *rgb*-CMFs for the CIE 1931 standard observer based on the colour matching data are presented in Figure 2-12, wherein the negative values represent the intensities of primaries added to certain monochromatic lights that were excessively saturated to be matched by mixing three primaries.

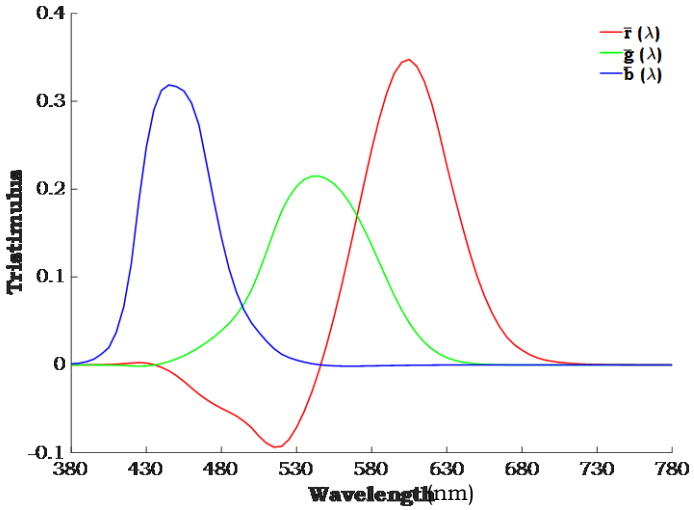

Figure 2-12 Wright & Guild 1931 2° *rgb*-CMFs.

Considering Judd's proposal that one of the three functions should correspond to the luminous efficiency function of photopic vision $V(\lambda)$ (i.e., function represented as solid lines in Figure 2-6), the *rgb*-CMFs was transformed into an imaginary set of primary colours, as depicted in Figure 2-13. In the CIE 1931 system, any colour can be represented by a vector of tristimulus values [*X*,*Y*,*Z*], which are the integrals of the set of CMFs ($\bar{x}(\lambda)$, $\bar{y}(\lambda)$, and $\bar{z}(\lambda)$) adopting imaginary primary colours and the SPD of the colour, as expressed in Equations (7)–(9). In particular, $\bar{y}(\lambda)$ corresponds to the luminous efficiency function of $V(\lambda)$, defined by CIE in 1924 [45] based on the measurements recorded by Coblenz and Emerson [46] and Gibson and Tyndall [47]. Thus, the tristimulus value *Y* in Equation (8) represents the luminance of the colour stimulus. The calculation of luminance value is defined according to the Abney's additivity law of luminance, a restatement of Grassmann's additive law, whose validity was verified in his experiment [48].

$$X = \int S(\lambda) \cdot \bar{x}(\lambda)\, d\lambda \tag{7}$$

$$Y = \int S(\lambda) \cdot \bar{y}(\lambda)\, d\lambda \tag{8}$$

$$Z = \int S(\lambda) \cdot \bar{z}(\lambda)\, d\lambda \tag{9}$$

In 1964, the CIE recommended a new set of CMFs for the extramacular vision in 10° FOV, denoted by the dashed line in Figure 2-13, based on the data acquired by Stiles and Burch [49] for a viewing field occupying a 14° FOV and including that collected by Speranskaya [50]. In Stiles and Burch's study, 53 sets of CMFs were acquired from 49 human observers using various primary colour sets, with four observers repeated twice. The recorded CMFs were the arithmetic mean of the 49 CMFs transformed using the primary colours in the wavelength of 645.2, 526.3, and 444.4 nm. Owing to the rod intrusion initiated in Speranskaya's experiments, the CMFs calculated in that study were assigned an extremely low weightage in the constitution of CIE 1964 standard CMFs. Similar to the definition of the CIE 1931 standard observer, the experimental results were transformed into the system with $\bar{y}_{10}(\lambda)$ corresponding to the luminance efficiency function $V_{10}(\lambda)$ for the 10° FOV, which was acquired by Stiles and Burch [49].

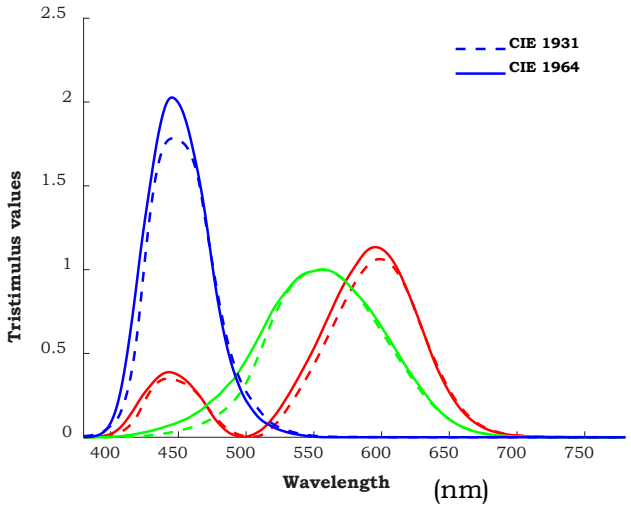

Figure 2-13 CIE 1931 2° and CIE 1964 10° CMFs.

CIE 2015 2° and 10° CMFs (based on CIE 2006 2° and 10° cone fundamentals)

Since the establishment of the trichromatic theory in the 19th century, several scientists have explored the sensitivity of cones to spectral lights. The pioneers of the trichromatic theory believed that the colour deficiencies were caused by the absence of the cones sensitized toward spectra light at certain wavelengths [51-53]. Based on this hypothesis, König and Dieterici [54] first recorded three hypothesis sensitivity curves for the three cones (i.e., cone fundamentals) from their experimental measurements on the protanopia and deuteranopia observers, who were considered exhibiting pure responses of L- or M-cones without intrusion from other cones on the monochromatic light in the range of middle to long wavelength.

Although the research on cone fundamentals started before the studies on CMFs, the CIE did not attend to it until the report of technical committee TC 1-36 published in 2006 [55], which defined two sets of cone fundamentals with 2° and 10° FOVs for the standard 32-year-old observer [55,56]. The curves are presented in Figure 2-14. The CIE 2006 10° cone fundamentals were transformed from the 10° CMFs compiled by Stiles and Burch [49], as expressed in Equation (10). $\bar{r}(\lambda)$, $\bar{g}(\lambda)$, and $\bar{b}(\lambda)$ denote the 10° CMFs reported by Stiles and Burch; $\bar{l}(\lambda)$, $\bar{m}(\lambda)$, and $\bar{s}(\lambda)$ were the cone fundamentals of three cones. The coefficients in the three-by-three matrix were derived based on the experimental results obtained by Stockman and Sharpe [56] on the colour deficiency observers with the FOV of 10° using heterochromatic flicker photometry [55].

$$\begin{bmatrix} \bar{l}_R & \bar{l}_G & \bar{l}_B \\ \bar{m}_R & \bar{m}_G & \bar{m}_B \\ 0 & \bar{s}_G & \bar{s}_B \end{bmatrix} \begin{bmatrix} \bar{r}(\lambda) \\ \bar{g}(\lambda) \\ \bar{b}(\lambda) \end{bmatrix} = \begin{bmatrix} \bar{l}(\lambda) \\ \bar{m}(\lambda) \\ \bar{s}(\lambda) \end{bmatrix} \tag{10}$$

The CIE 2006 system considered the function of age on the optical density of lens pigment and the function of FOV on the optical density of macular pigment, according to which the 2° standard cone fundamentals were deduced. In addition, the functions of cone fundamentals for observers aged between 20 and 60 years and for the FOV of 1° to 10° were stated in the report.

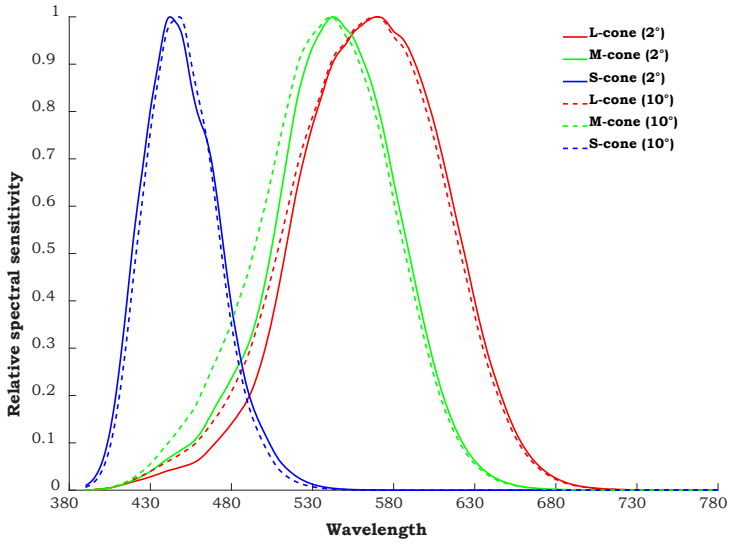

Figure 2-14 CIE 2006 2° and 10° cone fundamentals.

To introduce the system of cone fundamentals into the CIE system of tristimulus values, CIE TC 1-36 continued their investigation on deducing the CMFs that can characterize the colour matching of the CIE 2006 standard observers for FOV of 2° and 10° in 2015 [57]. The concluded CMFs were specified as CIE 2015 CMFs, as indicated in Figure 2-15. Moreover, $\bar{y}_2(\lambda)$ and $\bar{y}_{10}(\lambda)$ corresponds to the luminous sensitivity functions $V(\lambda)$ and $V_{10}(\lambda)$, which are similar to the definitions in the CIE 1931 and 1964 CMFs. As S-cones contribute negligibly toward luminance [57], the luminous sensitivity functions were evaluated through $\bar{l}(\lambda)$ and $\bar{m}(\lambda)$.

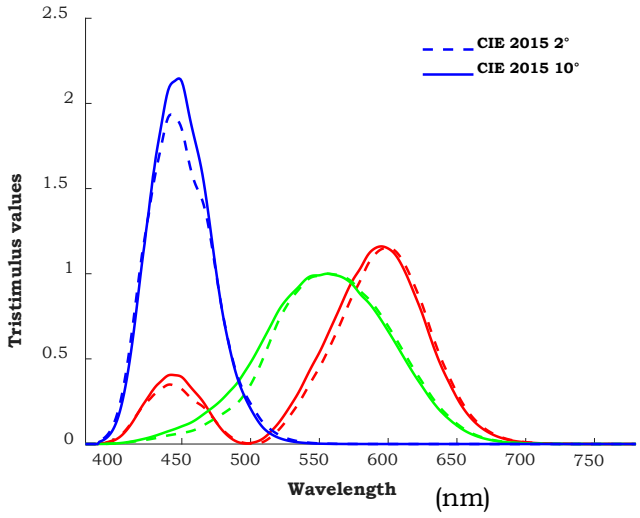

Figure 2-15 CIE 2015 2° and 10° CMFs.

2.2.3 Chromaticity Diagram

The chromaticity diagrams defined by CIE are widely used in the research of model colour science, such as the CIE 1931 *xy* and CIE 1976 *u'v'* chromaticity diagrams. Since Newton's dispersion of light experiment, scientists have attempted to diagrammatically represent spectral lights and their mixtures. The earliest example is the circle diagram developed by Newton (Figure 2-9) based on which Grassmann established a three-dimensional system of coordinate to characterize the colours using three-dimensional vectors, as described in Section 2.2.1. Thereafter, Helmholtz [58] reconstructed Newton's colour circle based on the complementary colours observed from his psychophysical experiment using monochromatic lights, as depicted in Figure 2-16. His study suggested that white cannot be positioned at the centre of the diagram and the yellow-to-green region of the spectrum cannot be achromatized by the colours from green to blue, and it worked in reverse. Therefore, in the modified diagram, the lines connecting the colours in these regions of the spectrum did not intersect the spectral locus. In his later study, Helmholtz [59] combined the chromaticity diagram with the trichromatic theory according to his hypothetical coterminal

response curves (Figure 2-1, prototype of cone fundamentals). This triangle chromaticity diagram is illustrated in Figure 2-17, wherein the any colour was characterized by the three primary colours located at the vertices of an equilateral triangle. As depicted in Figure 2-18, the prototype of the CIE chromaticity diagram was developed by Maxwell [52], who characterized the colours of monochromatic lights in terms of the projections of vectors in a three-dimensional colour space defined by three the primary colours on a unit plane. Maxwell characterized the colours as three-dimensional vectors [*r*,*g*,*b*] representing the contents of the three mixed primary colours (red, green, and blue). The spectral locus in his chromaticity diagram represented the projections of the monochromatic lights on the plane of $r + g + b = 1$. Thus, the colours on the plane exhibited equal luminance.

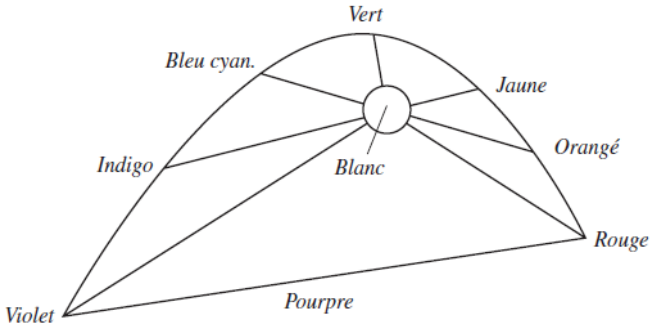

Figure 2-16 Schematic of Helmholtz's reconstructed chromaticity diagram based on Newton's colour circle [58].

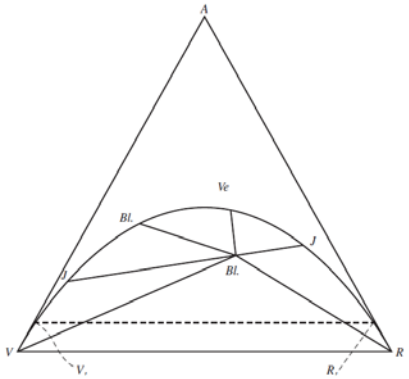

Figure 2-17 Schematic of Helmholtz's chromaticity diagram combining with trichromatic theory [59].

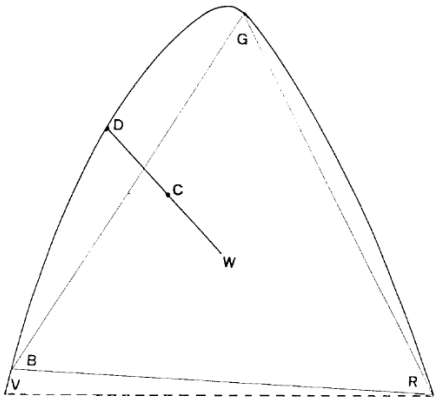

Figure 2-18 Schematic of Maxwell's chromaticity diagram [52].

The establishment of the CIE 1931 chromaticity diagram confirmed the same principle as the Maxwell chromaticity diagram. In case of using the *rgb*-CMFs observed from the colour matching experiments, the negative coordinates are presented in the chromaticity diagram in Figure 2-19. To correct this problem and reasonably modify the chromaticity diagram, CIE selected a set of imaginary primary colours to characterize the colours on the chromaticity diagram. The CIE 1931 2° CMFs described in Section 2.2.2 were established according to this set of primary colours. The CIE 1931 *xy* chromaticity diagram is presented in Figure 2-20, wherein the abscissa represents the line with "zero luminance" defined by Schrödinger [60]. The coordinates of colours (*x*,*y*) in the chromaticity diagram can be evaluated using Equations (11)–(12), with the *X*, *Y*, and *Z* tristimulus values calculated through Equations (7)–(9) described in Section 2.2.2. The CIE chromaticity diagram for 1964 10° CMFs was defined similar to the CIE 1931 system, with (x_{10},y_{10}) representing the coordinates of colours.

$$x = \frac{X}{X+Y+Z} \tag{11}$$

$$y = \frac{X}{X+Y+Z} \tag{12}$$

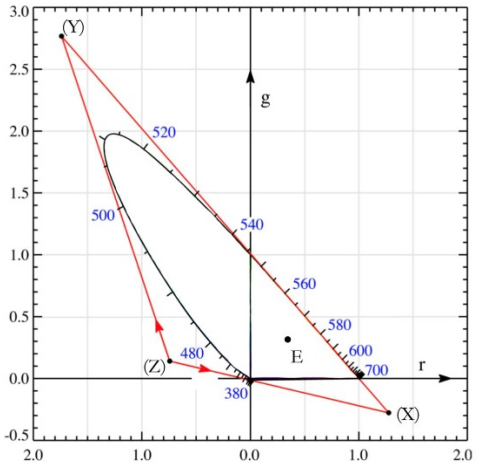

Figure 2-19 Chromaticity diagram plotted through CIE 1931 *rgb*-CMFs [64].

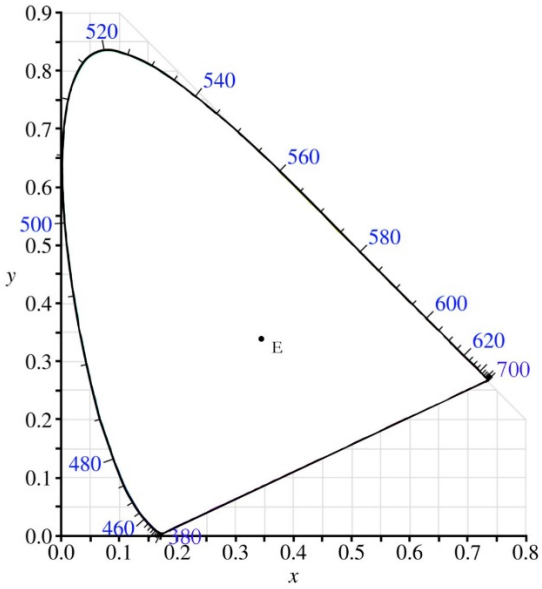

Figure 2-20 CIE 1931 *xy* chromaticity diagram plotted through CIE 1931 2° CMFs [64].

In 1960, a chromaticity diagram was proposed by CIE to specify the colours on uniform perceived scales based on MacAdam's work [61] in 1937. The chromaticity diagram was established to have equal Euclidean distances between the colours of the same perceived colour differences. MacAdam [62] conducted a psychophysical experiment to measure the perceived threshold of

colour difference for 25 colour centres in the CIE 1931 *xy* chromaticity diagram. In Figure 2-21, the distance between the perimeter of the circles to the colour centres represents the perceived colour difference threshold, which indicates nonuniformity in the perceptual scales of the CIE 1931 *xy* chromaticity diagram. Through projective transformation, chromaticity diagrams with more uniform scales were derived by CIE in 1960, which was referred to as the CIE 1960 *uv* uniform colour scale (UCS) chromaticity diagram. The coordinates (*u*,*v*) of colours can be evaluated from the tristimulus values *X*, *Y*, and *Z* in the CIE 1931 system through Equations (13) and (14).

$$u = \frac{4X}{X+15Y+3Z} \tag{13}$$

$$v = \frac{6Y}{X+15Y+3Z} \tag{14}$$

In 1976 [63], the uniformity of scale of the chromaticity diagram was improved by CIE, and new projection relationships were established by rescaling coordinate *v* by a factor of 1.5. The revised chromaticity diagram was referred to as the CIE 1976 *u'v'* UCS chromaticity diagram, which can be characterized through Equations (15) and (16). The concluded chromaticity diagram is presented in Figure 2-22, with more uniform scales of MacAdam's circles. This chromaticity diagram was recommended for use for both CIE 1931 2° and 1964 10° CMFs.

$$u' = \frac{4X}{X+15Y+3Z} \tag{15}$$

$$v' = \frac{9Y}{X+15Y+3Z} \tag{16}$$

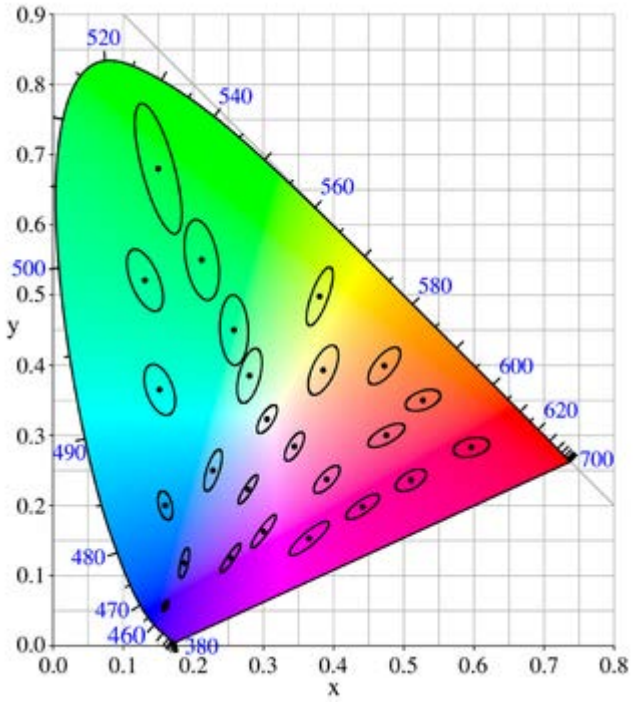

Figure 2-21 CIE 1931 *xy* chromaticity diagram with MacAdam's ellipses (Note: ellipses are ten times their actual size) [64].

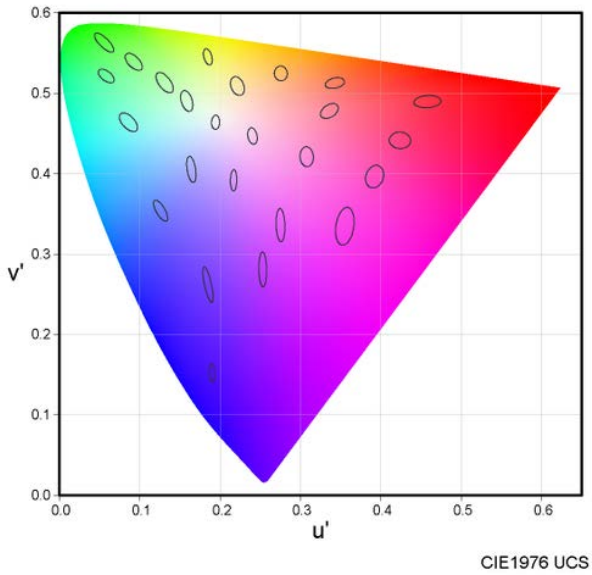

Figure 2-22 CIE 1976 *u'v'* chromaticity diagram with MacAdam's ellipses (Note: ellipses are ten times their actual size) [64].

2.2.4 Evaluation of Colour Difference

Based on the CIE 1960 *uv* chromaticity diagrams, a uniform colour space–CIEUVW colour space was developed in 1964 [64] based on the study of Wyszecki [65] to characterize the colour differences. In this colour space, a colour is specified using a three-dimensional vector involving lightness components *W* and two chromaticity components *U* and *V*. The Euclidean distance of the vectors of two colours was specified as the colour difference ΔE_{CIEUVW} between them. In 1976 [63], two uniform colour spaces CIELUV and CIELAB were developed by CIE based on the CIE 1976 *u'v'* chromaticity diagrams. Similar to the CIEUVW colour space, they comprised a lightness component *L*, two chromaticity components *u** and *v** in the CIELUV colour space, and *a** and *b** in the CIELAB colour space. The colour differences specified in the two colour spaces were based on the Euclidean distance of the colours in each colour space, as described in Equation (17) for the CIELAB colour space. A schematic of the CIELAB colour space is illustrated in Figure 2-23, wherein the chroma and hue can be calculated through the two chromaticity components *a** and *b** using Equations (18) and (19).

$$\Delta E_{ab} = \sqrt{\Delta L^{*2} + \Delta a^{*2} + \Delta b^{*2}} \tag{17}$$

$$h_{ab} = \arctan\left(\frac{b^*}{a^*}\right) \tag{18}$$

$$C^*_{ab} = \sqrt{a^{*2} + b^{*2}} \tag{19}$$

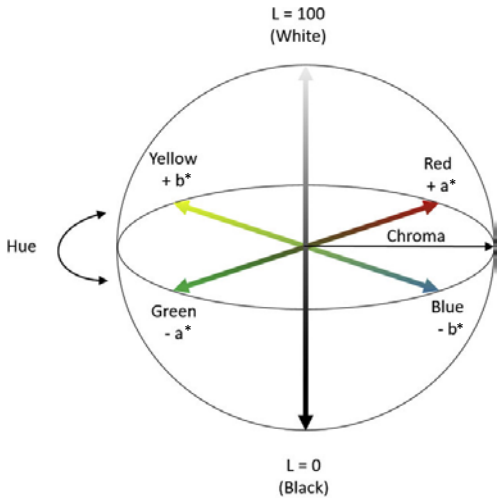

Figure 2-23 Schematic of CIELAB colour space.

Furthermore, CIE recommended a colour difference formula based on the CIELAB colour space, whose effectiveness can be supported by the 132 chromaticity discrimination ellipses reported by Luo and Rigg [66], the so-called Bradford Ellipses (BFD), expressed in Equation (20). The transformed results of these ellipses on the *a*–*b* plane of the CIELAB colour space are portrayed in Figure 2-24, wherein the long axes of the ellipses corresponds to the directions of chroma and the short axes corresponds to the directions of hue angles.

$$\Delta E_{ab}^{*} = \sqrt{\Delta L^{*2} + \Delta C_{ab}^{*\,2} + \Delta H_{ab}^{*\,2}} \tag{20}$$

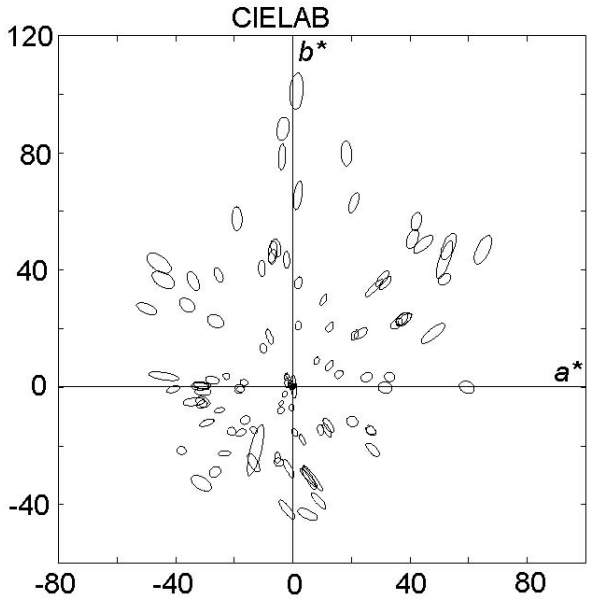

Figure 2-24 Bradford Ellipses (BFD) on a–b plane of CIELAB colour space.

Although the CIELAB colour space poses certain limitations such as the inconstancy of blue hue [67-69] and the conformity of perceptive colour difference threshold with the Euclidean distance in the colour space [70,71], the colour difference formula developed on it and the Euclidean distance of pair stimuli have been widely used since the CIE's recommendation. To date, several suggested corrections of the colour difference formula have been developed to improve the correlation between the colour measurement and visual perception, such as CMC [72], CIE1994 [73], and CIE2000 [74], but it did not substitute the Euclidean distance in CIELAB colour space or the CIELAB colour difference formula as the most widely used evaluations.

2.3 Categorical and Individual CMFs

2.3.1 Variations Among Observers

In the CIE colorimetry system, two colour stimuli with the same chromaticities but distinct SPDs are called metameric colours that would appear as the same colour for human observers. Standard observers were recommended to represent the colour matching of metameric colours by human observers with normal vision. However, researchers reported that pairs of metameric colours matched by a human observer appeared as large colour difference to another human observer [75]. This phenomenon is defined as observer metamerism by the CIE [76]. Thus, the standard observers were defined by CIE for various FOVs and did not account for observer variations; thus, they may not represent the colour matching by a normal observer group. Although certain researchers remarked that observer metamerism is not a significant problem and would not cause a large degree of colour mismatch [77], it was deemed as critical for applications of modern LCD and OLED displays with narrowband SPDs of primaries.

The variation in colour matching among observers was caused by the variations in their human visual system. As described in Section 2.1.2, three types of pigments exist in human eyes with functions on colour vision, lens pigments, macular pigments, and photopigments in the cones. Their optical densities varied among individuals and were influenced by multiple factors, which were not limited to the functions of age on the lens pigments [16-20]. Specifically, age can explain only 47% of the variations in the optical density of the lens, and additional factors such as oculopathy [78], smoking [79], and diabetes [80] have influences on the optical density of the lens. For the macular pigment, race [81,82], dietary habits [83,84], obesity [85], and gender [79] affects its density in addition to the FOV. In addition, variations were also detected on the photopigments

in the cones from various observers. The various gene sequences allow the differences either in the densities or in the peak sensitivities of the photopigments [86].

Thus, alternative methods have been developed to resolve the problem of observer metamerism with a group of CMFs to summarize the colour matching of normal observers in certain categories or develop a model to characterize the colour matching for individual observers.

2.3.2 Sarkar's Categorical CMFs

In 2011, Sarkar [87] reported a group of 10° CMFs based on which normal observers were classified into eight categories. The categorical CMFs were generated based on 61 sets of CIE 2006 10° cone fundamentals for observers aged between 20 and 80 (step = 1), and 47 sets of cone fundamentals transformed from the CMFs with completed data in the range of spectrum from the 49 CMFs required by Stiles and Burch [49].

The procedure can be separated into two steps. First, cluster analysis was applied to 108 *l*-cone, *m*-cone, and *s*-cone functions of the cone fundamentals, following which three, four, five, or six functions were ultimately selected. Each cone function was combined with two functions of the remaining two types of cones to generate a new set of cone fundamentals. For instance, one of the *l*-cone functions was combined with an *m*-cone and *s*-cone functions obtained from the cluster analysis. Thus, 3^3, 4^3, 5^3, or 6^3 sets of cone fundamentals were generated. The least number of cone fundamentals that can cover the variabilities of the normal observers were confirmed based on the CMFs transformed back from the derived combinations of cone fundamentals. The CIE2000 colour differences were evaluated between the chromaticities of colours characterized using each of the 47 CMFs collected by Stiles and Burch and each of the transformed CMFs described in Equation (21). The SPDs of the 240 colours of ColorChecker were adopted under the D65 standard

illuminance. The $CMF_{S\&B,n}$ denotes the *n*-th Stiles and Burch's CMFs; CMF_i indicates the *i*-th CMFs transformed back from the combinations.

$$\Delta E_{i,n} = mean\ \Delta E_{00}\big(SPD_{240\ color,\ illD65} \times CMF_{S\&B,\ n}, SPD_{240\ color,illD65} \times CMF_i\big) \quad (21)$$

The average and maximum colour differences calculated based on the 3^3, 4^3, 5^3, or 6^3 combinations are summarized in Table 2-1. According to the results, 5^3 sets of cone fundamentals could adequately cover the colour matching of normal observers, because the maximum colour difference was approximately equal to one unit of ΔE_{00}, which was generally considered the discrimination threshold of colour difference experienced by human observers.

Table 2-1 Colour differences for 3, 4, 5, and 6 clustered cone fundamentals.

Number of cluster centroids	Mean ΔE_{00}	Max ΔE_{00}
3	0.7	1.5
4	0.6	1.5
5	0.5	1.1
6	0.4	0.7

In the second step, 125 (5^3) combinations of the cones fundamentals representing the colour matching of normal observers were classified into seven or eight categories to cover the properties of Stiles and Burch's 47 observers. The colour differences between the chromaticities of the 240 colours characterized using each of the Stiles and Burch's 47 CMFs and the 125 CMFs were evaluated. Instead of the average value, the 90th percentile among the set of test colours was collected for each of the Stiles and Burch's observers, and subsequently, an observer-dependent threshold was selected as the 10th or 5th percentile of the 125 colour differences (90th percentile

among the test colours). This threshold was employed to assign Stiles and Burch's observers into seven categories, which were characterized using seven sets of CMFs selected from the 125 CMFs based on their discrimination threshold. For each of the 125 CMFs, the average colour differences among the test colours were evaluated for Stiles and Burch's 47 observers, and the number of colour differences smaller than the threshold for the 47 observers was recorded. The set of CMFs with the highest number of recordings was regarded as the first categorical CMFs, and the observers with calculated colour differences smaller than the threshold were assigned to this category. Thereafter, the first set of categorical CMFs was removed from the 125 CMFs and the observers assigned to the first category were excluded from the group of 47 observers; to select the second categorical CMFs, the same procedure was applied to the remaining 124 CMFs. The procedure was repeated until all 47 observers were assigned, which yielded seven categories for the usage of the 240 colour stimuli and eight categories for the usage of the 5832 colour stimuli developed by Sarkar [87]. The eight categorical CMFs recommended by Sarkar are depicted in Figure 2-25.

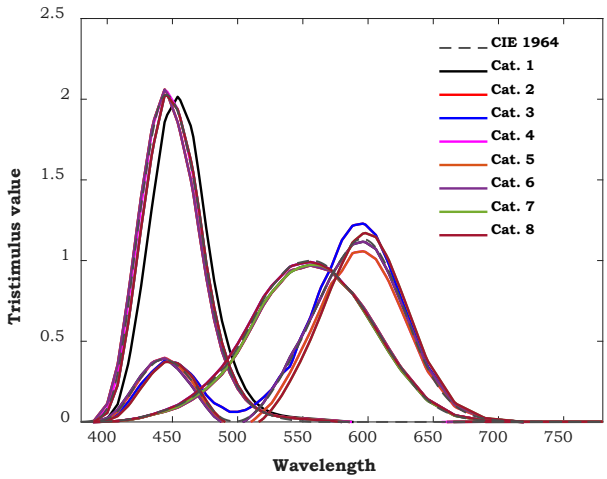

Figure 2-25 Sarkar's eight categorical CMFs compared with CIE 1964 10° CMFs.

2.3.3 Asano's Individual CMFs

Although CIE proposed functions to model the variations among observers of various ages in 2006 [55], the variations between the observers of the same age were not included.

In 2015, Asano [88] developed an individual cone-fundamentals model based on the model of CIE 2006 cone fundamentals. In addition to age (a) and FOV (f), the model added eight physiological parameters as the input variables of the model to generate the cone fundamentals for individual observers, as expressed in Equation (22). The D_{lens} and $D_{macular}$ denote the optical densities of the lens and macular, as described in Section 2.1.2. $D_{L,max}$, $D_{M,max}$, and $D_{S,max}$ indicate the peak photopigment densities of the *L*-, *M*-, and *S*-cone. $s_{L,max}$, $s_{M,max}$, and $s_{S\ max}$ denote the variations in the peak wavelength of the absorption spectra of the three photopigments.

$$LMS = f(a,\ f, D_{lens}, D_{macualr},\ D_{L,max}, D_{M,max}, D_{S,max}, s_{L,max}, s_{M,max}, s_{S,max}) \qquad (22)$$

The eight parameters were assumed to follow the normal distribution, and their mean values were adopted from the CIE 2006 standard cone fundamentals. Following a two-step algorithm, the standard deviations (SDs) of the normal distributions were calculated. In the first step, the SDs for the eight physiological parameters were evaluated from data sourced from all relevant previous studies. For each parameter, the adopted SD noted in the second row of Table 2-2 was calculated using Equation (23), wherein the subscript n represents the eight parameters, and m denotes the number of SDs obtained from the previous studies for the parameter n.

$$SD_n = \sqrt{\frac{SD_{n,1}^2 + SD_{n,2}^2 + \cdots + SD_{n,m}^2}{m}} \qquad (23)$$

In the second step, the adopted SDs were scaled using scalers c_1 for the optical densities of pigments of the pre-retinal ocular media (D_{lens} and $D_{macular}$) and c_2 for the remaining parameters. In particular, c_1 and c_2 were evaluated through the optimization based on the results of a colour

matching experiment conducted by Asano. The objective was to minimize the mean CIELAB colour difference between the colours characterized based on the CIE 1964 10° CMFs as well as the 1000 CMFs transformed from the model-evaluated cone fundamentals, as expressed in Equation (24). $XYZ_{1964,t}$ and $XYZ_{1964,s}$ denote the tristimulus values of colours adjusted by true observers and 1000 simulated observers following the CIE 1964 10° CMFs to match the colour appearances of the reference colours in the colour matching experiment, evaluated using Equations (25) and (26). SPD_t and SPD_P represent the SPDs of the colours adjusted by the true observers and those of the primary colours in the matching field, respectively. R denotes a vector incorporating the simulated intensities of the three primary colours evaluated using Equation (27), wherein CMF_i represents the individual CMFs of the simulated observer transformed from the model-evaluated cone fundamentals. SPD_r represents the SPDs of the reference colours. The optimized scalers c_1 and c_2 including the scaled SDs adopted in Asano's model are presented in Table 2-2.

$$\min \text{CIELAB}\left(XYZ_{1964,t},\ XYZ_{1964,s}\right) \tag{24}$$

$$XYZ_{1964,t} = CMF_{1964} \times SPD_t \tag{25}$$

$$XYZ_{1964,s} = CMF_{1964} \times SPD_p \times R \tag{26}$$

$$R = \frac{CMF_i \times SPD_r}{CMF_i \times SPD_p} \tag{27}$$

Table 2-2 SDs evaluated from previous studies, scalers of the SDs, and the scaled values adopted in Asano's model.

Parameters	D_{lens}	$D_{macular}$	$D_{L,\,max}$	$D_{M,\,max}$	$D_{S,\,max}$	$s_{L,\,max}$	$s_{M,\,max}$	$s_{S,\,max}$
Step 1	19.1	37.2	17.9	17.9	14.7	4.0	3.0	2.5
Scalers	0.98				0.5			

Step 2	18.7	36.5	9.0	9.0	7.4	2.0	1.5	1.3

Based on the results of a simple colour matching experiment, this model can generate a set of individual cone fundamentals for a human observer. Following the procedure described in Equations (24)–(27), the eight parameters can be calculated through optimization instead of evaluating only two scalers.

2.3.4 Asano's Categorical CMFs

Inspired by Sarkar's study, Asano [88] proposed his categorical CMFs model based on his individual cone-fundamentals model. A cluster analysis was performed on 1000 sets of CMFs transformed from the cone fundamentals generated through the model using Monte Carlo simulation. To confirm the number of categories required to cover the variations of normal observers, Asano evaluated the colour differences between the colours characterized using the clustered CMFs and another set of 1000 model-generated CMFs. The minimum colour differences were recorded for the 1000 CMFs among the clustered CMFs. The average colour difference among the 1000 recorded data was evaluated to determine the performance of the clustered CMFs group. The results revealed that if the CMFs were clustered into sets of ten, i.e., ten categorical CMFs were adopted, the performance did not increase with the numbers of the clustered sets. Thus, Asano recommended ten categorical CMFs for both 2° and 10° of FOV, as depicted in Figure 2-26.

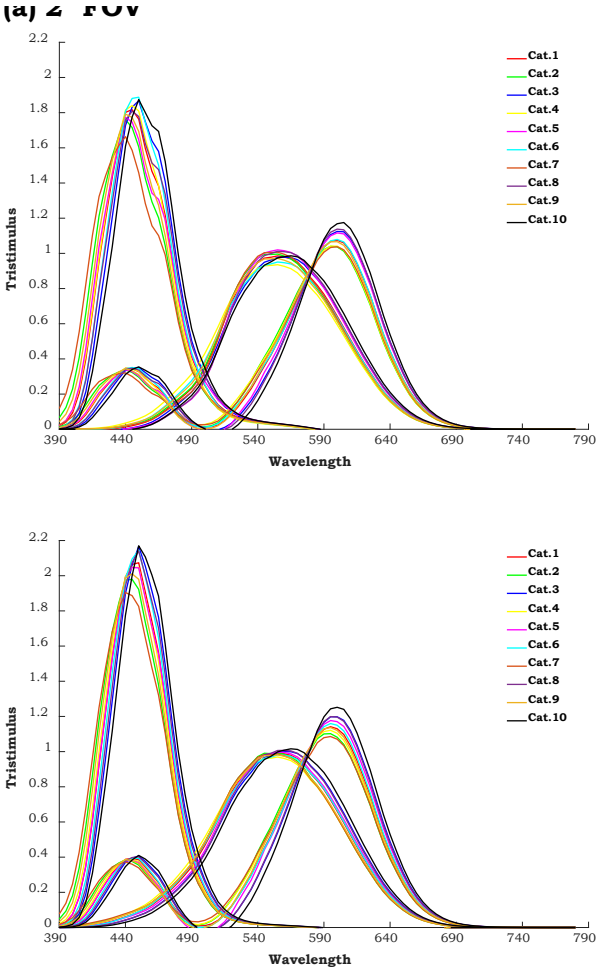

Figure 2-26 Ten categorical CMFs derived by Asano under (a) 2° and (b) 10° of FOV.

2.4 Digital Colours and Display Technologies

As the explanation for the human visual system (Section 2.1.2), colour vision was generated through the responses of the three cones with peak sensitivities of the lights in the long-, middle-, and short-wavelengths. Therefore, additive mixing of three primary colours corresponding to the sensitivities of cones is used to reproduce maximum numbers of colours on the electronic displays. In display technology, additive mixing occurs in “pixels,” which is the smallest unit that forms displays.

The relative intensities of the three primary colours (i.e., digital count values: R, G, and B) were intended to be independently controlled for each pixel to generate a colour image. Thus, the digital images used for the reproduction of colour images on the displays were stored in the electronic devices as multiple sets of three digital count values, corresponding to the resolution of the displays.

2.4.1 RGB Colour Space

In digital images, colours are represented using three numbers R, G, and B, the so-called digital count values, referring to the relative intensities of the three primary colours: red, green, and blue. In the procedure of reproducing the colours of objects in real world, the preliminary step involves capturing colours by measuring the contents of the three primaries required for their generation. The typically used devices include cameras, scanners, etc. Overall, the resultant values are scaled from 0 to 1. Upon application to display devices, the digital count values RGB were generated through the processes of display calibration, as described in Section 2.5, on the raw values captured by the measurement devices.

As depicted in Figure 2-27, the RGB colour space can be represented as a cube in a three-dimensional system of coordinates, wherein the origin represents the colour black and the three primary colours are specified on the axes.

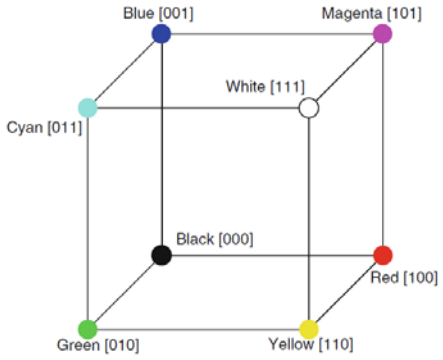

Figure 2-27 Illustration of RGB colour space.

2.4.2 Display Technologies

Based on the trichromatic theory of colour vision, display technologies have been developed based on the theoretical framework of additive mixing of three primary colours. Since invention of the first electronic display technology—cathode ray tube (CRT)—in the 19th century, numerous studies have focused on the developments of optical modulations. Further reformation of materials science improved the experiences to users through the invention of LCD and OLED displays.

In general, the invention of CRT is attributed to Karl Ferdinand Braun [89] in 1896. The CRT display was achieved through electron beam tubes, wherein the electron beams can be focused and emitted on the fluorescent screen in the tubes to generate colour lights. In principle, the colours of the lights were determined by the admixtures on the fluorescent screen, whereas the intensities of lights can be controlled by the number of electrons.

In the 20th century, electronic display users desired a display that can be viewed as a picture with a flat panel shape. Following the discovery of visible light emission from a diode in 1962 [90], the first flat-panel display was invented in 1968 [91] using the LED for optical modulation. However, it was replaced because of the large size of the modulations and high power consumption. In 1968 [92], the first LCD was invented and initially used on the displays of pocket calculators and digital watches [93]. Remarkably, LCD could solve the problems of the early LED display and rapidly became the most popular display technology of the latter half of the 20th century.

The technology of OLED was discovered in 1987 [94] and was demonstrated to be not limited by the size of LED modulations. After resolving certain technical limitations, the first OLED display with improved image quantity was invented in 1996 [94]. Since the first commercial release of an OLED device in 2013, the use of this technology became widespread in several industries, particularly in the smartphone industry owing to its low thickness and foldability.

2.5 Display Calibration

Owing to the use of various types of optical modulations on several display technologies, the primary colours of displays varied from each other, either in terms of shape or the peak wavelength of their SPDs. The colours specified in the RGB colour space relies on their primary set.

Display calibration involves the processing of raw data from digital images captured by certain measurement devices, e.g., cameras and scanners, in an RGB colour space that is used to drive the three primary colours in the displays. The processing aims to accurately reproduce the colours observed in the real world as well as those viewed on another display.

The general pipeline of display calibration is illustrated in Figure 2-28. The first stage involves characterizing the colours presented on the displays specified by the digital count values ($RGB_{display}$) in the CIE colorimetry system, typically CIEXYZ or CIELAB colour space, according to the CIE standard observer. Thereafter, the colours are specified in a standard RGB colour space specified using a set of primary stimuli with predefined chromaticity coordinates. Following this pipeline, the digital count values in the display RGB colour space are mapped into a standard RGB colour space that is independent of the devices. The colours from the real world or that displayed on another device would be consequently reproduced on the display if specified in the standard RGB colour space.

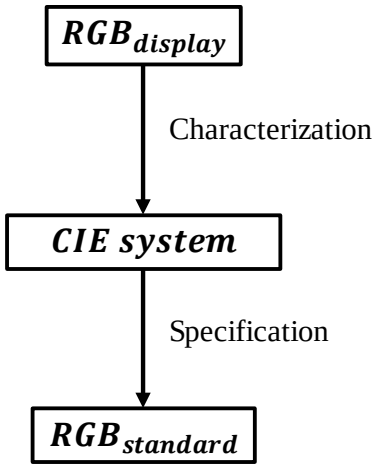

Figure 2-28 General pipeline of display calibration.

2.5.1 Display Colour Characterization

For the first stage of display calibration, the colour characterization models were generated for various display technologies. Generally, the models were used to predict the tristimulus values *XYZ*—specified using the CIE 1931 2° CMFs—of colours presented on the display based on its digital count values.

In 1980, Farley and Gutmann [95] first attempted to characterize the colour presented on the displays in terms of the CIE colorimetry system. According to the principle of additive mixing for electronic displays, they proposed a piecewise linear model assuming variations in chromaticity (PLVC model), which is representative of the CRT display at that time. The relative intensity responses (scaled in the range of 0–1) of the tristimulus values I_X, I_Y, and I_Z were characterized as functions of the digital count values R, G, and B of primary colours for each channel, which were referred to as linearization. As the characteristic of the intensity responses of CRT displays was unclarified during that period, the linearization was achieved through one-dimensional linear interpolations. Subsequently, a colorimetric transform was performed from the intensity responses to the tristimulus values *X*, *Y*, and *Z*, typically using the three-by-three matrix with tristimulus

values of primary colours in their maximum output. In 1989 [96], a simplified model referred to piecewise linear interpolation assuming constant chromaticity coordinates (PLCC) model, was proposed after the demonstration of constant chromaticity of CRT displays with varying luminance [96,97], in which the linearization was characterized to model only the intensity responses of luminance I_Y instead of the tristimulus values.

In 1983 [98], the characteristic of the intensity response for CRT displays was initially explored to derive a mathematical function for linearization. The response was determined according to the gamma law for CRT displays [98-100], which facilitated the development of the most widely used Gain–Offset–Gamma (GOG) model [101]. The linearization in the GOG model is described in Equation (28), wherein I_C denotes the relative intensity responses for channel C, representing the red, green, or blue channel, calculated through the gamma function with $gamma_c$. Additionally, a gain value $gain_c$ and an offset value $offset_c$ were applied to the equation. The colorimetric transformation from the relative intensity responses to the tristimulus values was completed using a three-by-three matrix containing the tristimulus values of three channels in their maximum output, as expressed in Equation (29). Note that this model is established assuming channel independence and constant chromaticity of displays.

$$I_C = (gain_c C + offset_c)^{gamma_c} \tag{28}$$

$$\begin{bmatrix} X \\ Y \\ Z \end{bmatrix} = \begin{bmatrix} X_{R,Max} & X_{G,Max} & X_{B,Max} \\ Y_{R,Max} & Y_{G,Max} & Y_{B,Max} \\ Z_{R,Max} & Z_{G,Max} & Z_{B,Max} \end{bmatrix} \times \begin{bmatrix} I_R \\ I_G \\ I_B \end{bmatrix} \tag{29}$$

However, the assumption of chromaticity constancy is found invalid for LCD technology [102-104,106], and even a part of CRT displays [105]. To correct the chromaticity inconstancy coming

from the black level of those displays, the colorimetric transform was modified using the measurement tristimulus values at zero digital count values [X_K,Y_K,Z_K], as shown in Equation (30). The modified version was referred to as Gain-Offset-Gamma-Offset (GOGO) model [106].

$$\begin{bmatrix} X \\ Y \\ Z \end{bmatrix} = \begin{bmatrix} X_{R,Max} - X_K & X_{G,Max} - X_K & X_{B,Max} - X_K \\ Y_{R,Max} - Y_K & Y_{G,Max} - Y_K & Y_{B,Max} - Y_K \\ Z_{R,Max} - Z_K & Z_{G,Max} - Z_K & Z_{B,Max} - Z_K \end{bmatrix} \times \begin{bmatrix} I_R \\ I_G \\ I_B \end{bmatrix} + \begin{bmatrix} X_K \\ Y_K \\ Z_K \end{bmatrix} \quad (30)$$

In addition to chromaticity inconstancy, another difference was observed between the LCDs and CRT displays in terms of the intensity response. The gamma function was developed particularly for the CRT displays, which could not be reasonably used in LCDs with responses consistent with the S-shaped curve [107,108]. For LCDs, two S-curve models were proposed for linearization [109]. Moreover, several researchers adopted polynomial regression and 3-D LUT to characterize the colours on the CRT [110] displays or LCDs [111-116], including the newly developed OLED displays [129].

Although the gamma function did not perfectly fit the intensity responses of LCDs, the GOG model, or the modified version, was widely used in the characterization of LCDs owing to its high efficiency and acceptable accuracy. However, a high level of channel dependency was observed on the newly developed OLED displays and components of LCDs, which caused the failure of the GOG model. Previous studies [117-124] proposed several models to consider the crosstalk effect, which can be described using Equation (31). In these models, the tristimulus values *X'Y'Z'* derived assuming channel independence were modified using a component *P(R,G,B)* that characterizes the crosstalk effect.

$$\begin{bmatrix} X \\ Y \\ Z \end{bmatrix} = \begin{bmatrix} X' \\ Y' \\ Z' \end{bmatrix} + P(R, G, B) \tag{31}$$

The crosstalk component P can be modelled in various manner. In the piecewise partition (PP) model [117], polynomial compensation (PC) model [118], compensation error (PCE) model [122], two-primary crosstalk (TPC) model [124], partition subspace compensation (SC) model [119], and two LCD characterization models [118,121], polynomial functions with various orders and terms are used to model the crosstalk effect. To further improve the accuracy, a 3D look-up-table (LUT) or multiple 2D LUTs are used with interpolation [121,123,125], which was verified to yield greater accuracy than the polynomial-based models [117,120,124].

In contrast, certain models directly developed the relationship between the digital count and tristimulus values, e.g., masking model [126], 3D LUT [127-129], and polynomial models [130]. Their performances were inferior compared with the models conforming to the format described in Equation (31) [119,122,123].

2.5.2 Display Colour Specification

To reproduce the colours on a display with respect to those on another display, the characterized colours were specified in a standard RGB colour space independent of the devices. This is a colour specification process achieved through the colour management system, wherein the chromaticity coordinates of primary colours and the white point defined by the CIE system were provided to develop the specification, typically the white point is set as D65 to scale the maximum light-emittance from the three colours. Consequently, accurate colours can be presented on the displays according to standard RGB colour spaces.

The colour specification was completed through a linear conversion from the tristimulus values XYZ to the RGB values in the standard colour space, as expressed in Equation (32), wherein *M* denotes a three-by-three transformation matrix that can be evaluated using Equations (33) and (34), given the chromaticity coordinates of primaries $[x_c,y_c,z_c]^T$ (*c* representing *R*, *G*, or *B*) and white $[x_w,y_w,z_w]^T$. In Equation (33), the relative contents of three primaries p_R, p_G, and p_B mixed to match the defined white point were calculated. The matrix *M* included the relative tristimulus values of primary colours with $y_R = y_G = y_B = 1$ scaled by the relative contents of primaries p_R, p_G, and p_B, as expressed in Equation (34). After the linear conversion, a gamma transformation was applied to the RGB colour space to adjust the contrast of images and achieve a high image quality on the display.

$$\begin{bmatrix} X \\ Y \\ Z \end{bmatrix} = M \times \begin{bmatrix} R \\ G \\ B \end{bmatrix} \tag{32}$$

$$\begin{bmatrix} p_R \\ p_G \\ p_B \end{bmatrix} = \begin{bmatrix} x_R & x_G & x_B \\ y_R & y_G & y_B \\ z_R & z_G & z_B \end{bmatrix}^{-1} \times \begin{bmatrix} x_W \\ y_W \\ z_W \end{bmatrix} \tag{33}$$

$$\mathrm{M} = \begin{bmatrix} p_R & 0 & 0 \\ 0 & p_G & 0 \\ 0 & 0 & p_B \end{bmatrix} \times \begin{bmatrix} x_R & y_R & z_R \\ x_G & y_G & z_G \\ x_B & y_B & z_B \end{bmatrix} \tag{34}$$

sRGB

In 1996 [131], HP and Microsoft created a set of standard RGB colour space (sRGB), which defined a colour gamut and white point on the CIE 1931 *xy* chromaticity diagram according to the capability of the most CRT displays during that period, as depicted in Figure 2-29. Although it was developed following the properties of CRT displays, it is still widely used in the display management system for LCDs, OLEDs, and other advanced displays. The HDTV standards for production and international program exchange recommended in 2015 also follow the

specifications of sRGB colour space [132]. A gamma of 2.2 was applied with an intention to be similar to the gamma response of CRT displays, which corresponds to the sensitivity responses of the human visual system on the luminance of lights explained in Stevens' power law [133].

DCI-P3

In 2005 [134], digital cinema initiatives (DCI) initially recommended a standard RGB colour space for the cinema industry, which was modified by the society of motion picture and television engineers (SMPTE) [135] in the definition of white point in 2011. The new version with the chromaticity coordinate of the white point in D65 is referred to as the DCI-P3 standard. The gamut of the DCI-P3 standard specified in the CIE 1931 *xy* chromaticity diagram is presented in Figure 2-29, which is 25% larger than the gamut of sRGB. To specify the intensity response, a gamma of 2.6 was used in DCI-P3, but it was later adjusted in certain documents published by other manufacturers, e.g., 2.2 used by Apple Inc. [136]. In the display industry, this standard is widely used to guide the production of large gamut OLED displays or certain types of LCDs.

Larger gamut colour spaces

Certain RGB colour spaces with larger colour gamut in the CIE chromaticity diagram have been recently recommended, such as the ITU-R Recommendation BT.2020, which covers an area of 75.8% on the CIE 1931 *xy* chromaticity diagram, as depicted in Figure 2-29. This standard was first published in 2012 [137] on the International Telecommunication Union (ITU) website, and further editions have been published in 2014 [138]. The definitions of primary colours were equivalent to the chromaticity coordinates of monochromatic light on the CIE 1931 spectral locus. For the limitation of the current display technologies, BT.2020 has not been widely adopted for the specification of most displays. Recently, a manufacturer reported that one of their new products—the RGB laser backlight system—achieved the BT.2020 standard [139].

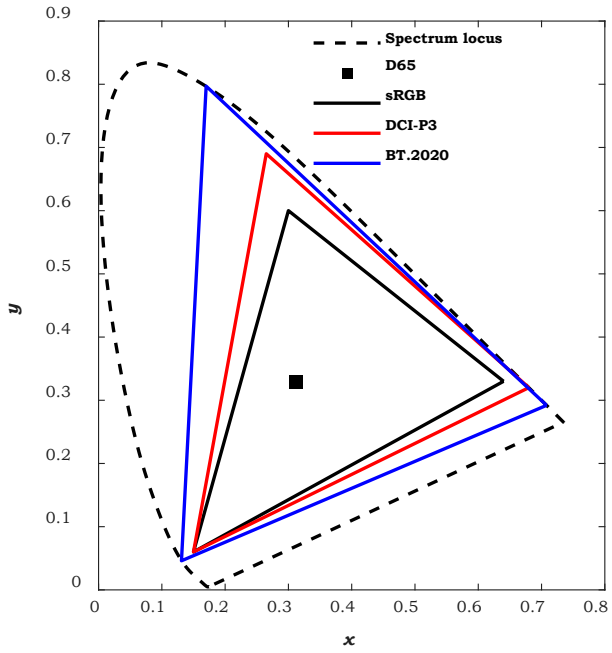

Figure 2-29 Comparison of colour gamuts of sRGB, DCI-P3, and BT.2020 standard colour spaces, together with the spectrum locus, on the CIE 1931 *xy* chromaticity diagram.

Chapter 3 Research Gap and Question

3.1 Research Gap

Since the invention of electronic displays, several explorations have been conducted on display calibration to achieve higher accuracy of colours on the displays. Accordingly, various models of colour characterization have been developed to build the relationship between the input digital count values and the tristimulus values, or values specified in other colour spaces, of the colours on the displays. In addition, a number of standard RGB colour spaces have been published to specify the tristimulus values of colours as the corresponding values in those colour spaces and achieve consistent colour reproduction among various devices.

The conventional colour characterization models were developed assuming channel independence and constant chromaticity according to the property of the CRT displays, as described in Section 2.5.1. As one of the conventional models, the GOG model is still widely used for the colour characterization of LCDs and OLED displays owing to its high efficiency. Only 17 (or less than 17) primary colours for each channel, black, and white are required to be measured to achieve an accurate prediction on the CRT displays or certain LCDs. However, it failed to characterize the newly developed OLED displays and a portion of the LCDs suffered from the issue of “crosstalk effect,” as described in Section 2.5.1. Although certain models can characterize these displays, most of them require an extensive number of measurements to achieve high accuracy. For instance, the PP model requires 91 colours, PCE model requires 729 colours, CS model requires 191 colours, and the LUT-based models require at least 125 colours [121,123]. Although the use of the TPC model only requires 49 measurements of colour stimuli as the training data, this model is effective only for the LCDs with the crosstalk arising from the interactions between two channels instead of three channels, which is invalid for the OLED displays. Although a model involves only 24

training stimuli to characterize the crosstalk effect [118], the same 24 stimuli are used for verification, and thus, the accuracy of the model prediction is implausible.

Another problem with the display calibration is that the colours with the same tristimulus values on varying displays were found to have different colour appearances by human observers. This phenomenon illustrated that the CIE colorimetry system may not represent the colour perception of the human visual system in certain conditions. As described in Section 2.2.1, the CIE colorimetry system was developed based on Grassmann's law, in which the law of additive colour mixture failed under certain conditions. In addition, psychophysical experiments reported mismatches between colour stimuli with the same chromaticities specified in the CIE system but with varying SPDs [140,141], or stimuli with matched colour appearance were determine to yield various chromaticities [39,40,142-144]. Moreover, the variations of densities of optical pigments in human eyes varied across individuals, which caused the phenomenon of observer metamerism—a pair of stimuli with a matched colour appearance to one observer exhibits a different appearance to another observer, as described in Section 2.3.1. Although the issues of colour mismatch and observer metamerism have not been recently detected, they become critically important to the display community owing to the wider usage of OLED displays. A study reported a colour mismatch between LCD and OLED displays in case of using the CIE 1931 2° CMFs for colour characterization [140]. However, their simulation results were not verified through psychophysical experiments, and no study has experimentally investigated the degrees of colour mismatch and observer metamerism between LCD and OLED displays. Furthermore, the characterization of the colour matches between these two display types based on the standard CIE CMFs (i.e., CIE 1931 2° CMFs) have not been verified.

3.2 Research Question

According to the reviewed literature and the discussed research gaps, this dissertation reports three studies investigating the following questions.

Study 1 investigates the efficient correction of the errors caused by the crosstalk effect during the characterization of OLED displays and a portion of LCDs in case of using conventional models, e.g., GOG model.

Study 2 experimentally investigated the degrees of colour mismatch and observer metamerism between the colours presented on the LCD and OLED displays in case of using the CIE standard CMFs for calibration. Moreover, the studies further investigated the performance of the CMFs on colour calibration under a smaller FOV (≈ 4.8º) and a larger FOV (≈ 20.2º) with the other experimental variables remaining constant.

Study 3 investigated a method for correcting the colour mismatch between LCD and OLED displays using the colour matching data collected through the colour matching experiments.

Chapter 4 Study 1: Display Colour Characterization Model for Solving the Problem of Crosstalk Effect

4.1 Motivations

The problem of crosstalk effects on displays creates channel dependency, which occurs in OLED displays and a portion of LCDs, but this effect is more concerning in OLED displays. The conventional display colour characterization models, such as the GOG model that is widely used for CRT displays and the portion of the LCDs displaying channel independence, failed to accurately predict the chromaticities of colours presented on the types of displays with channel dependence. Consequently, highly accurate display colour characterization models are required for those displays. Although certain models involving the correction of the crosstalk effect have been reported in existing studies, they are either inapplicable for the OLED displays or require complex measurements (more than 90 training colours; Section 3.1).

This study proposed a colour characterization model and verified the accuracy of the model using nine test OLED displays. Only 64 colour stimuli are required for developing the model and achieving an accurate prediction of tristimulus values of colours from the digital count values. The measurements required for the model and computational complexity are similar to that of the GOG model, which requires less than a minute to construct.

CIELAB colour differences, between the predicted tristimulus values using the model and the measured values, were adopted to evaluate the accuracy of the proposed model. Thereafter, the results were compared with the colour differences evaluated using the conventional GOG model. The tristimulus values and the colour differences reported in this study were calculated based on the CIE 1931 2° CMFs. The verification results indicated the high accuracy of the proposed model and a considerable improvement in comparison with the conventional GOG model.

4.2 Proposed 3D Piecewise Model

4.2.1 Model Establishment

The proposed 3D piecewise model is described in Equation (35), wherein $[X_{RGB},Y_{RGB},Z_{RGB}]^T$ denotes the tristimulus values derived assuming channel independence and is described in Equation (36); $[P_X,P_Y,P_Z]^T$ indicates the crosstalk effect on the tristimulus values; $[X_{RGB,CT}, Y_{RGB,CT}, Z_{RGB,CT}]^T$ represents the final tristimulus values with the input digital count values of (R,G,B).

$$\begin{bmatrix} X_{RGB,CT} \\ Y_{RGB,CT} \\ Z_{RGB,CT} \end{bmatrix} = \begin{bmatrix} X_{RGB} \\ Y_{RGB} \\ Z_{RGB} \end{bmatrix} + \begin{bmatrix} P_X \\ P_Y \\ P_Z \end{bmatrix} \tag{35}$$

$$\begin{bmatrix} X_{RGB} \\ Y_{RGB} \\ Z_{RGB} \end{bmatrix} = \begin{bmatrix} X_R \\ Y_R \\ Z_R \end{bmatrix} + \begin{bmatrix} X_G \\ Y_G \\ Z_G \end{bmatrix} + \begin{bmatrix} X_B \\ Y_B \\ Z_B \end{bmatrix} \tag{36}$$

Equation (37) can be used to model the relationship between the tristimulus values and the digital count values for each channel, as described in Equation (36), with T representing the tristimulus values X, Y, or Z derived based on the digital count values R, G, and B using n-th-order polynomials. For the three channels, the coefficients of the terms in the polynomials were c_{rj}, c_{gj}, and c_{bj} (j = 1 ~ n), which were constructed for all three tristimulus values. In particular, the digital count values were segmented into three ranges (i.e., 0 to M, M to N, and N to 255 for 8-bit displays), with a set of coefficients c_{rj}, c_{gj}, and c_{bj} derived for each range that increased the model accuracy. For instance, if M is specified as 64 and N as 128, the tristimulus values measured at (16,0,0), (32,0,0), (48,0,0), and (64,0,0) can be utilized to derive the relationship in case the red channel includes an input digital count value between 0 and M. The tristimulus values measured at (64,0,0), (80,0,0), (96,0,0), (112,0,0), and (128,0,0) were used to derive the relationship if the red channel includes an input

digital count value between *M* and *N*, and those at (128,0,0), (144,0,0), (160,0,0), (176,0,0), (192,0,0), (208,0,0), (224,0,0), (240,0,0) and (255,0,0) are used to derive the relationship if the red channel possesses an input digital count value between *N* and 255. In total, 27 relationships were derived (i.e., 3 channels × 3 digital count ranges × 3 tristimulus values).

$$\begin{cases} T_R = c_{r0} + c_{r1} \times R + c_{r2} \times R^2 + \cdots + \cdots c_{rn} \times R^{n-1} \\ T_G = c_{g0} + c_{g1} \times G + c_{g2} \times G^2 + \cdots + \cdots c_{gn} \times G^{n-1} \\ T_R = c_{b0} + c_{b1} \times B + c_{b2} \times B^2 + \cdots + \cdots c_{bn} \times B^{n-1} \end{cases} \quad (37)$$

Equation (38) was employed to model the crosstalk effect on the tristimulus values $[P_X, P_Y, P_Z]^T$ in Equation (35), wherein *R*, *G*, and *B* represent the digital count values. The polynomials with coefficients a_{Xi}, a_{Yi}, and a_{Zi} (i = 0, 1, 2, 3) for items 1, $R \times G$, $R \times B$, $G \times B$, and $R \times G \times B$ were used for modelling. The items were adopted to simulate the crosstalk effect between the corresponding channels. Based on past studies [121] and our measurements, it is obvious that the crosstalk effects cannot be modelled globally (i.e., to be applied to any combination of the digital count values). To achieve a higher accuracy of the model, the display RGB colour space specified by the three channels was separated into 27 subspaces from the digital count values at *M* and *N*, including a set of coefficients a_{Xi}, a_{Yi}, and a_{Zi} (i = 1, 2, 3) optimized for each subspace, as depicted in Figure 4-1. In particular, the 27 subspaces were segmented into two categories to select the training stimuli used in optimization. As depicted in Figure 4-2, the combinations of the digital count values at *M*/2, *M*, and 255 were selected to generate eight training stimuli for each subspace in the first category. Furthermore, *M*, *N*, *N*+(*255* – *N*)/2, and 255 were selected to generate the eight training stimuli for each subspace in the second category.

Specifically, the tristimulus values at (M/2, b_1, d_1), (M, b_1, d_1), (b_1, M/2, d_1), (b_1, M, d_1), (b_1, d_1, M/2), and (b_1, d_1, M), where b_1 and d_1 equal to M, N, or 255, were used to derive the relationship if the colour contained the input digital count values in the subspaces of the first category, whereas those at (b_2,d_2,f_2), with b_2, d_2, and f_2 equal to M, N, N + (255 – N)/2, or 255, were utilized to derive the relationship if the colour contained the input digital count values in the subspaces of the second category. The selection of the digital count values at M/2 instead of 0 used for the subspaces of the first category aimed to distinguish the modelling of crosstalk effect occurring between two and three channels. In case of modelling the secondary colours (e.g., colour with digital count values at (0,50,100)) only affected by the crosstalk effect between two channels, the new relationships were constructed using the training stimuli with one of the digital count values at 0.

$$\begin{cases} P_X = a_{X0} + a_{X1} \times R \times G + a_{X2} \times R \times B + a_{X3} \times G \times B + a_{X4} \times R \times G \times B \\ P_Y = a_{Y0} + a_{Y1} \times R \times G + a_{Y2} \times R \times B + a_{Y3} \times G \times B + a_{Y4} \times R \times G \times B \\ P_Z = a_{Z0} + a_{Z1} \times R \times G + a_{Z2} \times R \times B + a_{Z3} \times G \times B + a_{Z4} \times R \times G \times B \end{cases} \quad (38)$$

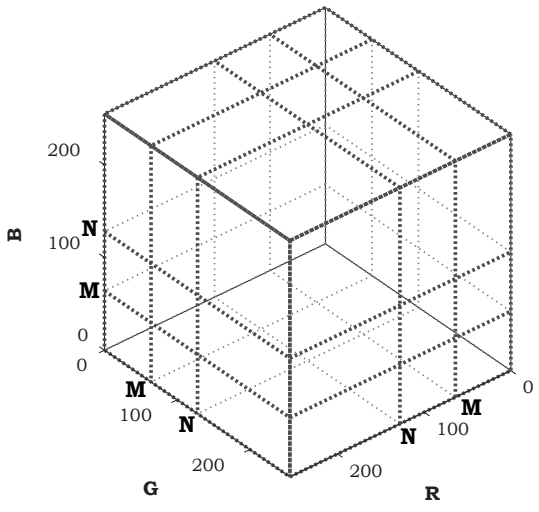

Figure 4-1 27 subspaces generated based on two piecewise points M and N on each channel in display RGB colour space.

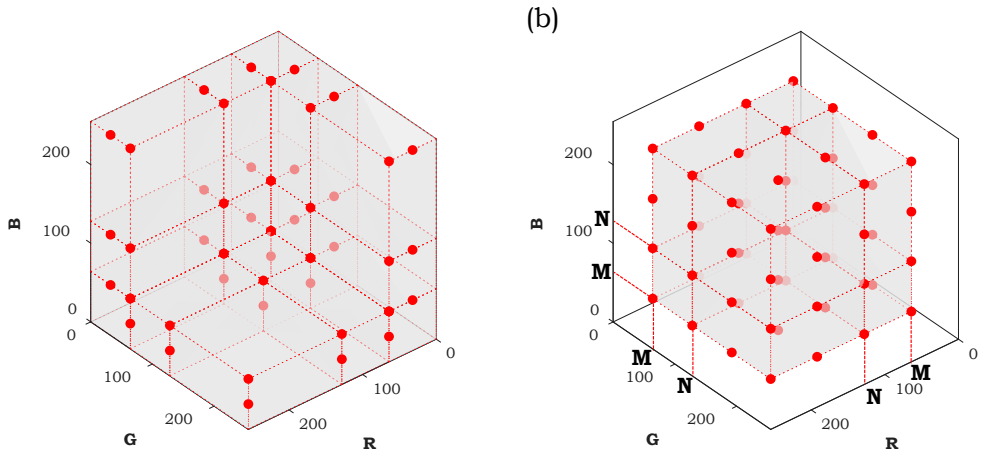

Figure 4-2 (a) 19 subspaces and corresponding training stimuli in first category, and (b) eight subspaces and corresponding training stimuli in second category.

For the secondary colours, $[P_X,P_Y,P_Z]^T$ in Equation (35) was modelled based on Equation (39), with C_1 and C_2 representing the two nonzero digital count values of colours. The polynomials with coefficients a_{Xi}, a_{Yi}, and a_{Zi} (i = 0, 1) for item 1 and $C_1 \times C_2$ were used for modelling.

$$\begin{cases} P_X' = a_{X0} + a_{X1} \times C_1 \times C_2 \\ P_Y' = a_{Y0} + a_{Y1} \times C_1 \times C_2 \\ P_Z' = a_{Z0} + a_{Z1} \times C_1 \times C_2 \end{cases} \quad (39)$$

The digital count values at M and N were applied to divided the three coordinate planes R0G, R0B, and G0B into 27 subplanes, as depicted in Figure 4-3. Specifically, the subplanes were separated into two categories for selecting the training stimuli used for optimization. As illustrated in Figure 4-4, the combinations of digital count values at $M/2$, M, and 255 were selected to generate three or four training stimuli for each subplan in the first category, and those at M, N, and 255 were selected to generate four training stimuli for each subplane in the second category. Specifically, the tristimulus values at (0,$M/2$,b_1'), (0,b_1',$M/2$), (b_1',0,$M/2$), ($M/2$,0,b_1'), (b_1',$M/2$,0), and ($M/2$,b_1',0),

with b_1' equal to M, N, or 255 were used to derive the relationship if the colour contained input digital count values in the subplanes of the first category, and those at $(0,b_2',d_2')$, $(b_2', 0,d_2')$, and $(b_2',d_2', 0)$ with b_2' and d_2' equal to M, N, or 255 were used to derive the relationship if the colour contained input digital count values in the subplanes of the second category.

According to Equations (35) to (39), the proposed model can predict the tristimulus values of any colour based on its digital count values.

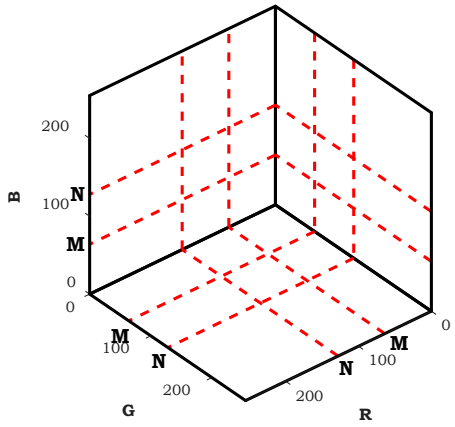

Figure 4-3 27 subplanes generated based on two piecewise points M and N on each channel in planes of R = 0, G = 0, or B = 0.

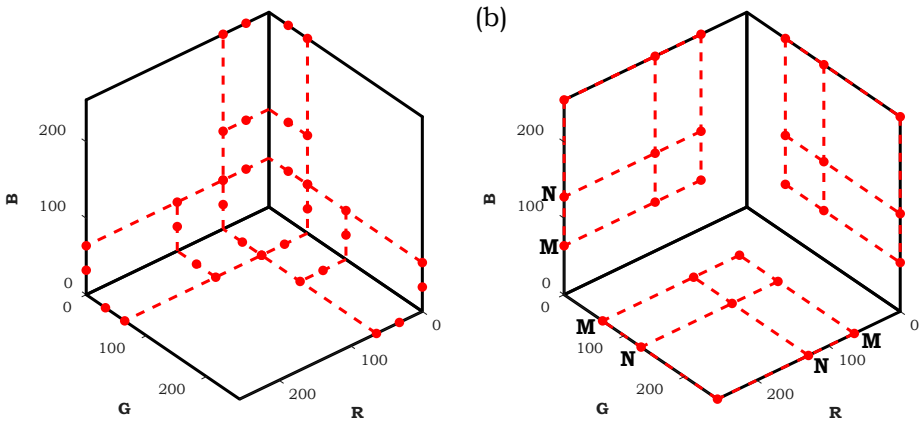

Figure 4-4 (a) 15 subplanes and corresponding training stimuli in first category, and (b) 12 subplanes and corresponding training stimuli in second category.

4.2.2 Model Simplified

Given its framework, the model was simplified to achieve an equivalent accuracy using less number of measurements.

Equation (40) can be used to model the relationship between the tristimulus values and the digital count values for each channel, as described in Equation (35), where T and C represent the tristimulus and digital count values, respectively. The coefficient a and the gramma value γ were derived using the digital count values at C_1 and C_2 as well as the corresponding measured tristimulus values T_1 and T_2 (Equations (41) and (42), respectively). In particular, the digital count values were segmented into two ranges (i.e., 0 to N and N to 255 for 8-bit displays), with a set of a and γ values derived for each range that increased the accuracy of the model. For instance, the tristimulus values measured at (M,0,0) and (N,0,0) were used to derive the relationship if the red channel included an input digital count value between 0 and N, and those at (N,0,0) and (255,0,0) were used to derive the relationship if the red channel contained an input digital count value between N and 255. In total, 18 relationships were derived (i.e., 3 channels × 2 digital count ranges × 3 tristimulus values). Therefore, the measurements of three colours, with the digital count values of 64, 128, and 255, are needed for each channel, with a total of nine colours.

$$T = \mathrm{a} \times (C/255)^{\gamma} \tag{40}$$

$$\gamma = \log(T_1/T_2)\ /\log\ (C_1/C_2) \tag{41}$$

$$\mathrm{a} = T_1/C_1^{\gamma} \tag{42}$$

The crosstalk effect on the tristimulus values $[P_X, P_Y, P_Z]^T$ in Equation (35) were modelled using Equation (43), with R, G, and B representing the digital count values. M_s denotes a three-by-five

matrix, as expressed in Equation (44). The tristimulus values *Xi*, *Yi*, and *Zi* (*i* = 0–4) in each row of M_s were multiplied by the vector coefficients $[1, R \times G, R \times B, G \times B, R \times G \times B]^T$ and the sum of these products were calculated as P_X, P_Y, and P_Z. The tristimulus values X_i, Y_i, and Z_i in M_s were evaluated through the Least-squares method expressed in Equation (45), which denotes the matrix multiplication product of the variations between the measured tristimulus values $[X_{RGB,CT}, Y_{RGB,CT}, Z_{RGB,CT}]^T$ and $[X_{RGB}, Y_{RGB}, Z_{RGB}]^T$ (Equation (35)) calculated using Equation (36), and the pseudo-inverse of the vector $[1, R \times G, R \times B, G \times B, R \times G \times B]^T$.

$$\begin{bmatrix} P_X \\ P_Y \\ P_Z \end{bmatrix} = M_s \times \begin{bmatrix} 1 \\ R \times G \\ R \times B \\ G \times B \\ R \times G \times B \end{bmatrix} \tag{43}$$

$$M_s = \begin{bmatrix} X_0 & X_1 & X_2 & X_3 & X_4 \\ Y_0 & Y_1 & Y_2 & Y_3 & Y_4 \\ Z_0 & Z_1 & Z_2 & Z_3 & Z_4 \end{bmatrix} \tag{44}$$

$$M_s = \left\{ \begin{bmatrix} X_{RGB,CT} \\ Y_{RGB,CT} \\ Z_{RGB,CT} \end{bmatrix} - \begin{bmatrix} X_{RGB} \\ Y_{RGB} \\ Z_{RGB} \end{bmatrix} \right\} \times \begin{bmatrix} 1 \\ R \times G \\ R \times B \\ G \times B \\ R \times G \times B \end{bmatrix}^{-1} \tag{45}$$

The display RGB colour space was categorized into 27 subspaces according to the digital count values at *M* and *N* on the three channels. In order to reduce the number of measurements, *M* and *N* are set to be the same as C_1 and C_2 (i.e., 64 and 128). For each subspace, the tristimulus values in Equation (44) were calculated. The digital count values required to generate eight training stimuli for each subspace were simply set at (*r*,*g*,*b*), with *r*, *g*, and *b* equal to *M*, *N*, or 255, thereby yielding the total number of training stimuli as 64, which were all possible combinations of four

digital count values (i.e., 0, 64, 128, and 255) for the three channels. According to the calculation of Equations (35), (40) and (43), the tristimulus values of any colour can be predicted based on its digital count values.

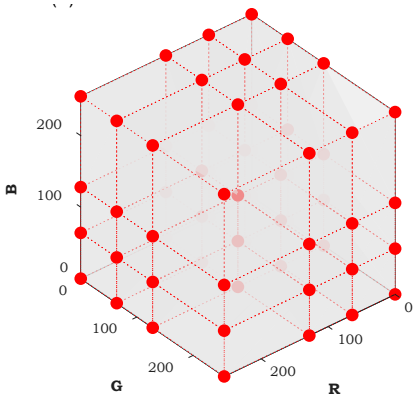

Figure 4-5 Illustration of (a) RGB colour space segmented into 27 subspaces based on digital counts values M and N on each channel, and (b) 64 training colours.

The segmentation of the display RGB colour space into subspaces considers that the relationship of the crosstalk effect with digital count values is not constant. The crosstalk effect for the colours can be more accurately predicted in their corresponding subspaces. According to the findings that the crosstalk effect is more crucial and challenging to be modelled on low emitting levels for OLED displays, the segmentation of the display RGB colour space should conform to the principle that higher precision is allocated to the characterization of the colours with lower digital count values. Therefore, *M* is defined as 128 for 8-bit displays because it is located at the centre of the range of digital count values, and *N* is defined as 64, because it is the centre of the front part of the range of digital count values.

4.3 Experiment

Nine smartphones (A to I) with OLED displays were used as test devices to explore the channel independence and chromaticity constancy, and verify the accuracy of the proposed colour characterization model. These displays were provided by different suppliers and had obvious perceived colour differences with the same input digital count values. As depicted in Figure 4-6, the gamut of these displays, together with the DCI-P3 gamut, were shown in the CIE 1931 2° chromaticity diagram. It is obvious that the colour gamuts of the displays were all similar to the DCI-P3 gamut, and the chromaticities of the primaries, especially for the blue and green, had very obvious differences. Each display was characterized by showing the 64 colours having the digital count values described above, with the tristimulus values measured using a PhotoResearch PR-655 spectroradiometer, using the proposed 3D piecewise model. The model accuracy was evaluated based on the average colour difference in terms of ΔE_{ab} in the CIELAB colour space, between the measured tristimulus values and the model predictions of 41 test colours. Thereafter, calculated colour differences were compared with the results obtained from the model before simplified and the GOG model. The digital count values of these 41 combinations are listed in Table 4-1, and the chromaticity coordinates of those colours on Display A are depicted in Figure 4-6 as an example.

Table 4-1 Digital count values of the 41 colours used to evaluate the performance of the colour characterization models.

No.	R	G	B	No.	R	G	B	No.	R	G	B
1	255	255	255	**15**	110	255	110	**29**	186	132	255
2	255	0	0	**16**	125	255	255	**30**	255	149	255
3	255	126	0	**17**	93	150	255	**31**	255	128	180
4	255	255	0	**18**	77	77	255	**32**	255	164	164
5	0	255	0	**19**	170	86	255	**33**	255	202	185

Table 4-1 (continued)

6	0	255	255	**20**	255	100	255	**34**	255	255	216
7	0	130	255	**21**	255	83	163	**35**	206	255	206
8	0	0	255	**22**	255	114	114	**36**	218	255	255
9	158	0	255	**23**	255	169	134	**37**	190	207	255
10	255	0	255	**24**	255	255	174	**38**	171	171	255
11	255	0	151	**25**	160	255	160	**39**	211	182	255
12	255	73	73	**26**	176	255	255	**40**	255	197	255
13	255	145	88	**27**	140	174	255	**41**	255	178	206
14	255	255	124	**28**	120	120	255				

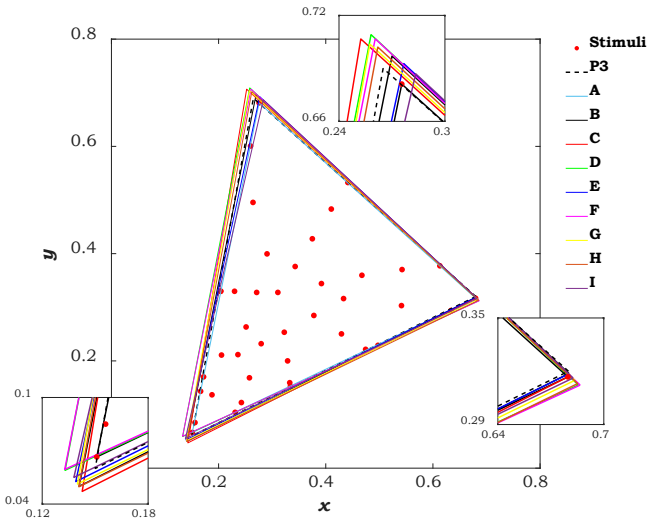

Figure 4-6 Colour gamuts of the nine OLED displays and the standard P3 gamut, together with the chromaticities of 41 combinations of the digital count values displayed using Display A in the standard P3 colour space, in the CIE 1931 2° chromaticity diagram.

4.3.1 Verification of Channel Independence and Chromaticity Constancy

The conventional colour characterization models, e.g., the GOG model, assume channel independence and chromaticity constancy. To verify the channel independence of OLED displays, we explored the relationships between the relative luminance of neutral colours with the three channels having the same digital count values, and the sum luminance of three stimuli with the

same digital count value to each channel individually (e.g., the luminance of (255,255,255) versus the sum of the luminance of (255,0,0), (0,255,0), and (0,0,255)). All the values were scaled using the white point luminance of each display. For the nine displays, this relationship is portrayed in Figure 4-7. The results indicated that the sum luminance of the three colours was larger than the corresponding luminance of the neutral colour for all displays, and increases of crosstalk effect with the luminances, excluding Display D and F. Then we calculated the chromaticity differences $\Delta u'v'$ between the measured chromaticities of a series colours whose digital count values of two or three channels were not zero and the calculated chromaticities of the colours assuming the channel independence (e.g., the measured chromaticities of (255,255,255) versus the calculated chromaticities by mixing (255,0,0), (0,255,0), and (0,0,255)), with Figure 4-8 showing the histograms of the $\Delta u'v'$ values for the nine displays. It also clearly shows the crosstalk effects. Overall, channel dependency was observed for all nine test displays.

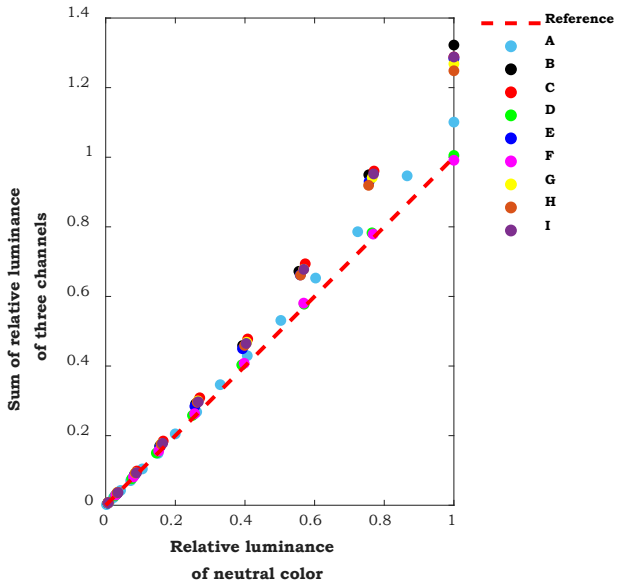

Figure 4-7 Relationships between relative luminance of neutral colours and sum of relative luminance of three channels.

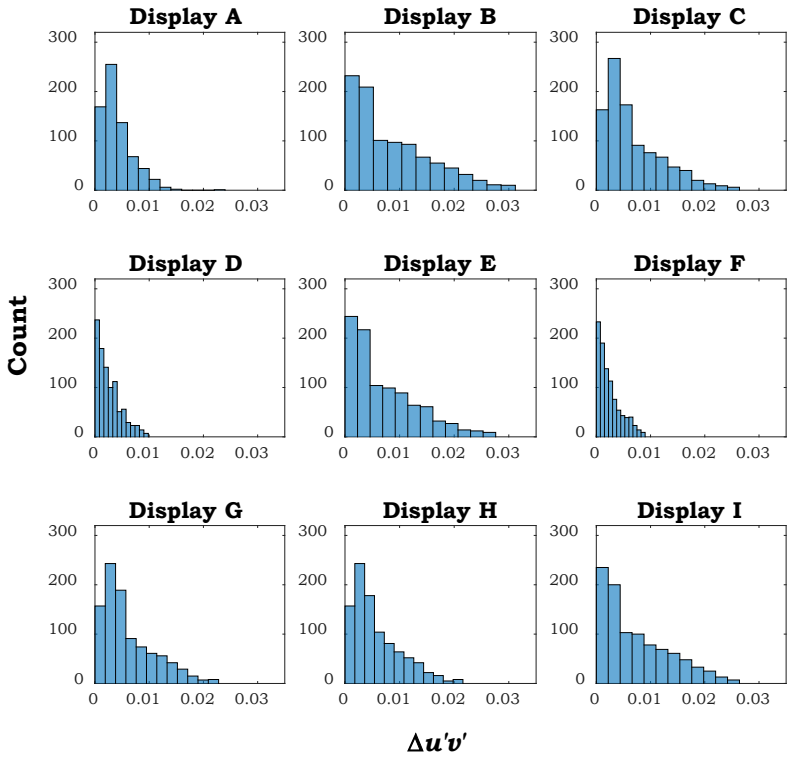

Figure 4-8 Histogram of the chromaticity differences Δ*u'v'* between the measured chromaticities of a series colours whose digital count values of two or three channels were not zero and the calculated chromaticities of the colours assuming the channel independence. There are 704 and 972 colours for Display A and Displays B to I respectively.

The chromaticity constancy of the test OLED displays was verified for each channel by comparing the chromaticities at a series of digital count values, as depicted in Figure 4-9. The results demonstrated the consistency in the chromaticities of the test OLED displays. Overall, the results indicated adequate chromaticity constancy. This figure, together with the chromaticity differences shown in Figure 4-8, clearly suggests the serious problem introduced by the crosstalk effects.

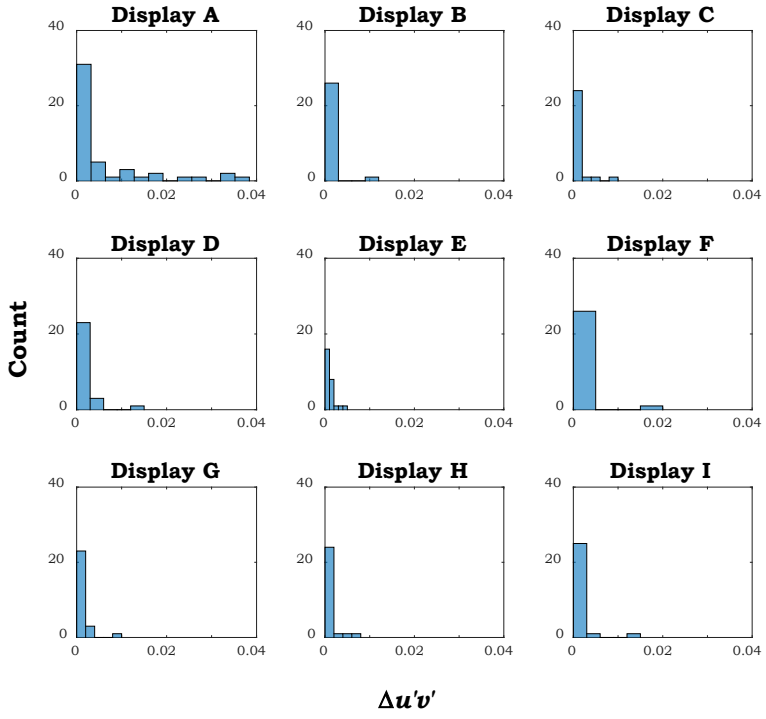

Figure 4-9 Histogram of the chromaticity differences Δ*u'v'* chromaticities at a series of digital count values and those at the digital count value of 255 for each channel for the nine displays.

4.3.2 Performance of the 3D Piecewise Model

The colour differences between the tristimulus values of the 41 test stimuli predicted from the models and the corresponding tristimulus values calculated using the measured SPDs are presented in Table 4-2 in terms of the minimal, maximal, and average ΔE_{ab} values. As expected, large errors were observed with the application of the GOG model for predicting the tristimulus values of the test stimuli based on the inputted digital count values. Among the nine test OLED displays, the average colour differences calculated based on the predicted tristimulus values of the test stimuli ranged from 5.03–15.99 units of ΔE_{ab} and averaged around 10.74 units of ΔE_{ab}. These results further established the failure of the GOG model in case of employing the colour characterization of the OLED displays.

The colour differences resulted from the proposed 3D piecewise model were calculated between the measurements and model predictions, also listed in Table 4-2. The values for the nine test OLED displays ranged from 0.61 to 1.46 units of ΔE_{ab} and averaged around 0.92 units of ΔE_{ab}, which signifies a considerable improvement in comparison with the results predicted by the GOG model. Furthermore, these results verified that the accuracy of the proposed model was constant after the simplification. The colour differences computed using the preliminary model are listed in Table 4-2. The values for the nine test OLED displays ranged from 0.55 to 1.58 units of ΔE_{ab} and averaged around 1.03 units of ΔE_{ab}, suggesting that the average colour difference is similar with the results calculated using the proposed model.

Table 4-2 Comparisons of the performance between proposed 3D piecewise model and the GOG, as well as the model before simplified, in terms of the colour differences ΔE_{ab} of the 41 combinations of the digital count values between the chromaticities predicted by the models and those based on the measurements, in the CIELAB colour space for the nine displays.

Displays	GOG model			Proposed 3D piecewise model before simplified			Proposed 3D piecewise model		
	Mean	Max	Min	Mean	Max	Min	Mean	Max	Min
A	5.03	7.74	0.03	0.55	1.52	0.01	0.61	1.96	0.06
B	15.99	27.20	0.12	1.04	3.69	0.00	1.46	4.15	0.06
C	12.40	19.99	0.08	1.00	4.57	0.06	1.02	3.24	0.06
D	4.45	12.07	0.08	1.58	7.92	0.04	0.51	2.64	0.01
E	13.66	24.01	0.11	0.89	3.26	0.00	1.18	3.48	0.04
F	3.75	8.74	0.09	0.97	5.00	0.00	0.49	3.12	0.03
G	11.21	17.59	0.10	1.03	4.16	0.07	0.94	2.71	0.05
H	10.58	16.25	0.15	0.87	3.44	0.04	1.00	3.29	0.03
I	13.88	23.61	0.12	0.89	3.21	0.00	1.08	3.40	0.05
Mean	10.74	-	-	1.03	-	-	0.92	-	-

4.4 Model for a display with breakpoints on the channels

In practice, the breakpoints were observed for the three channels in characterizing a special type of OLED display, as depicted in Figure 4-10, which shows the obvious discontinuity between the tristimulus values and the digital count values. Under the circumstances, the proposed 3D piecewise model may cause large degrees of inaccuracy because the breakpoints may be involved in certain subspaces in case of using 64 and 128 to divide the range of digital count values on the three channels.

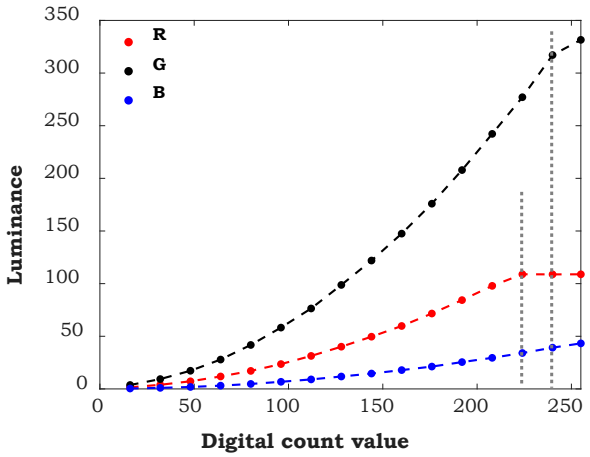

Figure 4-10 Relationships the luminance and the digital count values for each of the three channels.

To resolve this issue, *M* and *N* were redefined according to the measured breakpoints of displays. For example, the relationships between the relative luminance of neutral colours and the relative luminance of three channels for a OLED display are presented in Figure 4-10. The breakpoints were prominently observed on the red and green channels at the digital count values R = 224 and G = 240 for the 8-bit display. Based on this result, *M* and *N* were redefined as 112 and 224 on the red channel and 120 and 240 on the green channel, because *M* was always defined as the centre of the front part of the range of digital count values. For the blue channel without an evident

breakpoint, 64 and 128 were still set as *M* and *N*. The new set of 27 subspaces were segmented based on the redefined *M* and *N* for each channel, as depicted in Figure 4-11. The model with the redefined values of *M* and *N* was applied to characterize this OLED display using the digital count values and corresponding measured tristimulus values of the 64 colours used for deriving the models for characterizing the crosstalk effects for the 27 subspaces, as portrayed in Figure 4-11. The remaining portions of the model remained unchanged.

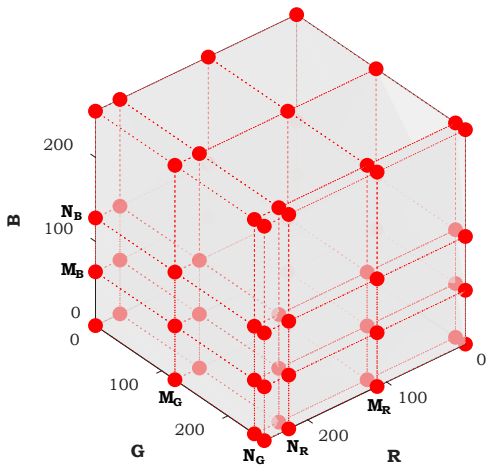

Figure 4-11 Illustration of the 27 subspaces with the revised M and N values based on the breakpoints for each channel, with the dots showing the 64 combinations of the digital count values.

In Figure 4-12, the tristimulus values *XYZ* between the measurements and the model predictions using the redefined *M* and *N* for the three channels were compared. The lines indicate the prediction relationship of tristimulus values of colours for each channel with the digital count values. The three channels with digital count values at (*j*, 0, 0), (0, *j*, 0), and (0, 0, *j*), with *j* equal to 16, 32, 48, 64, 80, 96, 112, 128, 144, 160, 176, 192, 208, 224, 240, or 255, were used to verify the accuracy of the predictions. The dots represent the measured tristimulus values, signifying

small colour differences between the measurements and model predictions. The average colour differences ΔE_{ab} in CIELAB colour space between the predicted and measured tristimulus values of the 41 test colours are summarized in Table 4-3. The prediction results exhibited remarkable improvement in comparison with the results calculated through the GOG model and the proposed 3D piecewise model without redefinition. The average colour difference evaluated based on the redefined piecewise model was 2.40 units, which performed great improvement compared with the results calculated using the GOG model (13.8 units), and the proposed 3D piecewise model without redefinition (14.95 units).

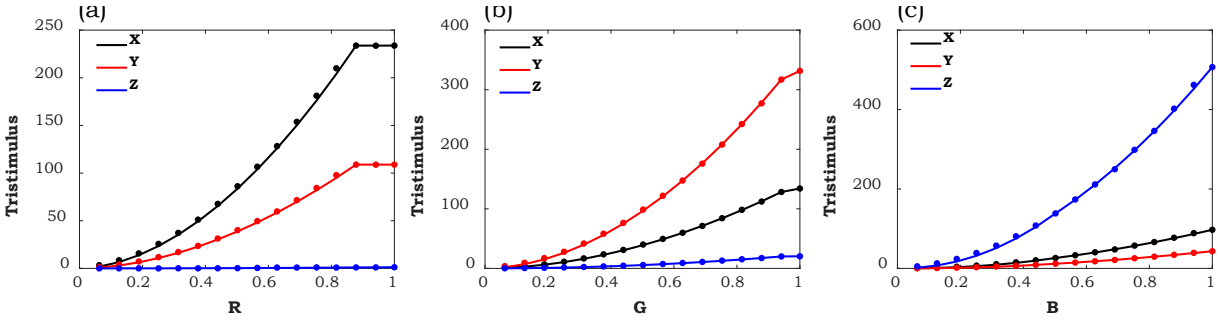

Figure 4-12 Relationships between predicted tristimulus values and relative digital counts (a) R, (b) G, and (c) B of three channels; dots represent measured tristimulus values.

Table 4-3 Average CIELAB colour difference between the measurements and model predictions of 41 test stimuli for display with breakpoints on channels.

GOG model			3D piecewise model (PP: 64, 128)			3D piecewise model (PP: Breakpoints)		
Mean	Max	Min	Mean	Max	Min	Mean	Max	Min
13.08	32.84	0.84	14.95	30.36	3.21	2.40	6.27	0.52

4.5 Inversion of the proposed 3D Piecewise Model

For industry applications, the displays are calibrated and specified to produce colours according to standard RGB specifications. The inverse models are useful to predict the display digital count values based on the values with standard RGB specifications.

The derive the inversion of the proposed 3D piecewise mode, the tristimulus values of 16777216 combinations of digital count values, which were all possible combinations of 256 digital signal levels for the RGB channels, were calculated. At the same time, the tristimulus values of the standard P3 RGB combinations were also calculated, which were considered as target values. The combination of digital count values having the smallest colour differences ΔE_{ab} in the CIELAB colour space to the target values was identified from the above 16777216 ones. Meanwhile, the combination for the white point was identified by finding the smallest chromaticity distance $\Delta u'v'$ to the standard P3 white point (i.e., D65) and the highest luminance level.

Based on such a method for inverting the model, an 8 × 8 × 8 3D LUT was derived between the values with standard P3 RGB specifications and the display digital count values for calibrating smartphone displays, with the standard P3 RGB specifications of all combinations of 8 levels of R, G, and B values (i.e., 0, 40, 80, 120, 160, 200, 240, and 255). The display will automatically perform interpolations based on the 3D LUT.

The performance of the inversion of the 3D piecewise model and the development of the LUT were tested using 94 OLED smartphone displays. The ΔE_{ab} colour differences were calculated between the chromaticities of the colours with the P3 standard specification and those measured on the displays before and after the calibration. Figure 4-13 shows the histograms of the ΔE_{ab} for the 94 displays. The 64 training colours were used to characterize the display accuracy without calibration, and the 41 test colours were used to characterize the display accuracy after the

calibration. It can be found that such methods resulted in good performance, with the average color difference reduced from 11.81 to 1.63.

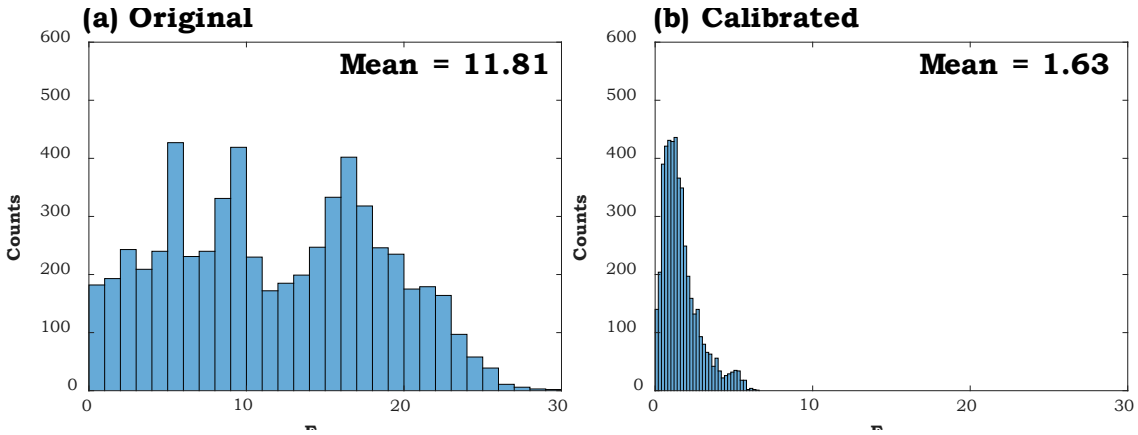

Figure 4-13. Histogram of ΔE_{ab} between the chromaticities of the colors with the P3 standard specification and those measured on the displays before and after calibrated using the inverse model.

4.6 Conclusions

As a newly developed display technology, OLED is widely used in the smartphone industry. However, the crosstalk effect resulting from the special structure of the OLED display panels causes the failure of channel independence. Owing to this problem, conventional colour characterization models assuming channel independence, e.g., GOG model, cannot accurately calibrate modern OLED displays. Although certain models of colour characterization have been developed to calibrate the displays that fail to satisfy channel independence, these models require extensive number of measurements. Thus, colour characterization models that can accurately and efficiently correct the crosstalk effect on OLED displays are required. This study proposed a 3D piecewise model using only 64 measurements, wherein display RGB colour space was divided into 27 subspaces, with two separation points on each channel. The accuracy of the model predictions was verified using nine test OLED displays. The average colour difference in terms of

ΔE_{ab} in the CIELAB colour space, between the measurements and model predictions of 41 test colours were calculated using the proposed model and the conventional GOG models. Among the nine test OLED displays, the 3D piecewise model yielded average values of 0.92 units, which was significantly smaller than that based on the GOG model. In addition, for the displays having obvious breakpoints on each channel, the 27 subspaces are proposed to be redefined by adjusting the separation points on each channel. Such an adjustment can maintain the good performance of the proposed model.

Chapter 5 Study 2-1: Colour Mismatch and Observer Metamerism between LCD and OLED Displays for Smaller FOV (≈ 4.8°)

5.1 Motivations

Colour mismatch and observer metamerism are observed between devices with multiple spectra. Although these problems have not been recently reported, they are crucial for the display community owing to the wider usage of OLED displays. On online forums, certain users have recently reported the appearance of a green tint on OLED displays of a specific smartphone brand, and its reason remains unidentified. In addition, a study investigated the possible effect of using the CIE 1931 2° CMFs on colour calibration and the specification for OLED displays and LCDs through mathematical calculations [140]. However, no study has experimentally investigated the degrees of colour mismatch and observer metamerism between OLED displays and LCDs.

In this study, human observers adjusted the colour appearance of the stimuli produced by four smartphone displays, including one LCD and three OLED displays, to match the colour appearance of the six colour stimuli produced by another OLED display. The results of the colour matching experiment enabled us to quantify the performance of four standard CIE CMFs, especially the CIE 1931 2° CMFs, in characterizing the colours between LCD and OLED displays.

5.2 Method

5.2.1 Apparatus and Setup

In this study, we constructed a 60 cm × 60 cm × 60 cm viewing booth for the experiment, painted the interiors with Munsell N7 spectrally neutral paint, and created two 5 cm × 5 cm square openings at the centre of the rear panel. The distance from the centre edge of an opening to that of another

opening was 6 cm. Thereafter, we mounted a chin rest on the exterior side of the viewing booth to ensure that an observer is capable of simultaneously detecting the display centres of the two smartphones through the openings. The FOV of each stimulus was 4.77°, and the experimental steps are displayed in Figure 5-1.

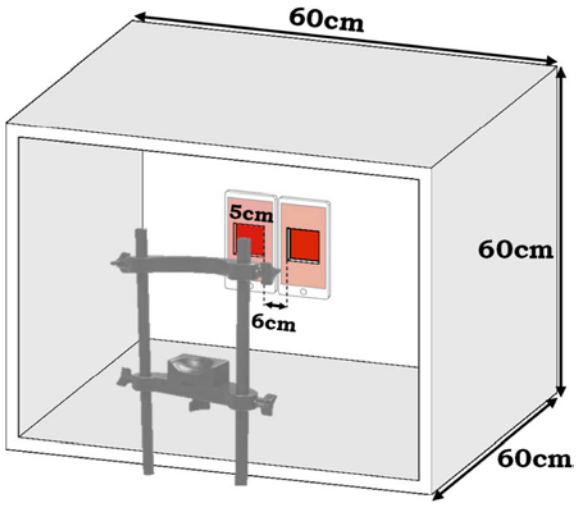

Figure 5-1 Schematic illustration of experimental setup. Chin rest was mounted immediately outside the booth such that the viewing distance is 60 cm.

Despite the similarity between the use of the entire display as a stimulus and the practical viewing of the display, only a small area at the display centre was used to produce the stimuli and avoid the possible problems resulting from the nonuniformity of the displays. Moreover, if the two stimuli were placed in vicinity of each other without any significant separation distance, colour matching could be easily achieved. However, the distance of 6 cm was the least distance for the openings to exhibit the centre of displays.

5.2.2 Displays and Colour Stimuli

In the experiment, we employed five smartphone displays including one LCD and four OLED displays. The dimensions of these smartphones were 70 mm (width) × 140 mm (height), with small variations. The characteristics and algorithms of the displays were tested based on the

configurations of the five smartphones. Among eight OLED displays, selected four OLED displays to ensure marginal differences in their primaries, which was manifested by the peak wavelength and shape of the SPDs. Despite the small differences between various OLED displays, prominent colour differences were observed. Accordingly, we selected the OLED display that exhibited the smallest colour gamut as the reference display, for comparison between LCD and OLED displays as well as between various OLED displays. The colour gamut of displays derived with the CIE 1931 2° CMFs is depicted in Figure 5-2, and the SPDs of the primaries are illustrated in Figure 5-3.

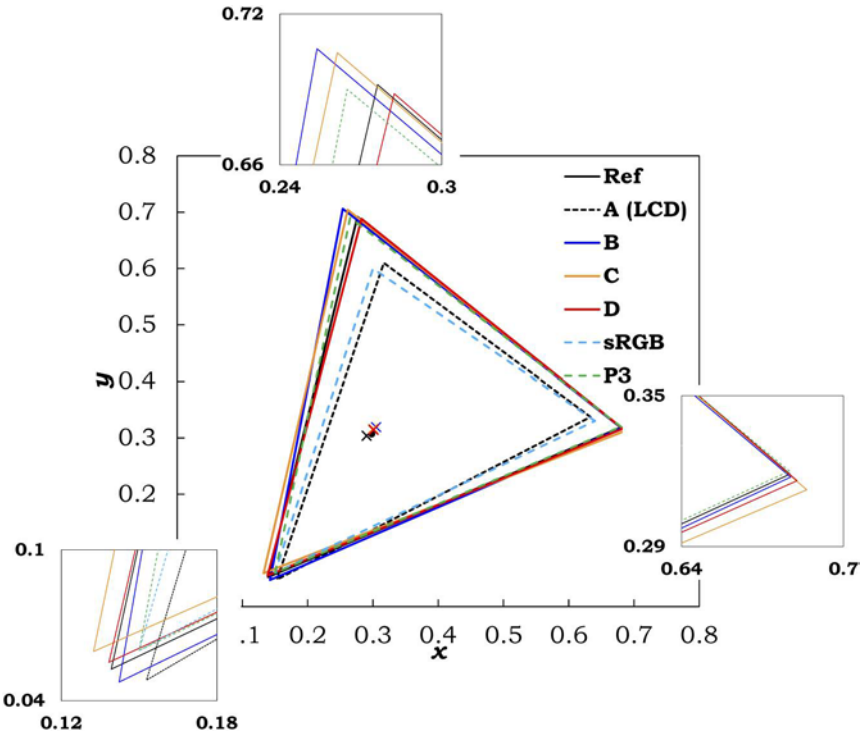

Figure 5-2 Colour gamut and white points of five displays derived using CIE 1931 CMFs along with standard sRGB and P3 colour gamut. Note: white point of reference display is labelled with a circle and those of other four displays are labelled with crosses.

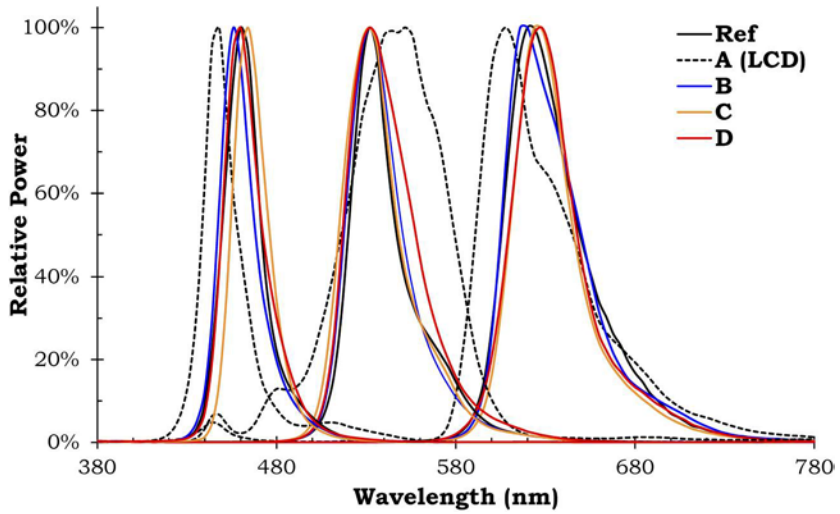

Figure 5-3 Relative SPDs of primaries of five displays.

With careful consideration, we selected six colour stimuli and presented them on the reference display in the MacLeod–Boynton chromaticity diagram [145] for 2° FOV [57]. The MacLeod–Boynton chromaticity diagram is based on physiology, forming the rectangular axes—*l* and *s* with the cone sensitivity functions, for improving the representation of the relative cone excitation (l = L/(L + M) and s = S/(L + M)). According to Figure 5-4, we selected all stimuli from the colour gamut of all displays to ensure that human observers were capable of matching these stimuli. In particular, Stimuli 1 and 2 possessed similar values along *s*-axis, but they significantly varied along the *l*-axis; Stimuli 2 and 3 covered similar values along *l*-axis but dissimilar values along *s*-axis; the values of Stimuli 2, 4, and 5 varied along both the axes. Stimuli 6 was a neutral colour, and the CIE D70 illuminant served for calculating the target values along the two axes. To minimize any possible impact caused by adaptation to observation under dark conditions, the luminance ranges of the displays exhibiting the six chromaticities were considered and the luminance of the six stimuli was set at 93 cd/m^2.

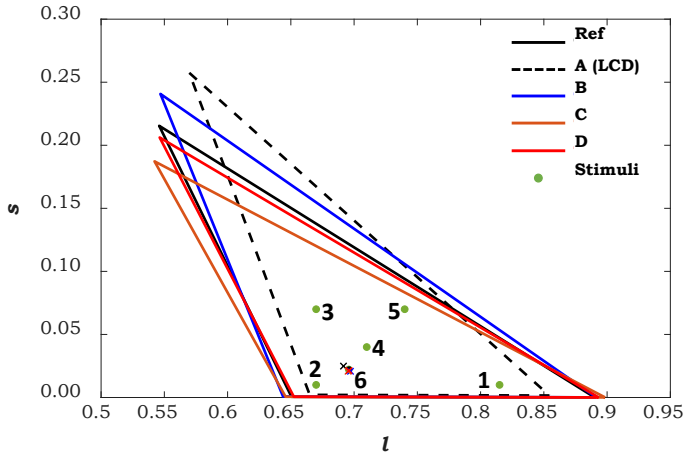

Figure 5-4 Display colour gamut and white points in MacLeod–Boynton chromaticity diagram for 2° FOV [10] and chromaticities of stimuli exhibited on reference display for colour matching.

5.2.3 Display Calibration and Control Program

A calibrated JETI Specbos 1811 spectroradiometer was used for calibrating the six stimuli on the reference display.

We developed a customized control program with respect to the four displays used for matching the colour appearance of six stimuli. The observers were requested to adjust the related chromaticities along the *u'*- and *v'*-directions in the CIE 1976 *u'v'* chromaticity diagram, thereby adjusting the colour appearance of the stimuli. In the CIE 1976 *u'v'* chromaticity diagram, + *u'*, – *u'*, +*v'*, and –*v'* represented the directions of reddish, greenish, yellowish, and blueish, respectively. A prior research [146] once adopted such an adjustment method that can be comprehended by naïve observers.

Specific to each display, we employed the spectroradiometer to measure the SPDs of 1000 colours, corresponding to all the possible combinations of the ten digital count levels specific to the RGB channels (0, 28, 56, 85, 113, 141, 170, 198, 226, and 255). Relevant measurements were recorded by placing the display at the experimental position and placing the spectroradiometer at the eye

position of the observer. These data served for building a 10 × 10 × 10 3D LUT between the RGB combinations and the corresponding tristimulus values *XYZ*. Subsequently, we determined the stimuli with luminance ranging from 88.35–97.65 cd/m^2 (±5% of 93 cd/m^2) to estimate the colour gamut at 93 cd/m^2, as depicted in Figure 5-5. The colour with the smallest colour difference ΔE_{ab} was identified from the target stimulus from the 1000 colours, thereby estimating the RGB combination that could generate a target stimulus with chromaticities (*u'*,*v'*) in the gamut.

All possible combinations, regarding the contiguous six digital count levels, and the corresponding tristimulus values *XYZ* were acquired to construct another 3D LUT (6 × 6 × 6). The three values above and below the digital count values of the colour exhibiting the smallest colour difference compared to the target colour were selected as the six values. The corresponding tristimulus values *XYZ* were trilinear interpolated from the 1000 sets of data. We considered the RGB combination bearing the smallest colour difference ΔE_{ab} value between the target colour and the 216 colours as the estimated RGB combination for the generation of stimulus with chromaticities (*u'*,*v'*). The stated process served for estimating the RGB combinations specific to all chromaticities within the display colour gamut at 93 cd/m^2 with a step of 0.0015 along the two directions (*u'*,*v'*).

In the experiment, if the observer adjusted the stimulus chromaticities to alter the colour appearance, the control program could determine the corresponding RGB combination for generating the colour on displays. Conventional models that are employed for developing control programs for display characterization include the GOG model or PLCC model, described in Section 2.5.1. However, these models cannot be applied to the OLED displays adopted in the experiment.

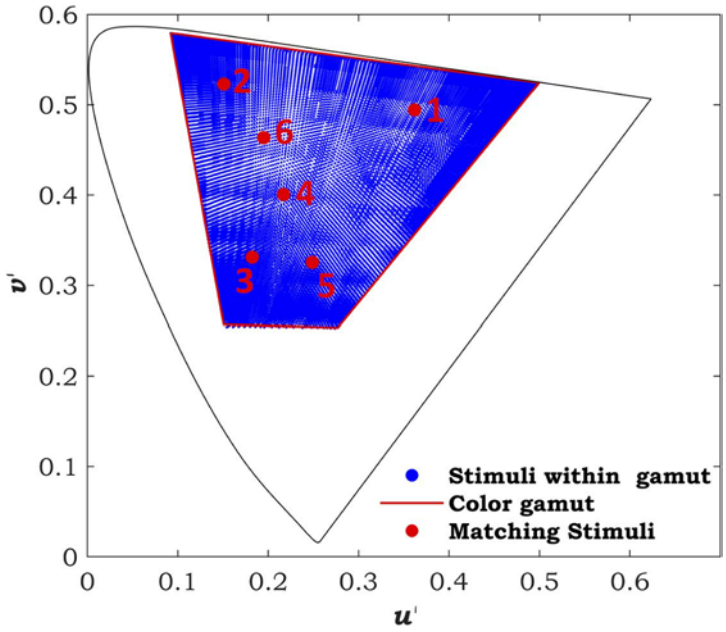

Figure 5-5 Illustration of using 3D LUT to identify colour gamut at luminance of ~93 cd/m^2 for Display B.

5.2.4 Observers

The experiment included 50 observers (36 males and 14 females) aged in the range of 19–38 years (mean = 22, SD = 3.01). The Ishihara Color Vision Test was used for testing whether the observers exhibited normal colour visions.

5.2.5 Experimental Procedure

Prior to the experiment, the observers underwent the Ishihara Color Vision Test and completed a survey on their general information. Thereafter, the observers were guided toward the front of the viewing booth with the illumination turned off. The experimenters informed the observers regarding the manner in which the stimulus colour appearance can be adjusted using the four arrow keys on the keyboard (right: $+u'$, left: $-u'$, up: $+v'$, down: $-v'$) to render the two stimuli with the same colour appearance. Thereafter, the observers were instructed to place their chins on the chin-rest. Before initiating the recorded trials, the observers were familiarized with the control program

with two practice trials. During the colour matching process, the reference display produced a stimulus on the left-hand side, and any one of the four test displays produced a stimulus on the right-hand side. Although a possible positional bias existed in such a setup, the positions were not altered to ensure the stability of the displays. Specific to each test display, seven adjustments were enacted by the observers, wherein Stimulus 2 was adjusted two times to evaluate the intra-observer variations. Twenty-eight adjustments were completed by each observer in a total duration of one hour. We warmed up all the displays for almost half an hour before the experiment to ensure the stable performance of displays. In particular, the displays were attached on various tripods and two lines were marked on the rear side of the booth to ensure that the alternation between various displays can be executed by simply adjusting the location of the tripods aligned toward the left edge and on the top of the displays with respect to the markers.

5.3 Results and Discussion

5.3.1 Verification of Control Program Accuracy

Although the observers adopted the customized control program to adjust the stimulus colour appearance by altering the related chromaticities, we recorded the RGB combinations used for producing the stimuli. After the experiment, the RGB combinations were recorded for reproducing the stimuli on the corresponding displays, and the spectroradiometer was employed to measure the SPDs. The chromaticities (u',v') regarding all the adjusted stimuli from the SPDs measured by the control program and the corresponding predicted chromaticities are presented in Figure 5-6(a). $\Delta u'v'$ values were in the range of 0 to 0.0053 and the average $\Delta u'v'$ was 0.0017. The luminance levels of the stimuli adjusted according to the measured SPDs are presented in Figure 5-6(b), wherein the average value of 91.9 cd/m^2 validated the reliability of the control program.

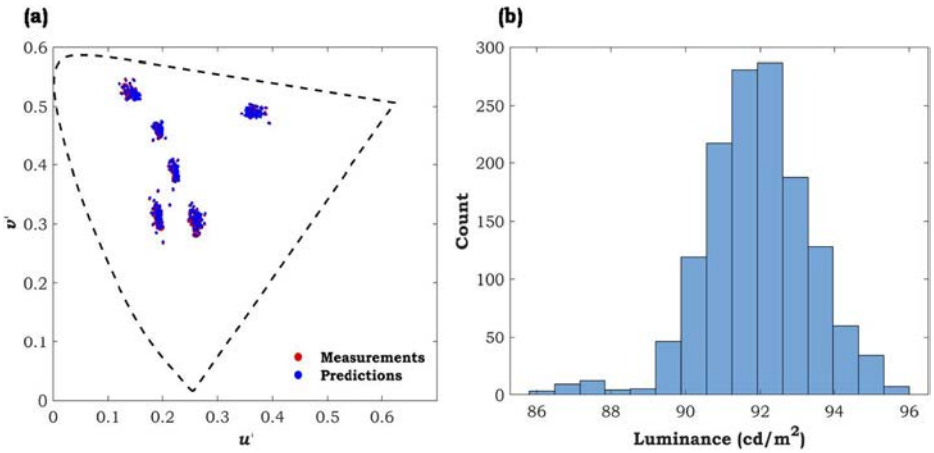

Figure 5-6 Accuracy of control program, in terms of chromaticities and luminance. (a) Chromaticities of adjusted stimuli derived from measured SPDs and predictions using control program in CIE 1976 *u'v'* chromaticity diagram; (b) Histogram of luminance of adjusted stimuli derived from measured SPDs.

5.3.2 Intra- and Interobserver Variations

The mean colour difference from the mean (MCDM) in the CIE 1976 *u'v'* chromaticity diagram was adopted for characterizing the intraobserver and interobserver variations. Specifically, the characterization of the intraobserver variation considered the average colour differences between the chromaticities of the two matching results from Stimulus 2 and the average chromaticities of the two matching results. Each observer used the four test displays to perform the matches for Stimulus 2, with the related chromaticities and the 95%-confidence error ellipses displayed in Figure 5-7, and the histograms of MCDM for intraobserver variation are presented in Figure 5-8. Specific to Displays A, B, C, and D, the average MCDM among the observers was 0.0020, 0.0031, 0.0026, and 0.0024, respectively, less than the 0.004 units of *u'v'* (≈ one unit of just-noticeable colour difference, JND).

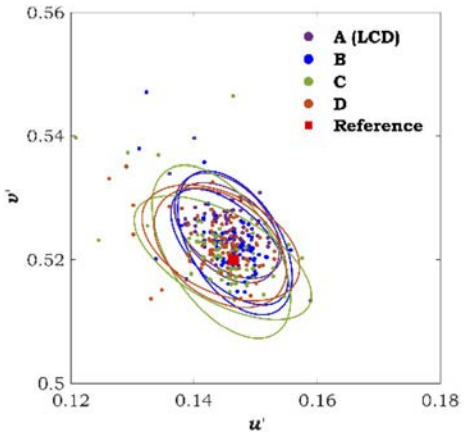

Figure 5-7 Chromaticities, together with 95%-confidence error ellipses, of two matches performed by each observer for Stimulus 2 using four test displays.

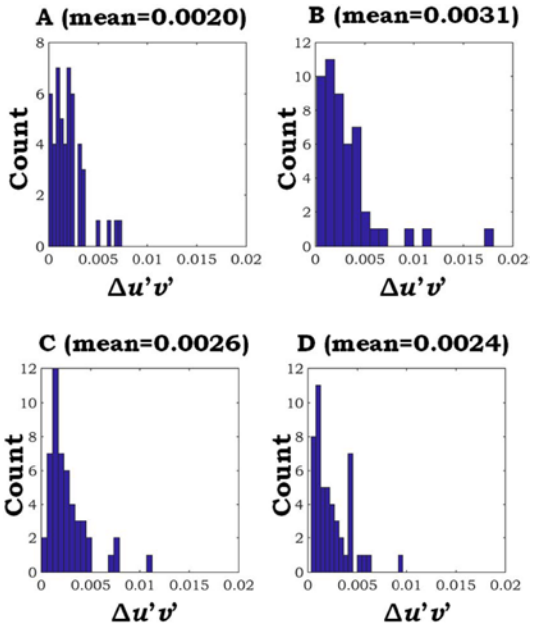

Figure 5-8 Histogram of MCDM values of the intra-observer variations for each display.

To characterize interobserver variations, the differences in chromaticity between the 28 adjustments regarding each observer and the 28 mean adjustments among the 50 observers were recorded. The MCDM value was in the range of 0.0027 to 0.0122 and the average MCDM was 0.0059. The MCDM values regarding the intraobserver and interobserver variations conformed to

a recently conducted colour matching experiment [17], which established the high reliability of experimental results.

5.3.3 Characterization of Colour Matching Results using Four CMFs

The chromaticities of the stimuli adjusted by the observers using the four test displays are depicted in Figure 5-9, wherein the 95%-confidence error of the observers are marked with ellipses. The four standard CMFs were employed to characterize the chromaticities. In Figure 5-10, the chromaticities of the reference stimuli have been transposed to the origin, and the chromaticities of the adjusted results varied with the reference stimuli. In case of using various CMFs, the majority of the ellipses exhibited similar orientations. In addition to the chromaticities of the stimuli on the reference display, the average chromaticities of the stimuli adjusted on the four displays are illustrated in Figure 5-11, wherein the four CMFs were used for related calculation. The Euclidean distances from the average chromaticities of the adjusted results to the chromaticities of the reference stimuli in the chromaticity are portrayed in Figure 5-12, and the ellipse areas of the chromaticities adjusted by the observers are plotted in Figure 5-13. Interestingly, the longer axes of the ellipses were oriented toward the centre of the chromaticity diagram, and the ellipses of Stimulus 6 (white colour) became circles. In particular, the chromaticities characterized using the two 10° CMFs were more representative to the adjusted results. Compared to the LCD, the OLED displays were more strongly influenced by the four CMFs.

The CIE 1931 2° CMFs are closely associated with display calibration. To apply this set of CMFs, Display A (LCD) exhibited the largest chromaticity distances and areas of ellipses relative to the three OLED displays. The chromaticity distances produced by all six stimuli were over 0.004 units of $u'v'$ (1 JND), implying a prominent colour difference. Moreover, for Display A, the chromaticities shifted toward the $-u'+v'$-direction to render an appearance that corresponds to the

colours of the stimuli on the reference OLED display. Therefore, the application of the CIE 1931 2° CMFs to ensure the same chromaticities of Display A (LCD) and the reference OLED display would yield a severe colour mismatch. More specifically, a stimulus appearing neutral on an LCD may appear yellowish green on a OLED display, which exhibited the same chromaticities between the stimuli on the two displays. Comparatively, a stimulus appearing neutral on an OLED display may appear pinkish on an LCD at the same chromaticity, which confirms the recent discovery that colour mismatches may generate pinkish or greenish chromaticities [148]. The shifts occurred for neutral colours as well as for other colours (Figure 5-11). Specific to Displays B, C, and D, the majority of the chromaticity distances were below 0.004 units of *u'v'* (1 JND).

Notably, the comparison between the calculated chromaticity distances and the MCDM values for the intraobserver variations deepens our understanding of the distinction between LCDs and OLED displays. The average difference in the chromaticity between the OLED displays (Displays B, C, and D) and the reference display confirmed the intraobserver variations. However, the average difference between Display A (LCD) and the reference OLED display was substantially larger than the intraobserver variation. In case of Displays A, B, C, and D, the chromaticity distances were 0.0051, 0.0025, 0.0021, and 0.0032, and the MCDM values were 0.0020, 0.003, 0.0026, and 0.0024, with the ratio of the former to the latter at 2.55, 0.81, 0.81, and 1.33, respectively.

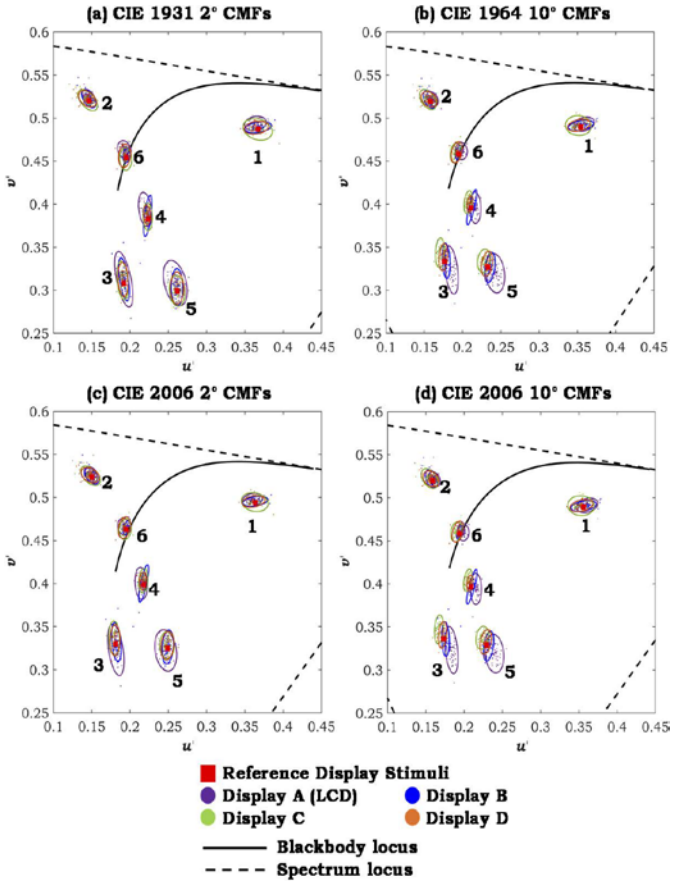

Figure 5-9 Chromaticities with 95%-confidence error ellipses of stimuli adjusted by 50 observers using four displays to match the colour appearance of the stimuli displayed on reference display based on four CMFs. (a) CIE 1931 2° CMFs; (b) CIE 1964 10° CMFs; (c) CIE 2006 2° CMFs; (d) CIE 2006 10° CMFs. (Note: numbers on figures represent stimuli 1 to 6).

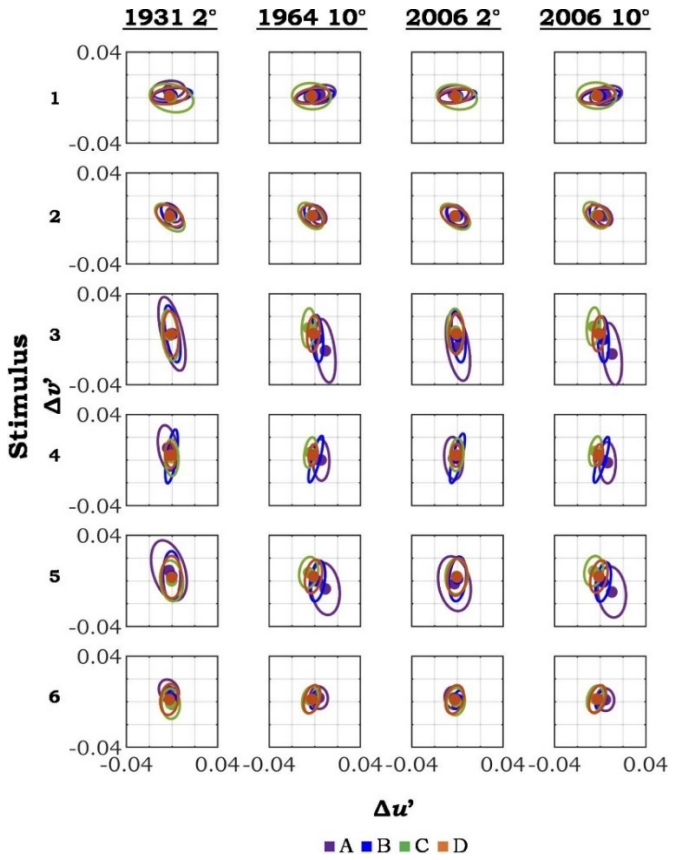

Figure 5-10 95%-confidence error ellipses of chromaticities adjusted by observers with relation to chromaticities of corresponding reference stimuli, plotted using four CMFs.

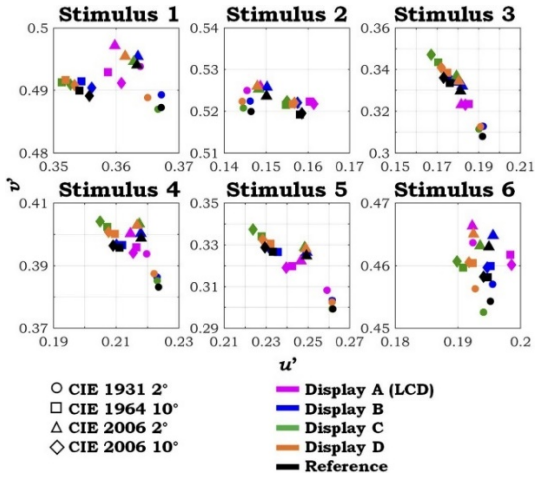

Figure 5-11 Average chromaticities of stimuli adjusted by observers using four displays and corresponding stimuli on the reference display calculated using four CMFs. (Note: for illustration, axis ranges varied, but each gird corresponds to 0.01 unit in *u'* and *v'*)

5.3.4 Comparisons among Four CMFs

According to Figure 5-11, in case of adopting two sets of 2° CMFs, the average chromaticities of the stimuli generated by Displays B, C, and D were similar among the observers. Comparatively, the average chromaticities of Stimuli 3 and 5 generated by the three OLED displays varied in normal situations. The variation in the chromaticities between the adjusted and reference stimuli, including the ellipse size obtained by fitting the chromaticities of the adjusted stimuli, enabled a quantitative comparison of the performance of the CMFs. The chromaticity distance facilitated the evaluation of the accurate characterization of the colour match by an average observer using a set of CMFs, wherein a smaller distance indicates a higher accuracy. The ellipse area can be utilized for assessing the characterization of the variations among the observers using a set of CMFs, and a smaller area represents a smaller variation [144]. According to Table 5-1, the CIE 2006 2° CMFs yielded the smallest chromaticity distance, followed by the CIE 1931 2°, CIE 1964 10°, and CIE 2006 10° CMFs. This finding does not reflect that the 10° CMFs are suitable for an FOV beyond 4° [149]. Considering observer variations, the two 10° CMFs presented the best performance, the CIE 2006 2° CMFs produced a moderate performance, and the CIE 1931 2° delivered the worst performance. Therefore, the adoption of the CIE 1931 2° CMFs can result in severe observer metamerism.

The chromaticity distances or ellipse areas calculated using various CMFs cannot be directly compared because of the various scales. Despite the fixed perceived colour difference between the standard D65 and D70 illuminants, the chromaticity distances varied with the CMFs, and the CIE 1931 2°, 1964 10°, 2006 2°, and 2006 10° CMFs exhibited the values of 0.005701, 0.005675, 0.00594, and 0.005698 $\Delta u'v'$ units, respectively. Therefore, to comprehensively compare the performance of the four CMFs, the chromaticity distances and the ellipse areas were scaled based

on the chromaticity distance between the standard D65 and D70, and the same trend was obtained, as described in Table 5-1.

Notably, the above-mentioned comparisons between the LCD (Display A) and the reference OLED display were meaningful, because these calculated chromaticity distances could be compared with the MCDM values for the intraobserver variations. Generally, the chromaticity differences between the test OLED displays (i.e., Displays B, C, and D) and the reference OLED display were consistent with the intraobserver variations, whereas the difference between the LCD and the reference display was significantly larger than the intraobserver variation. The ratios of the chromaticity distances of Stimulus 2 to the MCDM value was 2.55, 0.81, 0.81, and 1.33 for Displays A, B, C, and D, with chromaticity distances of 0.0051, 0.0025, 0.0021, 0.0032 and MCDM values of 0.0020, 0.0030, 0.0026, 0.0024, respectively.

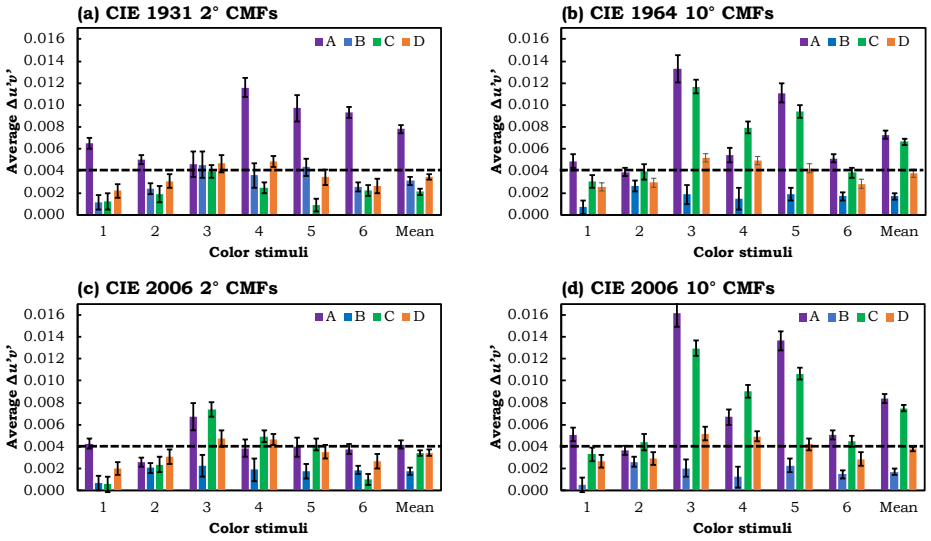

Figure 5-12 Average Δu'v' between chromaticities of stimuli adjusted by 50 observers using four displays and chromaticities of stimuli on reference display calculated using four CMFs. (a) CIE 1931 2° CMFs; (b) CIE 1964 10° CMFs; (c) CIE 2006 2° CMFs; (d) CIE 2006 10° CMFs. (note: dash line labels 1 just-noticeable colour difference, JND. However, it was developed based on only CIE 1931 CMFs and may be inapplicable to other CMFs).

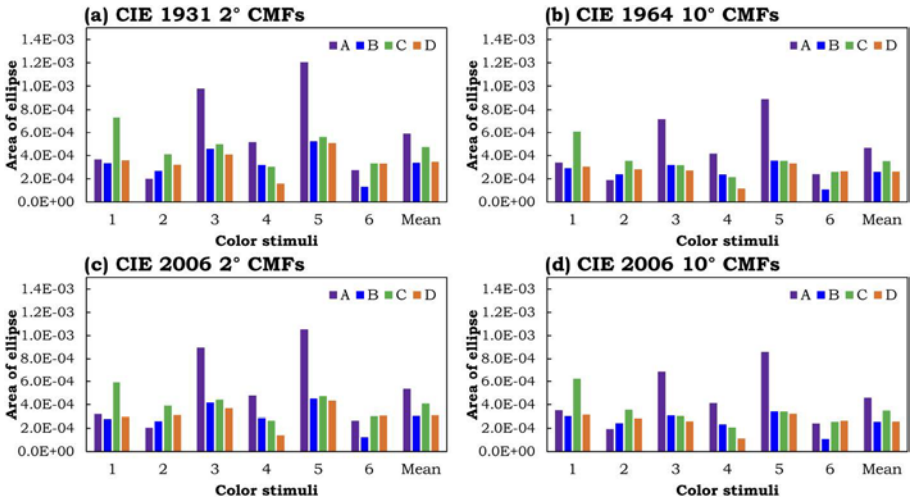

Figure 5-13 Area of 95%-confidence error ellipses for chromaticities of stimuli adjusted by 50 observers using four displays calculated using four CMFs. (a) CIE 1931 2° CMFs; (b) CIE 1964 10° CMFs; (c) CIE 2006 2° CMFs; (d) CIE 2006 10° CMFs.

Table 5-1 Summary of average chromaticity distances and areas of 95%-confidence error ellipses using four CMFs.

	1931 2°	1964 10°	2006 2°	2006 10°
Original				
Chromaticity distance in *u'v'* units ($\times 10^{-3}$)	4.17	4.98	3.29	5.47
Area of ellipses in *u'v'* units ($\times 10^{-4}$)	4.37	3.34	3.89	3.30
Scaled				
Chromaticity distance in *u'v'* units ($\times 10^{-3}$)	7.32	8.77	5.53	9.60
Area of ellipses in *u'v'* units ($\times 10^{-4}$)	7.67	5.89	6.55	5.79

5.4 Quantitative Comparison of Performance of Various CMFs

The comparison between various CMFs for characterizing the colours presented on the test displays and matching the appearance of the reference stimuli based on the colour difference calculated from the tristimulus values were characterized according to the multiple sets of CMFs

considered herein. However, the values could not be directly compared for the various scales. The colour differences between the illuminants on the blackbody locus with fixed and perceived colour differences when characterized based on the four standard CMFs are presented in Figure 5-14. The results revealed the performance ranking of the four CMFs and the corresponding variations in the chromaticity distances. Thus, to quantitatively compare the performance of various CMFs, the chromaticity characterized using various CMFs should be represented in the colour space specified by the same primaries. For instance, transformation of the chromaticities characterized using the CIE 1964 10° CMFs into the CIE 1931 2° CMFs. As the just-noticeable colour difference value with $\Delta u'v' = 0.004$ unit was developed based on the CIE 1931° CMFs, it provided a reference to evaluate the chromaticity distances. Thus, to compare the performance of CMFs, the chromaticity characterized using the remaining CMFs should be represented in the $u'v'$ chromaticity diagram based on the CIE 1931° CMFs.

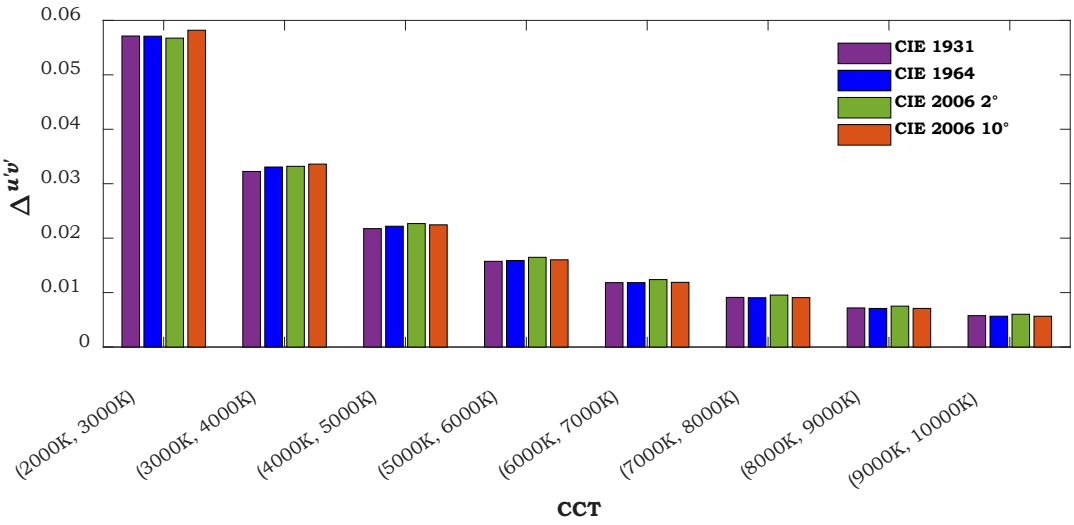

Figure 5-14 Colour differences between adjacent stimuli on blackbody locus based on four standard CMFs

Most existing studies did not consider this issue. The performances of various CMFs were compared following the same method as that used in this study, i.e., the colour difference. In this

case, the distance between the chromaticity diagrams of the reference stimuli and the stimuli adjusted by the observers before scaling were calculated based on the colour differences between D65 and D70 illuminances. As such, three methods can be utilized to compare the performance of various CMFs in the same colour space [150], excluding the method in the current study that scales the chromaticities distances using the distance of a pair of fixed perceived stimuli. In these three methods, the comparison was performed between the chromaticities of the simulated adjustments for a given set of CMFs and the stimuli adjusted by the true observers or simulated for another set of CMFs. For the given set of CMFs, the SPDs of the simulated adjustments $SPD_{simulated}$ can be evaluated using Equation (46). The $SPD_{primary}$ is a three-column matrix containing the SPDs of the three primaries of the display used for colour matching. The digital count values *RGB* used for depicting colours with the same tristimulus values were characterized using the given CMFs, because the reference stimuli can be evaluated using Equation (47), wherein CMF_i denote the given CMF and SPD_{ref} represents the SPDs of the reference stimuli.

$$SPD_{simulated} = RGB \times SPD_{primary} \tag{46}$$

$$RGB = \left(CMF_i \times SPD_{ref}\right) \times \left(CMF_i \times SPD_{primary}\right)^{-1} \tag{47}$$

Following this procedure, the simulated adjustments on the test displays of the four standard CMFs were estimated to match the colour appearance of the 12 stimuli on the reference OLED. The chromaticities of the simulated adjustments for the four standard CMFs along with those adjusted by the observers and characterized using the CIE 1931 2° CMFs are portrayed in Figure 5-15. The performance of the four standard CMFs was quantized using the chromaticity distances between the four simulated adjustments and those by the true observers in the *u'v'* chromaticity diagram

following the CIE 1931 CMFs. The average distances for the four test displays and the six stimuli are portrayed in Figure 5-16, wherein the four subplots indicate the distances of the four standard CMFs. The distances calculated using the method that directly characterizes the chromaticities of the reference stimuli and that adjusted by the observers using the four CMFs are plotted in Figure 5-17. The results revealed the similar performance rankings of the four CMFs, regardless of calculating the chromaticities distances in the same chromaticity diagram. The relationship between the chromaticities distance evaluated using the two methods is depicted in Figure 5-18. Although a positive correlation was observed, the chromaticities distances between the adjustments simulated using the two 10° CMFs were larger than the distances directly characterized using the two sets of CMFs. This finding signified that the performance of the CMFs cannot be quantized for comparison with the distances of reference stimuli and the adjusted results in several chromaticity diagrams. Overall, the comparison yielded effective results.

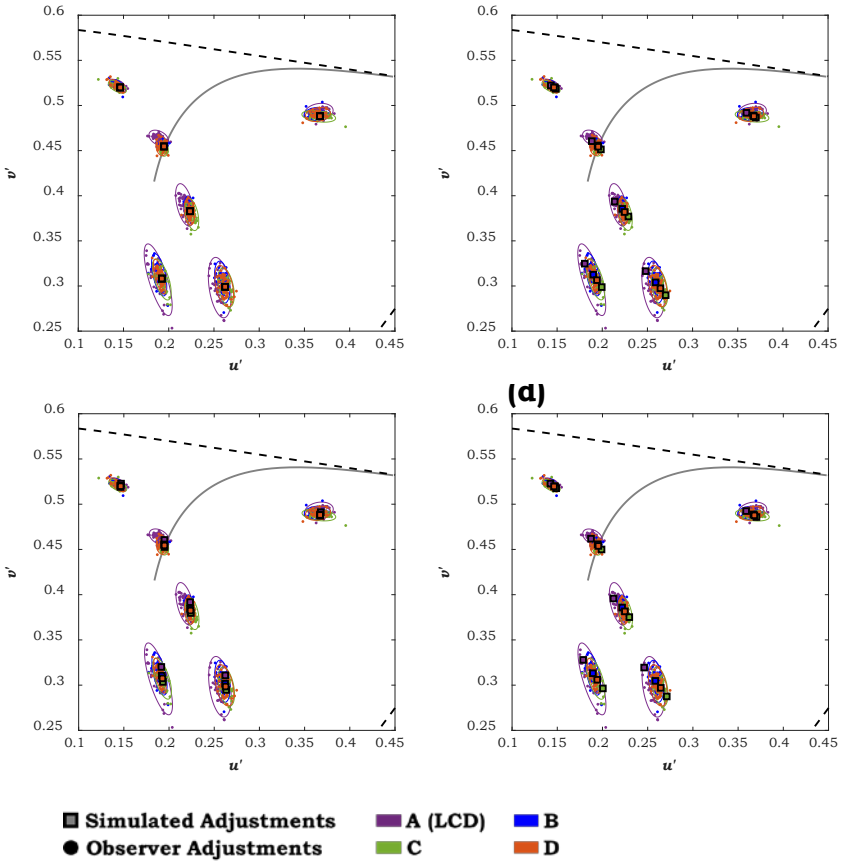

Figure 5-15 Chromaticities with 95%-confidence error ellipses of stimuli adjusted by 50 observers using four displays to match the colour appearance of stimuli on reference display using CIE 1931 2° CMFs, including the chromaticities of the stimuli of simulated adjustments for (a) CIE 1931 2° CMFs; (b) CIE 1964 10° CMFs; (c) CIE 2006 2° CMFs; (d) CIE 2006 10° CMFs.

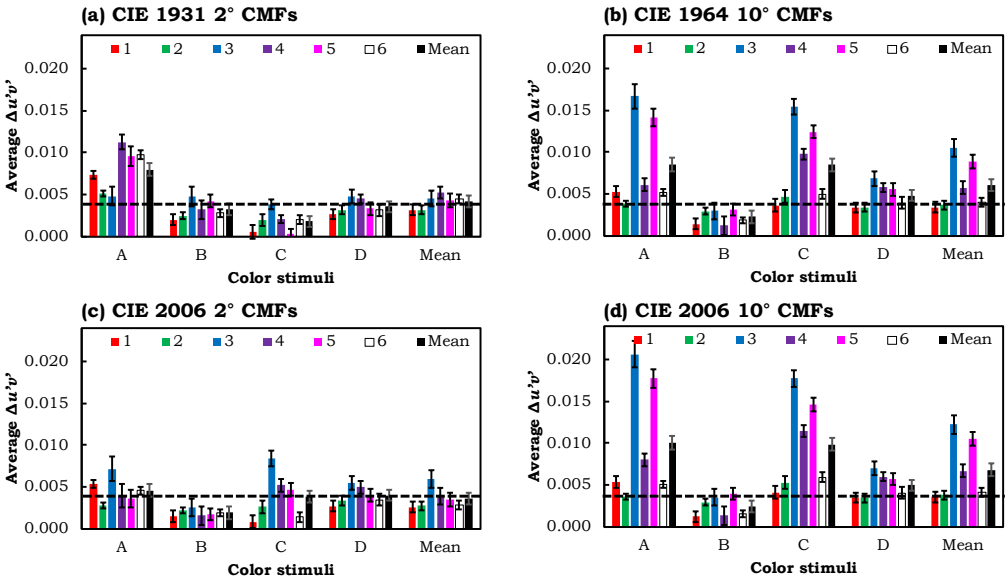

Figure 5-16 Average Δ*u'v'* between chromaticities of stimuli adjusted by 50 observers using four displays and the chromaticities of stimuli of simulated adjustments for (a) CIE 1931 2° CMFs; (b) CIE 1964 10° CMFs; (c) CIE 2006 2° CMFs; (d) CIE 2006 10° CMFs, calculated using the CIE 1931 2° CMFs. (note: dashed-line labels 1 just-noticeable colour difference, JND).

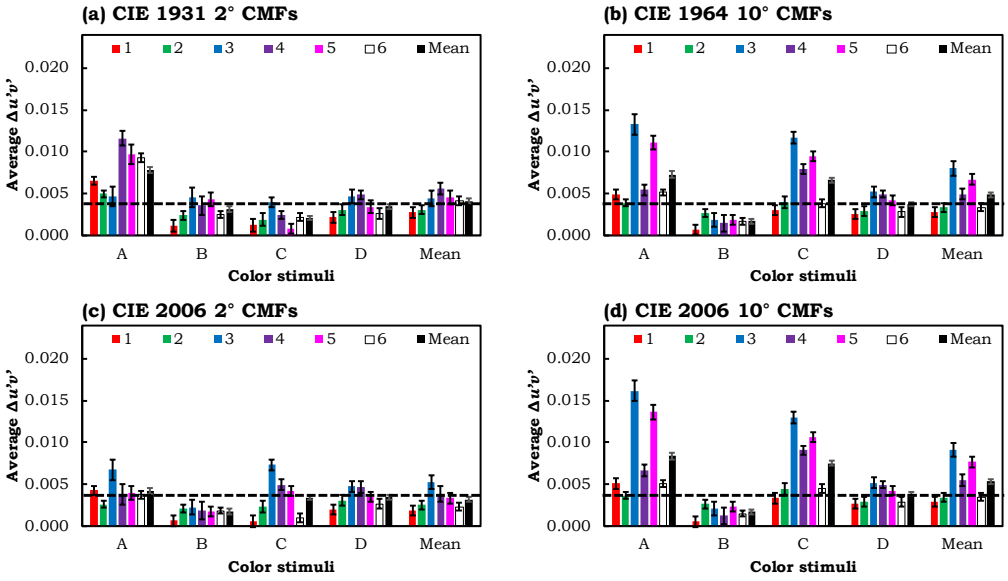

Figure 5-17 Average Δ*u'v'* between chromaticities of stimuli adjusted by 50 observers on four displays and the chromaticities of stimuli presented on reference display calculated using (a) CIE 1931 2° CMFs; (b) CIE 1964 10° CMFs; (c) CIE 2006 2° CMFs; (d) CIE 2006 10° CMFs (note: dashed-line labels 1 just-noticeable colour difference, JND).

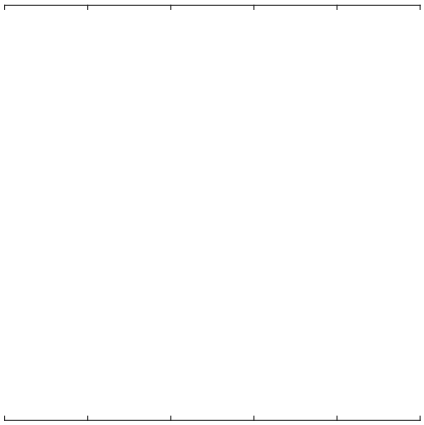

Figure 5-18 Relationship between average Δ*u'v'* between reference stimuli and stimuli adjusted by 50 observers calculated using four CMFs, and average Δ*u'v'* of stimuli of simulated adjustments and stimuli adjusted by 50 observers calculated using CIE 1931 CMFs.

5.5 Conclusions

Recently, OLED displays have garnered increasing scholarly attention, as they can adopt primaries with higher saturation and are capable of generating larger colour gamut compared to traditional LCDs. Despite previous studies demonstrating the possibilities for such types of primaries resulting in severe colour mismatch and observer metamerism, no experiments have been conducted to evaluate the impact of the standard CIE CMFs on the colour match between the LCD and OLED display. This study performed a colour matching experiment with 50 observers, who used four smartphone displays (one LCD with sRGB colour gamut; three OLED displays with P3 colour gamut) for matching the colour appearance of six stimuli produced by another OLED smartphone display. The six stimuli were selected from a chromaticity diagram combining physiological observations. Given that the displays presented a nonuniformity, the centre of 4.77° FOV displays produced the colour stimuli. Considering the CIE 1931 2° CMF to characterize the colour matches, the chromaticities of the stimuli generated by the LCD exhibited a prominent

difference from that generated by the OLED displays. Moreover, the chromaticities exhibited an $-u'+v'$ shift in the CIE 1976 $u'v'$ chromaticity diagram. Accordingly, if the CIE 1931 2° CMFs were used for calibrating the LCD and OLED displays and generating the same chromaticities, the LCD displayed neutral colours and the OLED displays projected a yellowish green colour. Despite the slight difference in the primaries of all OLED displays, their chromaticities were similar. The CIE 2006 2° CMFs could more effectively characterize the colour matches compared with the other three CMFs (CIE 1931 2°, CIE 1964 10°, and CIE 2006 10°), which did not follow the recommendation of adopting 10° CMFs for a FOV beyond 4°. Regardless of adopting the four CMFs, the LCD and OLED displays exhibited a larger difference in terms of the observer metamerism compared to that between OLED displays.

Chapter 6 Study 2-2: Colour Mismatch and Observer Metamerism between LCD and OLED Displays for Larger FOV (≈ 20.2°)

6.1 Motivations

In previous studies, psychophysical experiments were performed to compare and verify the performance of the four standard CMFs (CIE 1931 2°, CIE 1964 10°, CIE 2006 2°, and CIE 2006 10°) [71,135-137,151-158]. In those experiments, the spectral composition of the colour stimuli, in terms of spectral shape (i.e., narrow-band versus broad-band) and peak wavelength, was varied as the critical independent variable. This is because it significantly affects the performance of CMFs, and an optimal CMF should function appropriately for any spectral composition. The colour stimuli with various spectral compositions were produced using several types of devices such as CRT display, LCD, OLED display, LED lamps, projector, broadband lamps with filters, and illuminated colour samples. The observers adjusted the colour appearance of one stimulus to match that of the reference stimulus, and the chromaticities of the two stimuli were considered to compare the performance of various CMFs. However, the performances of the 2° and 10° CMFs were inconsistent. For instance, although 10° CMFs are recommended for stimuli with an FOV > 4°, results in Study 2-1 reported that the performance of 2° CMFs was superior to that of the 10° CMFs. However, Li et al. demonstrated that 10° CMFs provided superior performance [39]. More importantly, no existing study has considered maintaining constant spectral compositions and varying the FOV as an independent variable, which does not clearly relate the poor performance of CMFs to the FOV.

In Study 2-1, we investigated the colour mismatch and observer metamerism between conventional LCD and OLED displays. In total, 50 human observers completed colour matching tasks for two 4.77° colour stimuli, located 5.72° apart and produced by displays. The CIE 2006 2° CMFs exhibited improved performance than the other three CMFs, which did not support the recommendation of the CIE. To further investigate whether this result is attributed to the relatively small FOV, we increased the FOV of the stimuli to 20.2° in this experiment, which is similar to the typical viewing condition of smartphone displays in daily life. Moreover, the two stimuli in this experiment were placed adjacent to each other, thereby enabling an easy match of the colour appearance, which was not observed in Study 2-1 and most past studies.

6.2 Method

6.2.1 Apparatus

For the experimental setup, we designed and constructed a black metal viewing box (50 cm (width) × 28.5 cm (depth) × 28.5 cm (height)), with two 5.5 cm × 10 cm openings on the ceiling and rear panels. The smartphone was attached at each opening with a holder, and to produce a colour stimulus, the smartphone display centre area appeared at the opening. As the viewing window, a 10 cm × 10 cm opening was created on the front panel. Thereafter, we carefully placed a mirror with a 45° tilt angle inside the box to ensure that the observer can simultaneously view the two adjacent stimuli from the two displays through the viewing window. Specifically, the top stimulus was provided from the display above the ceiling panel and could be viewed *via* the reflection in the mirror, whereas the bottom stimulus was projected from the display located behind the rear panel and could be directly observed. The size of the stimuli was 5 cm × 5 cm, with a prominent dividing edge between the two stimuli, which was specially designed for achieving highly accurate colour matching, similar to that in Study 2-1. Notably, we used the carefully placed mirror to

ensure a smooth spectral reflection across the visible spectrum, and the average reflectance factor was approximately 93%.

As the experiment started, the viewing box was placed in front of the observers, and the front panel of the viewing box was situated 28 cm farther from the eye position of the observers. The observers were required to place their chins on a rest and allowed to adjust the chair height such that the two stimuli appear to be the same size for observers (FOV around 20.2°). The viewing box design, experimental setup, and the stimuli viewed by observers are illustrated in Figure 6-1.

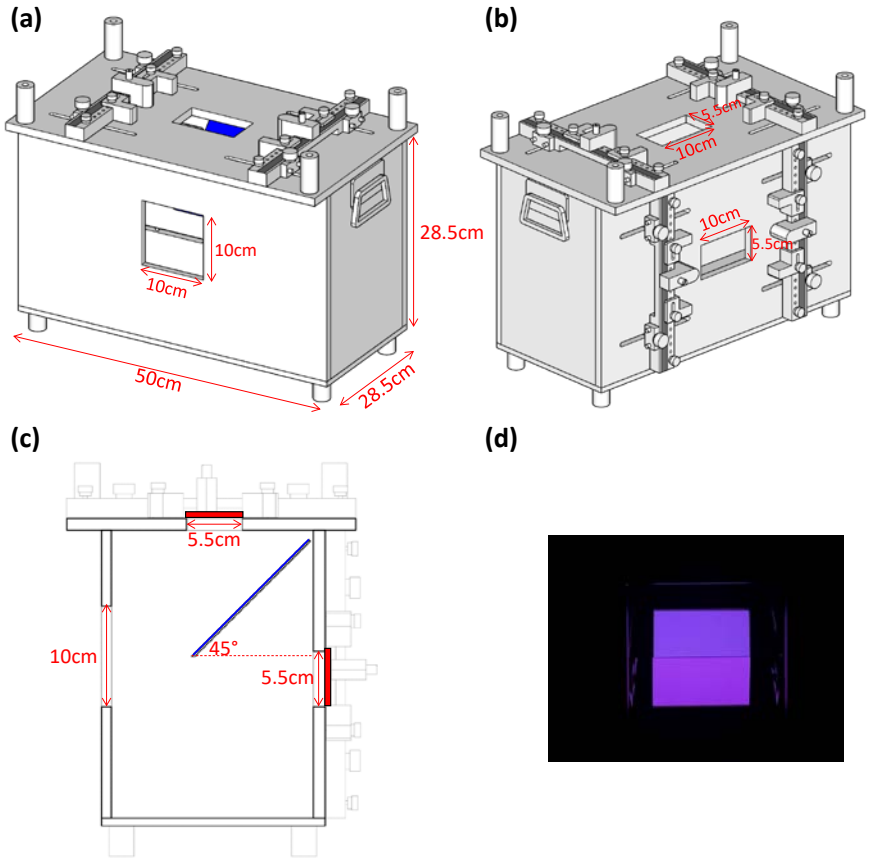

Figure 6-1 Apparatus and experiment setup. (a) Perspective front view of the apparatus; (b) Perspective back view of the apparatus; (c) Cross section view of the apparatus and the positions of the two smart phones; (d) Photograph of the two stimuli viewed from the observer's eye position. (Note: the mirror is shown in blue in (a) and (c)).

6.2.2 Display, Colour stimuli, Display Calibration, Control Program, and Experimental Procedure

Study 2-1 adopted five smartphone displays (one LCD and four OLED displays) for producing the colour stimuli. With careful considerations, we selected four OLED displays from eight OLED displays to ensure that they contained various primaries (in terms of peak wavelengths and SPD shape) and multiple colours. The OLED display with the smallest colour gamut was set as the reference display for comparison between the LCD and OLED displays and that between various OLED displays. In above-mentioned five displays, the gamut and SPDs of the primaries are illustrated in Figure 5-2 and Figure 5-3, respectively.

As the experiment initiated, we affixed the reference display behind the rear panel to generate the bottom stimulus and placed one of the four displays above the ceiling panel to generate the top stimulus, ensuring that the experimenters were capable of conveniently adjusting the displays placed above the ceiling panel. Considering a smooth spectral reflectance distribution on the mirror, we expected that the reflection could reduce the luminance while maintaining the chromaticities, which was verified from the measurements of the SPDs of 20 stimuli generated by one of the four displays in the presence and absence of the mirror. Moreover, to ensure a direct application of the LUTs and the control program in the experiment, the luminance level exhibited by the stimuli was altered from 93 cd/m^2 to 88 cd/m^2 in Study 2-1. Comparatively, the spectroradiometer was used to recalibrate the six stimuli on the reference display and ensure their luminance at 88 cd/m^2. The chromaticities of the six stimuli as well as the display colour gamuts in the MacLeod–Boynton chromaticity diagram (2° FOV) are presented in Figure 5-4. The general locations of the chromaticities exhibited by the six stimuli in the CIE 1976 *u'v'* diagram are presented in Figure 6-2.

The experimental procedure in this chapter remained the same as that in Study 2-1. Briefly, each observer adjusted the colour appearance of the seven stimuli (Stimuli 1 to 6 and two adjustments of Stimuli 2 to evaluate intraobserver variations) generated by the four displays and appearing at the top for matching the colour appearance presented by the relevant reference stimuli from the reference display appearing at the bottom. Both the seven stimuli and the four test displays followed a randomized order.

6.2.3 Observers

The experiment recruited 53 observers (28 males and 25 females) aged between 19 and 38 years (mean = 24.1, std. dev. = 3.28). The Ishihara Color Vision Test was employed to verify if all observers had normal colour visions. Although a number of observers were sourced from Study 2-1, not all the enrolled observers were common between the two experiments.

6.3 Results and Discussions

6.3.1 Verification of Control Program Accuracy

Using the control program, the observers could adjust the chromaticities of stimuli along the *u'*- and *v'*-directions in the CIE 1976 *u'v'* chromaticity diagram to alter their colour appearance. The control program used the LUTs for revising the RGB digital count values. Upon terminating the experiment, we used the RGB combinations adjusted by the observers to reproduce the stimuli on relevant displays and measured the SPDs from the eye positions of the observers. The chromaticities (*u'*,*v'*) exhibited by all the adjusted stimuli derived from the measured SPDs including the chromaticities predicted using the control program are presented in Figure 6-2 (a). The luminance of the adjusted stimuli derived from the measured SPDs is presented in Figure 6-2 (b), with an average value of 87.06 cd/m^2. Considered together, the control program and the calibration in Study 2-1 produced reliable data in this experiment.

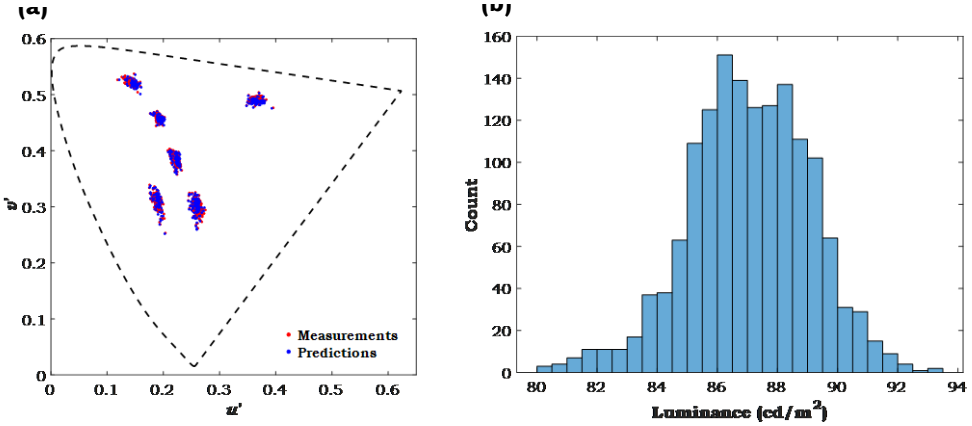

Figure 6-2 Accuracy of control program in terms of chromaticities and luminance. (a) Chromaticities of adjusted stimuli derived from measured SPDs and predictions using control program in CIE 1976 *u'v'* chromaticity diagram. (b) Histogram of luminance of adjusted stimuli derived from measured SPDs; average: 87.06 cd/m^2.

6.3.2 Intra- and Interobserver Variations

The MCDM in the CIE 1976 *u'v'* chromaticity diagram served for characterizing the intraobserver and interobserver variations, as described in Study 2-1. Each observer used the four test displays to perform repeated matches of stimulus, with the chromaticities and 95%-confidence error ellipses displayed in Figure 6-3. The ellipses covered adequately overlapped sizes and orientations. The histograms of the MCDM values for the four displays are plotted in Figure 6-4. The average MCDM values for Displays A, B, C, and D were 0.0023, 0.0023, 0.0020, and 0.0021, respectively, which were smaller than 0.004 units of *u'v'* (1 JND). In particular, these values were even smaller than those in Study 2-1, because the two stimuli could become adjacent to each other in the experiment because of the new apparatus. For the characterization of the interobserver variations, the MCDM values ranged from 0.0022–0.0095, with an average of 0.0047, also smaller than those in Study 2-1. Therefore, the experiment results exhibited strong reliability.

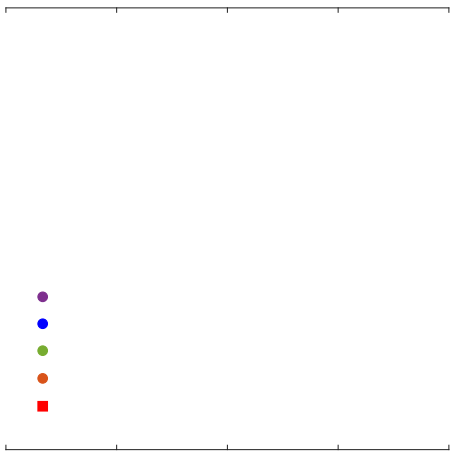

Figure 6-3 Chromaticities including 95%-confidence error ellipses of the repeated matches performed by each observer for Stimulus 2 using four test displays.

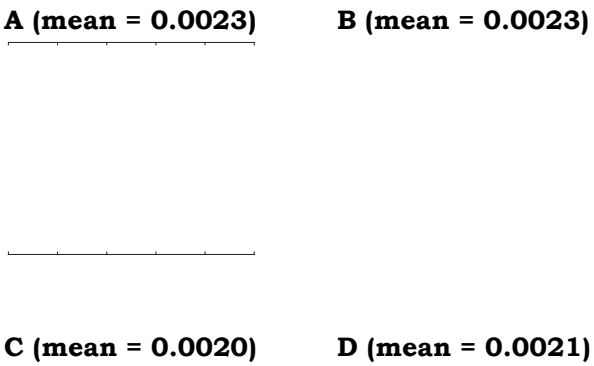

Figure 6-4 Histogram of MCDM values of intraobserver variations for each test display.

6.3.3 Performance of Four CMFs in Characterizing Colour Matches

All observers used the four displays to adjust the chromaticities of the stimuli. The four standard CMFs used in calculating the related chromaticities and the 95%-confidence error ellipses, displayed in the CIE 1976 *u'v'* chromaticity diagram, are presented in Figure 6-5. The average chromaticities of the adjusted stimuli (centre of each ellipse in Figure 6-5) including those of the relevant reference stimuli obtained through the four CMFs were shown in Figure 6-6. The chromaticity differences $\Delta u'v'$ calculated for the four displays are summarized in Figure 6-7 and Table 6-1. Overall, the chromaticity and ellipse distributions observed in this study herein were similar to those in Study 2-1, as depicted in Figure 6-5.

The colour matching experiments preferred a smaller calculated $\Delta u'v'$ between the reference stimuli and the stimuli adjusted by observers, because an optimal set of CMFs should ensure zero value of $\Delta u'v'$ for colour stimuli with matched colour appearance. Generally, the average $\Delta u'v'$ calculated using the CIE 2006 2°, CIE 1964 10°, and CIE 1931 2° CMFs were similar (~0.004) but smaller than that for the CIE 2006 10° CMFs (0.005). The $\Delta u'v'$ values calculated using the four CMFs in the experiment as well as those obtained in Study 2-1 (FOV of 20.2° *versus* 4.8°) are comparatively presented in Figure 6-8. Generally, the data points were scattered around the diagonal line, implying the similarity between the results both experiments. In case of Display D, which includes primaries most representative to those of the reference display, the four data points were under the diagonal line, as depicted in Figure 6-8 (b), i.e., the adoption of four CMFs for a larger FOV created small differences in the chromaticity of stimuli with matched colour appearance. Specific to Display A, the CIE 2006 2° CMFs created larger differences in the chromaticity from ~0.004 to ~0.008 units for larger FOV, whereas the two 10° CMFs resulted in smaller differences in chromaticity corresponding to the two FOVs (near the diagonal line).

Specific to the three OLED displays, namely, Displays B, C and D, the CIE 2006 2° CMFs delivered the best average performance for all six colour stimuli. Despite the increase in the stimuli sizes in the experiment, the results did not support the application of 10° CMFs to characterize the stimuli colour with an FOV > 4°.

In all cases, Display A (LCD) possessed the largest average of $\Delta u'v'$ values in which CMFs were used, possibly because its primaries presented an evident difference from the reference display. Comparatively, under the same situations, Display D possessed the smallest average $\Delta u'v'$ values that were always less than 0.004 (1 JND) in all cases, because its primaries were extremely similar to those of the reference display (both Display 4 and the reference display are produced by the same manufacturer). For the four displays, the six stimuli calculated by the CIE 1931 2° CMFs produced average $\Delta u'v'$ values of 0.0066, 0.0040, 0.0023, and 0.0024, which were 2.87, 1.74, 1.15, and 1.14 times of the MCDM values, respectively. The intraobserver variations presented in Figure 6-4 demonstrates the larger significance of the comparisons. Therefore, the primary sets affected the performance obtained using the CMFs.

With respect to the reference display, the chromaticities of Display A (LCD) presented the $-u'+v'$ shift, as depicted in Figure 6-6. The result implies that the use of the CIE 1931 2° CMFs for calibrating the colour stimuli on Display A and the reference display to ensure the same chromaticities within them would yield severe colour mismatches. In particular, a stimulus appearing neutral on an LCD may appear yellowish green on an OLED display, whereas a stimulus appearing neutral on an OLED display may appear pinkish on an LCD. The colour mismatch and the colour appearance were recorded in the present observations. In addition, the variations of CMFs failed to diminish the $\Delta u'v'$ values of the six colour stimuli simultaneously. The reduced $\Delta u'v'$ values for Stimuli 2 (green), 4 (purple), and 6 (neutral) were typically accompanied with

increased Δ*u'v'* values for Stimuli 1 (red), 3 (blue), and 5 (reddish purple). Thus, the variation in the performance of CMFs relied on the colour stimuli. In case of using CIE 1931 2° CMFs, which is a common CMF used in calibrating and characterizing displays, Display A presented the largest chromaticity differences Δ*u'v'*, all of which were larger than 0.004 (1 JND).

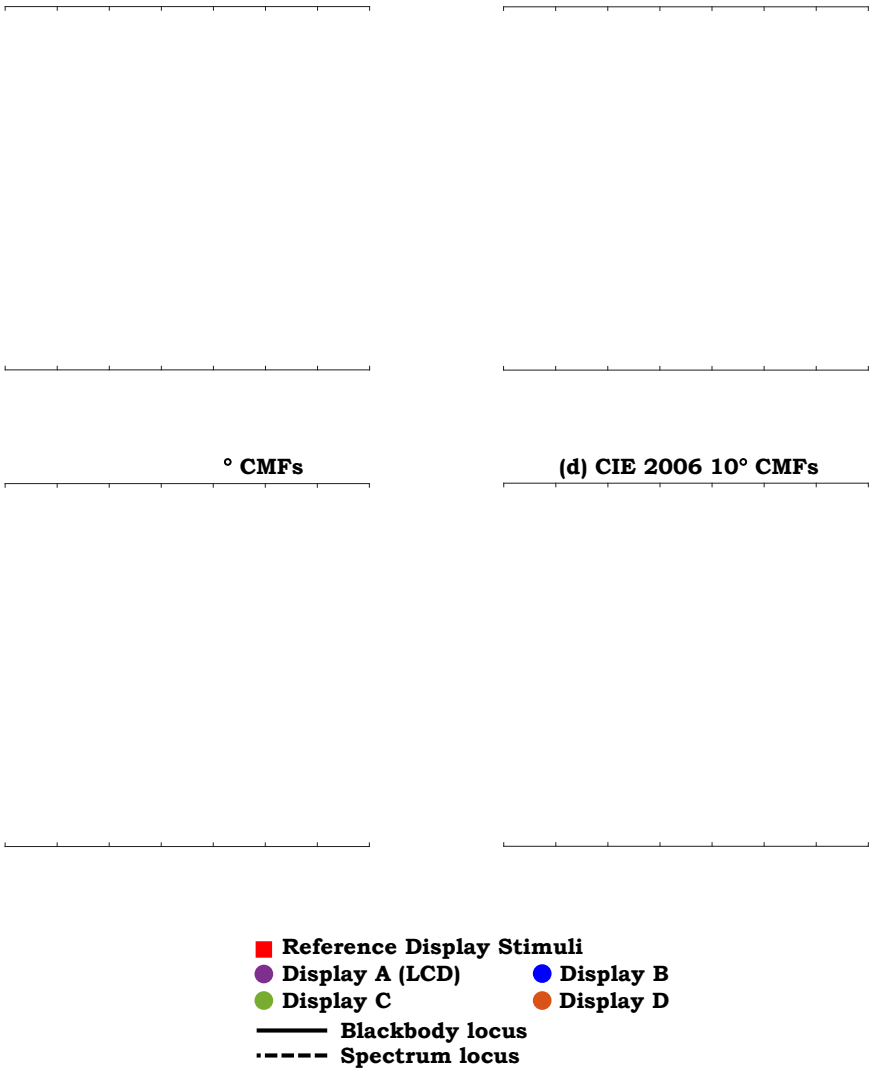

Figure 6-5 Chromaticities of stimuli adjusted by 53 observers using four displays to match colour appearance of reference stimuli on reference display, including fitted 95%-confidence error ellipses, calculated using four CMFs. (a) CIE 1931 2° CMFs; (b) CIE 1964 10°; (c) CIE 2006 2° CMFs; (d) CIE 2006 10° CMFs. (Note: numbers in the figures represent Stimuli 1 to 6).

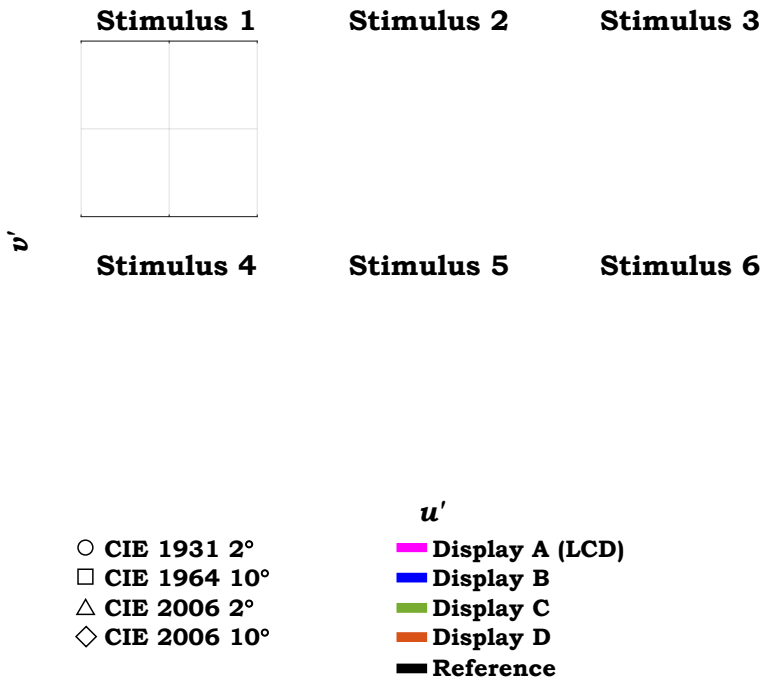

Figure 6-6 Average chromaticities of stimuli adjusted by 53 observers using four displays and corresponding reference stimuli on reference display calculated using four CMFs. (Note: for illustration purposes, the axis ranges were varied, but each grid corresponds to 0.01 unit in *u'* and *v'*). (Note: blackbody locus exhibited with Stimulus 6 was plotted using CIE 1931 2° CMFs).

Table 6-1 Average difference Δ*u'v'* between average chromaticities adjusted by observers of six colour stimuli using each display and chromaticities of reference stimuli on reference display calculated using four CMFs.

	Display A	Display B	Display C	Display D	Average
CIE 1931 2°	0.00660	0.00403	0.00230	0.00243	0.00384
CIE 1964 10°	0.00802	0.00159	0.00461	0.00229	0.00413
CIE 2006 2°	0.00738	0.00241	0.00222	0.00234	0.00359
CIE 2006 10°	0.00913	0.00172	0.00537	0.00226	0.00462

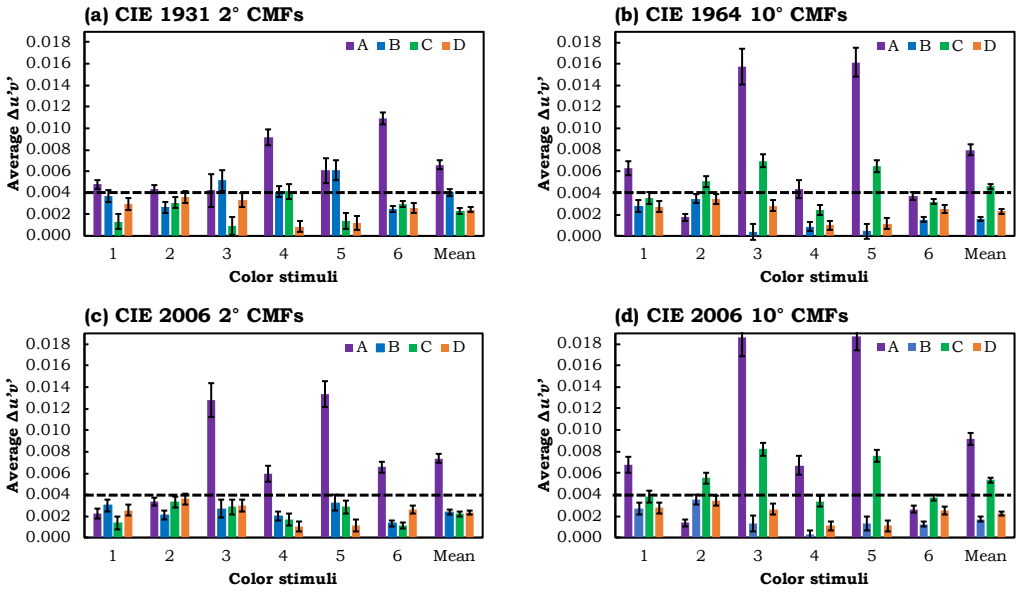

Figure 6-7 Chromaticity differences Δ*u'v'* between average chromaticities of stimuli adjusted by 53 observers and chromaticities of reference stimuli on reference display calculated using four CMFs. (a) CIE 1931 2° CMFs; (b) CIE 1964 10° CMFs; (c) CIE 2006 2° CMFs; (d) CIE 2006 10° CMFs. (Note: dashed-line labels 1 just-noticeable colour difference, 1 JND. However, it was developed only based on CIE 1931 2° CMFs and may not be applicable to remaining three CMFs).

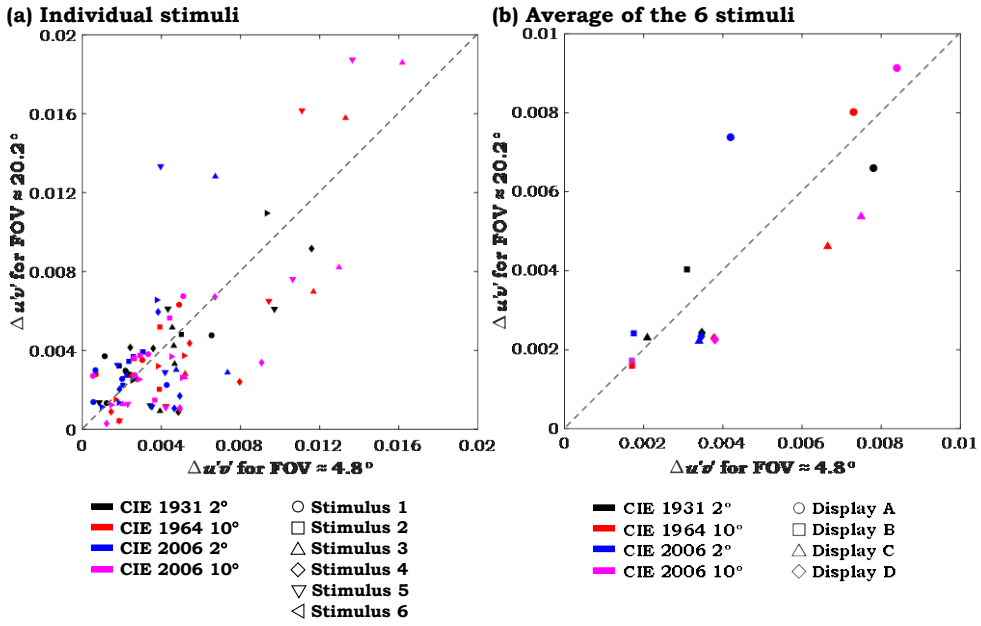

Figure 6-8 Scatter plots of Δ*u'v'* values calculated using four CMFs between this experiment with an FOV ≈ 20.2° and part I with an FOV ≈ 4.8°. (a) Individual stimuli (6 stimuli × 4 displays × 4 CMFs = 96 data points); (b) Average of six stimuli for each display (4 displays × 4 CMFs = 16 data points).

6.3.4 Performance of Four CMFs in Characterizing Observer Metamerism

The 95%-confidence error ellipses of various sizes are presented in Figure 6-5, which were accounted for characterizing the degrees of observer metamerism. For a more clear comparison, the chromaticities of the stimuli on the reference display were transposed to the origin. The 95%-confidence error ellipses are plotted in Figure 6-9 and the ellipse areas are indicated in Figure 6-10.

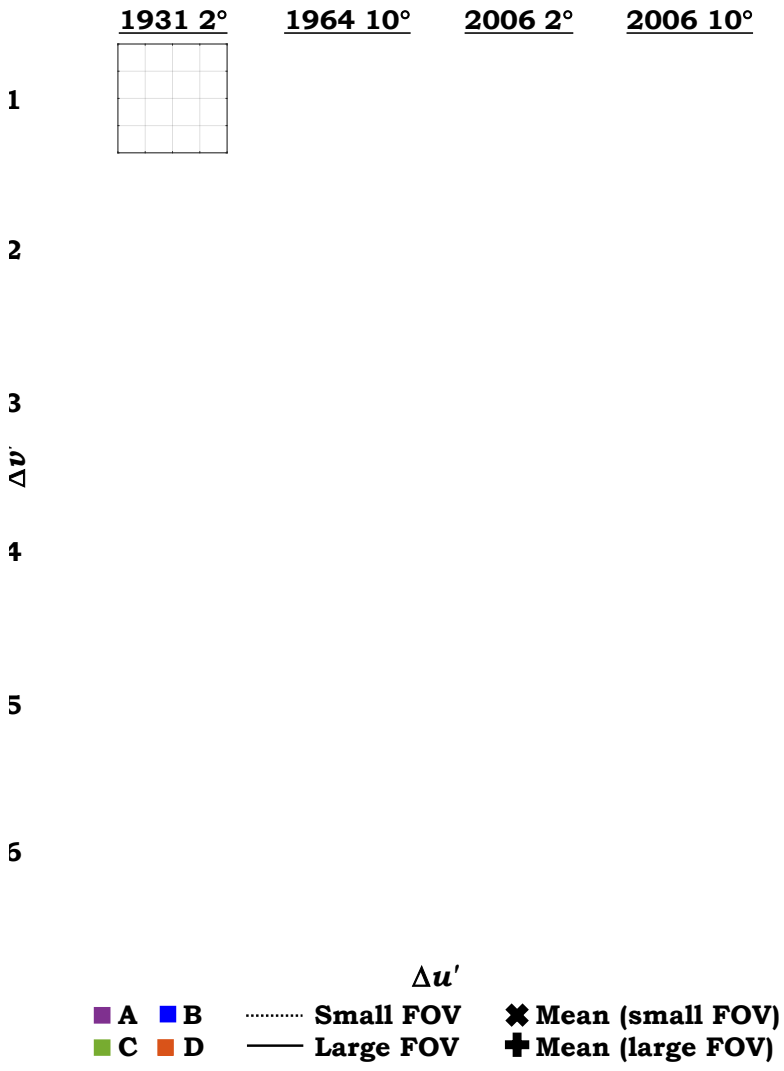

Figure 6-9 Average chromaticities of stimuli adjusted by 53 observers in this experiment and 50 observers in part I (ellipse centres) and fitted 95%-confidence error ellipses with respect to chromaticities of the corresponding reference stimuli on reference display, plotted using four CMFs. (Note: blackbody loci calculated using four CMFs are plotted with Stimulus 6).

The four CMFs presented similar ellipse sizes and orientations. Displays B, C, and D possessed similar degrees of observer metamerism, which were much smaller in relation to Display A, especially for Stimuli 3 (blue), 4 (purple), and 5 (reddish purple). We compared the ellipse areas derived from the experiment with those depicted in Figure 5-12 in Study 2-1. The data points were much more proximate to the diagonal line with respect to those portrayed in Figure 6-8, revealing that the observer metamerism degree was less affected by the FOV. Accordingly, the two 10° CMFs produced smaller ellipse areas, indicating their enhanced predictive ability over observer variations.

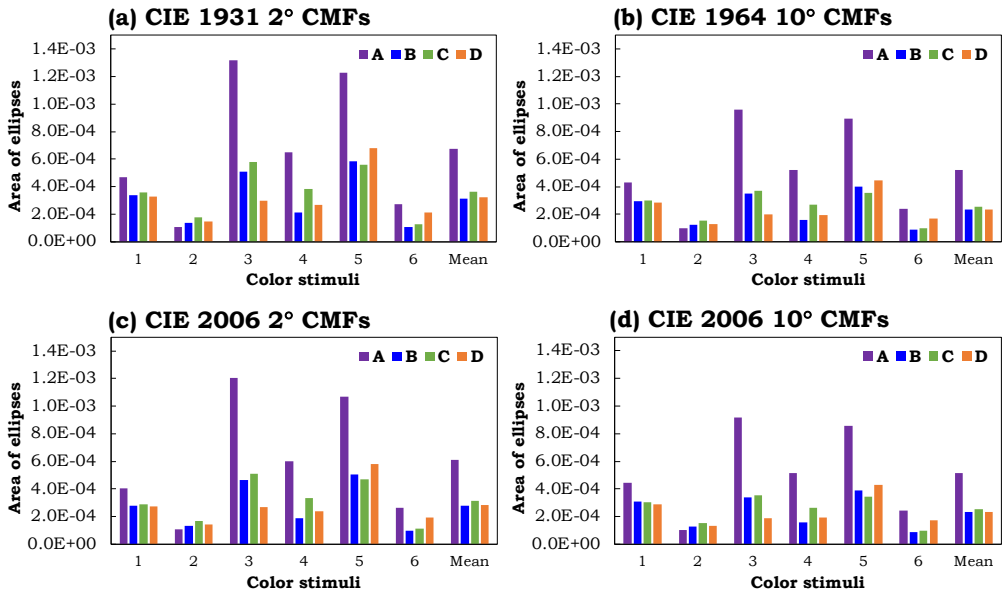

Figure 6-10 Areas of fitted 95%-confidence error ellipses of stimuli adjusted by 53 observers calculated using four CMFs, as depicted in Fig. 10. (a) CIE 1931 2° CMFs; (b) CIE 1964 10° CMFs; (c) CIE 2006 2° CMFs; (d) CIE 2006 10° CMFs.

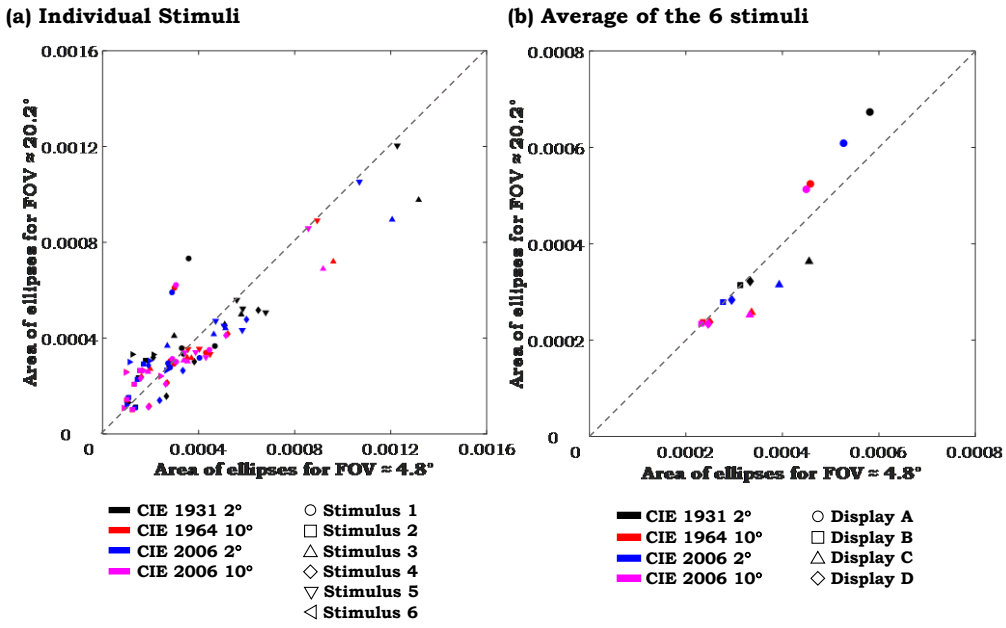

Figure 6-11 Scatter plots of areas of fitted 95%-confidence error ellipses of stimuli adjusted by 53 observers using four CMFs between this experiment with an FOV ≈ 20.2° and part I with FOV ≈ 4.8°. (a) Individual stimuli (6 stimuli × 4 displays × 4 CMFs = 96 data points); (b) Average of six stimuli for each display (4 displays × 4 CMFs = 16 data points).

6.4 Conclusions

In this study, 53 observers used four smartphone displays (one LCDs with sRGB colour gamut; three OLED displays with P3 colour gamuts) along with an OLED reference display to match the colour appearance of six stimuli selected from a chromaticity diagram combining physiology. Relative to the experiment in Study 2-1, we designed and constructed a new apparatus that could project the colour stimuli generated by the test displays and the reference display adjacent to each other to facilitate the observers to more easily perform the colour match. In addition, the FOV was increased from 4.77° to 20.2° to render the display size with the conventional viewing condition. The MCDM values calculated to characterize the inter- and intraobserver variations were smaller than those in Study 2-1.

The LCD exhibited prominent differences in comparison to the reference OLED display. In general, the four CMFs cannot be used to accurately characterize the colour matches between the above-mentioned two types of displays. The LCD manifested observer metamerism to a larger degree, indicating that colour primaries could remarkably influence the perceived colour matches as well as the observer metamerism in terms of the spectral shape and peak wavelength.

Compared to the results of Study 2-1, the four CMFs produced similar performance in characterizing the colour matches and observer metamerism. To characterize the colour matches using the CIE 1931 2° CMFs, the LCD produced remarkably variant stimuli chromaticities with respect to the reference OLED display, and the chromaticities exhibited an $-u'+v'$ direction shift in the CIE 1976 $u'v'$ chromaticity diagram. If the CIE 1931 2° CMFs were used for calibrating the LCD and OLED displays for producing stimuli that possessed the same chromaticities, the stimuli appearing neutral on the LCD would appear yellowish green on the OLED display. Despite the 20.2° FOV of the stimuli in the experiment, the CIE 2006 2° CMFs exhibited the best performance for all the displays compared to the remaining three sets of CMFs and considering the average chromaticity difference between stimuli with matched colour appearance. Nonetheless, the present findings do not suggest the adoption of 10° for stimuli with an FOV > 4°. Overall, the performance of the CMFs varied with the colour stimuli.

Chapter 7 Study 3: Correction of the Colour Mismatch between LCD and OLED Displays

7.1 Motivations

In Study 2, colour matching experiments were conducted between LCD and OLED displays as well as between several OLED displays under small (4.77°) and large FOV (20.2°), while maintaining other experimental variables constant. In these experiments, large chromaticity differences were observed between the colours matched by human observers in the 1976 *u'v'* chromaticity diagram characterized based on the four CIE standard observers between LCD and OLED displays. The results suggested the significance of the primary colours in terms of the peak wavelengths and spectral shapes for perceived colour matches and observer metamerism. The use of the most widely used CMFs for display calibration, CIE 1931 2° CMFs, caused the most serious colour mismatches and observer metamerism between LCD and OLED displays.

In this study, a colour matching experiment was conducted. The data collected from the experiment were used to correct the colour mismatch between LCD and OLED displays when the displays were characterized using the CIE 1931 2° CMFs. In the experiment, a greater number of colour stimuli covering a large area of the chromaticity diagram were adopted as the test colour stimuli. Similar to previous experiments, the participating observers performed the task of adjusting chromaticities on LCD or OLED displays to match the colour appearances on a reference OLED display. The LCD used in the study included different primary colours—both in shape and peak wavelength on the SPDs—compared to that used in Study 2.

7.2 Method

7.2.1 Apparatus

A viewing booth with dimensions of 60 cm (width) × 60 cm (depth) × 60 cm (height) was constructed for the experiment. The interiors of the booth were painted using Munsell N7 spectrally neutral paint. The two phone holders were placed on the bottom of the booth, with two smartphones placed on the holders adjacent to each other. The angle of the holders was adjusted to ensure that the displays are tilted at an angle of 60º with the horizontal plane. The observers were asked to place their chin on a rest and adjust the height of the chair to ensure that the viewing angle is perpendicular to the screen. The two displays occupied an FOV of ~20.2° to the observer. The experiment setup is illustrated in Figure 7-1.

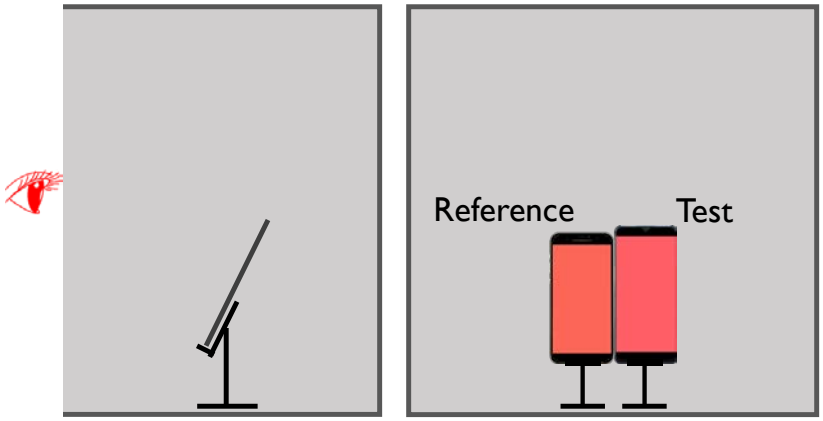

Figure 7-1. Schematic illustration of experimental setup.

7.2.2 Displays and Colour Stimuli

Four smartphones were used in this experiment, i.e., one LCD and three OLED displays. The size of the displays of these smartphones was around 70 mm (width) × 140 mm (height) with small variations. The gamuts and the chromaticities of the white points for these displays are comparatively presented with the sRGB and P3 standard gamuts in Figure 7-2. The SPDs of the

primaries of these displays are plotted in Figure 7-3. As earlier, an OLED display was set as the reference display to present the colour stimuli to the observers for comparison of the colour appearance of the stimuli on the LCD (Display A) as well as on the two remaining OLED displays (Displays B and C).

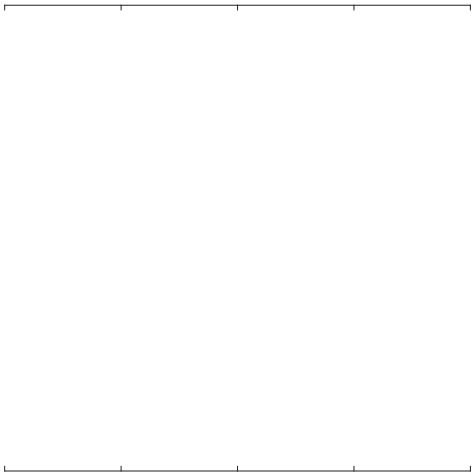

Figure 7-2 Colour gamuts and white points of five displays derived using CIE 1931 CMFs, including standard sRGB and P3 colour gamuts.

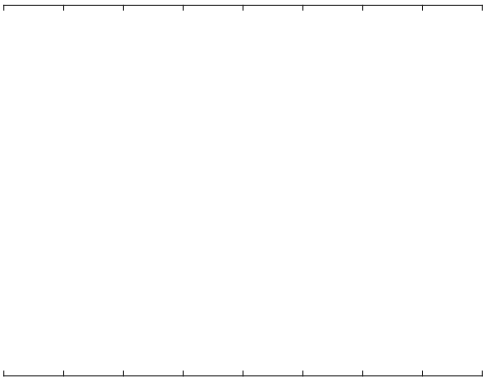

Figure 7-3 Relative SPDs of primaries of four displays.

In total, 12 colour stimuli were carefully selected for presentation on the reference display in the CIE1976 *u'v'* chromaticity diagram, which was uniformly distributed in the P3 standard gamut, as

depicted in Figure 7-4. The coordinates of Stimuli 1 to 3 segment the line connecting D65 to the red primary into four equal components. Stimulus 4 corresponds to the coordinates dividing the line connecting D65 with the intersection of the line extended from the red primary to D65 and that of the green and blue primaries into two equal segments. The coordinates of Stimulus 5 divided the line of D65 to green primary into two equal segments. The coordinates of Stimuli 6 and 7 divided the line connecting D65 to the intersection of the line extended from the green primary to D65 and that of the red and blue primaries into three equal segments. The coordinates of Stimuli 8, 9, and 10 included three stimuli with higher *v'* values than the four stimuli dividing the line connecting D65 to the blue primary into five equal segments. The coordinates of Stimuli 11 divided the line connecting D65 to the intersection of the line extended from blue primary to D65 and that of the red and green primaries into two equal segments. Stimulus 12 was selected as a neutral colour with the chromaticity coordinate evaluated from the CIE D65 illuminant.

The luminance of the 12 stimuli was set at 78.87 cd/m^2 according to the maximum luminance that can be achieved by the displays. The definition of the luminance of colour stimuli followed two principles: to ensure all the stimuli can be presented on the displays in the target chromaticities and the observers can broadly adjust these chromaticities. According to the colour matching experiments conducted in Study 2, the bluish stimuli (Stimuli 3 and 5) were adjusted up to 0.042 units in the direction of $-v'$. Consequently, the $\Delta v'$ of lower boundaries of the gamuts at the defined luminance and the coordinate of the most bluish stimulus (Stimuli 10) should be at least larger than 0.042 unit in the CIE1976 *u'v'* chromaticity diagram.

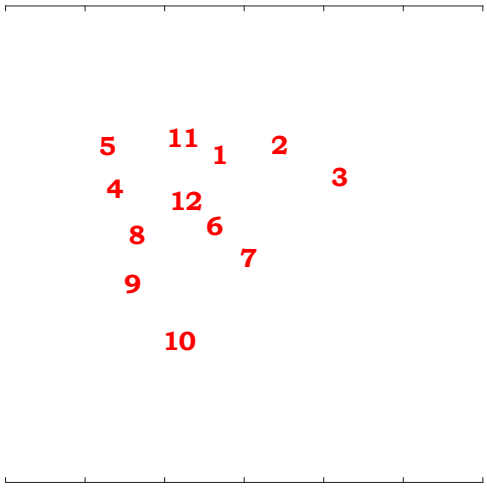

Figure 7-4 Target chromaticities of stimuli selected based on P3 standard gamut in CIE1976 *u'v'* chromaticity diagram.

7.2.3 Display Calibration and Control Program

A calibrated JETI Specbos 1811 spectroradiometer served for calibrating 12 stimuli on the reference display.

Furthermore, we developed a customized control program for the three test displays used in matching the colour appearance of the stimuli presented on the reference display. This customized control program enabled the observers to adjust the colour appearance of the stimulus by controlling its chromaticities along the *u'*- and *v'*-directions in the CIE 1976 *u'v'* chromaticity diagram, with + *u'* for red, –*u'* for green, +*v'* for yellow, and –*v'* for blue, which is similar to the method used in Study 2. All the chromaticity coordinates of the colours in the gamut at the luminance of 78.87 cd/m^2 with a step of 0.0015 along the *u'*- and *v'*-directions were recorded for the three test displays, as depicted in Figure 7-5. The chromaticities were specified as the target values for the calibration of the displays. To present the colour stimuli with the target chromaticities, the corresponding digital count values were calculated for each test display.

As the colour management profile has been integrated into the smartphones to correct the crosstalk effect between channels, the problem of channel dependency was alleviated to a certain extent. In case of these displays, the accuracy of the GOG model predictions was verified using the 41 combinations of RGB listed in Table 4-1. The spectroradiometer was used to measure the SPDs of the three channels in 17 digital levels, black, and white as the training data to construct the GOG model. Moreover, the stimuli generated using the 41 digital counts values of RGB combinations were regarded as the test data. The colours on each display were measured by placing the display in which they would be placed in the experiment. The lens of the spectroradiometer was placed at the observer's eye position and enabled the light to display vertical incidence. Following the calculation procedure of the GOG model, the tristimulus values of the 41 test colours were predicted for each display. The chromaticities (*u'*,*v'*) of the model predictions and measurements are presented in Figure 7-5. The average colour differences for the test colours in the CIELAB colour space were 1.14, 3.72, and 1.73 for Displays A, B, and C, respectively. Although the colour differences were larger than one unit of colour difference ΔE_{ab} in the CIELAB colour space, which were larger than the errors of the control program in Study 2, the control program was developed based on the inverse algorithm of the GOG model, because the adjusted chromaticities followed the measured values instead of the target values.

For the three test displays, 34874, 36904, and 33030 colour patches were generated based on the calculated digital count values and transformed into P3 standard colour space through an ICC profile. During the experiment, if the observer adjusted the colour appearance of the stimulus by controlling its chromaticities, the control program fetched the storage of the smartphone and presented the corresponding colour patch on the full-screen display.

Figure 7-5 Target stimuli in gamut of displays at luminance of 78.87 cd/m^2 with a step of 0.0015 along *u'*- and *v'*-directions.

7.2.4 Observers

Eight observers (3 females and 5 males) between 19 and 33 years of age (mean = 22, std. dev. = 2.26) participated in this experiment. All the observers had normal colour vision, as tested with the Ishihara Color Vision Test.

7.2.5 Experimental Procedure

The procedure of the current colour matching experiment is similar to that described in Study 2. The experiment was performed in a dark environment. After being escorted to the viewing booth and instructed on their tasks, the observers adjusted the colour appearance of a stimulus to ensure that the colour appearance of the two stimuli appear the same. In all experimental cases, the stimulus on the left-hand side was produced by the reference display, whereas that on the right-hand side was produced by one of the three test displays. Excluding Display C, the observer enacted 12 adjustments for all test displays in a random order. For Display C, Stimulus 11 was adjusted twice to evaluate the intraobserver variations. Moreover, the order of the three test displays was randomized for each observer. In total, each observer made 37 adjustments, spanning

a duration of approximately one hour. To ensure stabilization, all the displays were warmed up for at least 30 min prior to the experiment.

During the experiment, the device holders were affixed in the booth to ensure the constant location and angle of the smartphone displays in case of switching between multiple test displays during the experiment.

7.3 Results

7.3.1 Verification of Control Program Accuracy

The digital count values of colour patches used in the control program for the test displays were generated through the inverse algorithm of the GOG model. If the colour appearance of the two displays matched during the experiment, the target chromaticities marked for the currently displayed colour patch were recorded. The measured chromaticities of the patches and the corresponding recorded target chromaticities are presented in Figure 7-6 (a), with the colour difference $\Delta u'v'$ averaged at 0.0061. The histogram of various luminance of the adjusted stimuli calculated from the measured SPDs is plotted in Figure 7-6 (b), wherein the average luminance was 73.62 cd/m^2.

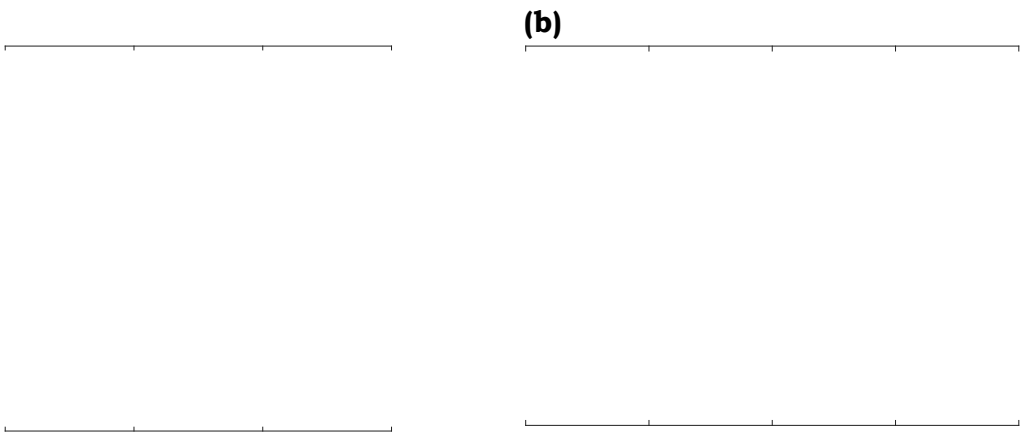

Figure 7-6 Accuracy of control program in terms of chromaticities and luminance. (a) Chromaticities of adjusted stimuli derived from measured SPDs and predictions using control program in CIE 1976 *u'v'* chromaticity diagram; (b) Histogram of luminance of adjusted stimuli derived from measured SPDs.

7.3.2 Intra- and Interobserver Variations

The intraobserver variation for each observer was characterized using the Euclidean distance of the coordinates of the two matches for Stimulus 11 on Display C in the CIE 1976 *u'v'* chromaticity diagram. The variations for the eight observers ranged from 0.0002 to 0.0058, with an average value equal to 0.0019 that is less than 0.004 units of $\Delta u'v'$ (1 JND). The chromaticities, along with the 95%-confidence error ellipses, of the two matches performed by each observer for Stimulus 11 using Display C are presented in Figure 7-7.

The interobserver variation for each display and each colour stimulus was characterized using the MCDM calculated based on the chromaticity distances in the CIE 1976 *u'v'* chromaticity diagram, which represented the average distances between the chromaticities of the stimulus matched by the eight observers and the average chromaticities of the eight matches, as demonstrated in Figure 7-8. Similar to the results of Study 2, the bluish stimuli (Stimuli 6 to 10) caused larger levels of

interobserver variations. Specifically, this phenomenon was observed between the LCD and reference OLED displays.

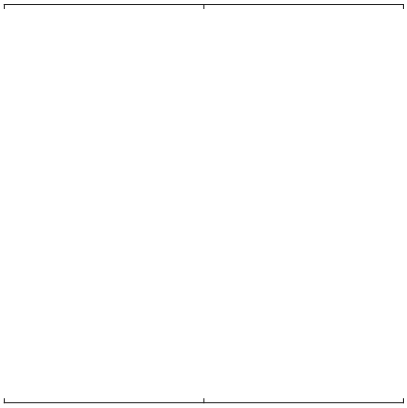

Figure 7-7 Chromaticities along with 95%-confidence error ellipses of two matches performed by each observer for Stimulus 11 using Display 3.

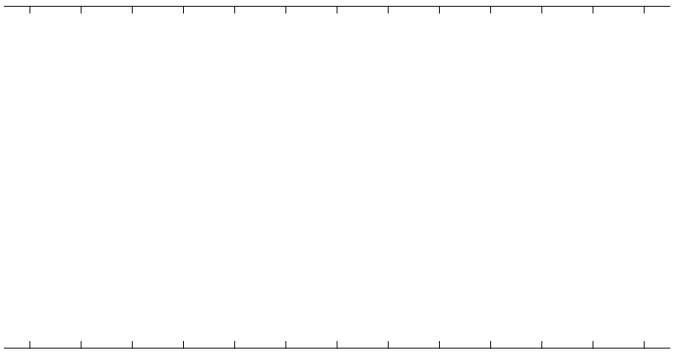

Figure 7-8 Histogram of MCDM values of interobserver variations for each display and each colour stimulus.

7.3.3 Characterization of Colour Matching Results using Four CMFs

The chromaticities of the stimuli adjusted by the observers on the three displays based on the four standard CMFs, including the 95%-confidence error ellipses, are depicted in Figure 7-9. Similar to the results in Study 2, most ellipses exhibited similar orientations if various CMFs were used. The shifts of the average chromaticities adjusted by the observers with the three test displays by shifting the chromaticities of the reference stimuli to the origin are presented in Figure 7-10. The chromaticities distances between reference stimuli and the average chromaticities adjusted by observers for the three displays and the 12 stimuli are depicted in Figure 7-11. The areas of 95%-confidence error ellipses of the adjusted chromaticities were demonstrated in Figure 7-12. The values of the distances and the ellipses areas are summarized in Table 7-1. For the majority of the colour stimuli, Display A (LCD) exhibited the largest chromaticities distances and ellipses areas, especially for the bluish stimuli (Stimulus 6 to 10), compared to the remaining two OLED displays. A prominent colour mismatch was observed between Display A and the reference display according to the chromaticity distances of the 12 stimuli, averaged at 0.00882, which were all greater than 0.004 units of $\Delta u'v'$ (i.e., 1 JND). Upon evaluating using the CIE 1931 2° CMFs, the average distances of the stimuli for Displays B and C were 0.00361 and 0.00307, respectively, thereby indicating a colour correspondence between the test OLED displays and the reference display.

The results in Figure 7-10 suggest that the usage of the CIE 1931 2° CMFs in the characterization of the colours on Display A caused chromaticities shifts of colours towards the $-u'+v'$ direction in case of comparing the stimuli displayed on the reference display. In case of using the two 10° CMFs, the chromaticities of colours adjusted using Display A shifted towards the $+u'-v'$-direction

for the bluish colours (Stimuli 6 to 10), which is in contrast to the results characterized by CIE 1931 2° CMFs.

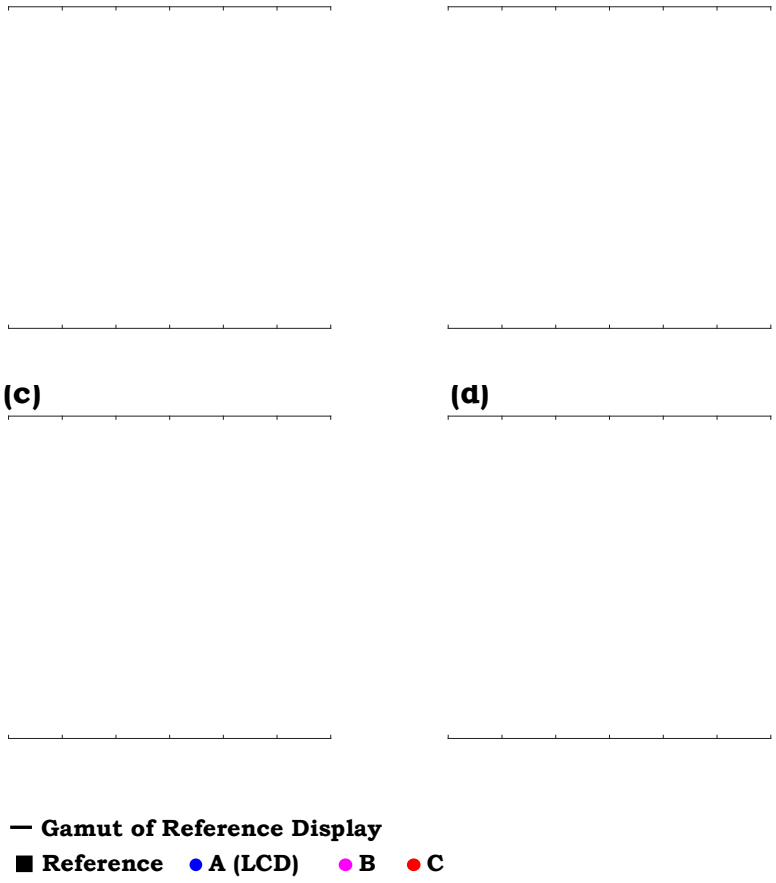

Figure 7-9 Chromaticities, including 95%-confidence error ellipses, of stimuli adjusted by 50 observers using four displays to match colour appearance of stimuli on reference display calculated using four CMFs. (a) CIE 1931 2° CMFs; (b) CIE 1964 10° CMFs; (c) CIE 2006 2° CMFs; (d) CIE 2006 10° CMFs.

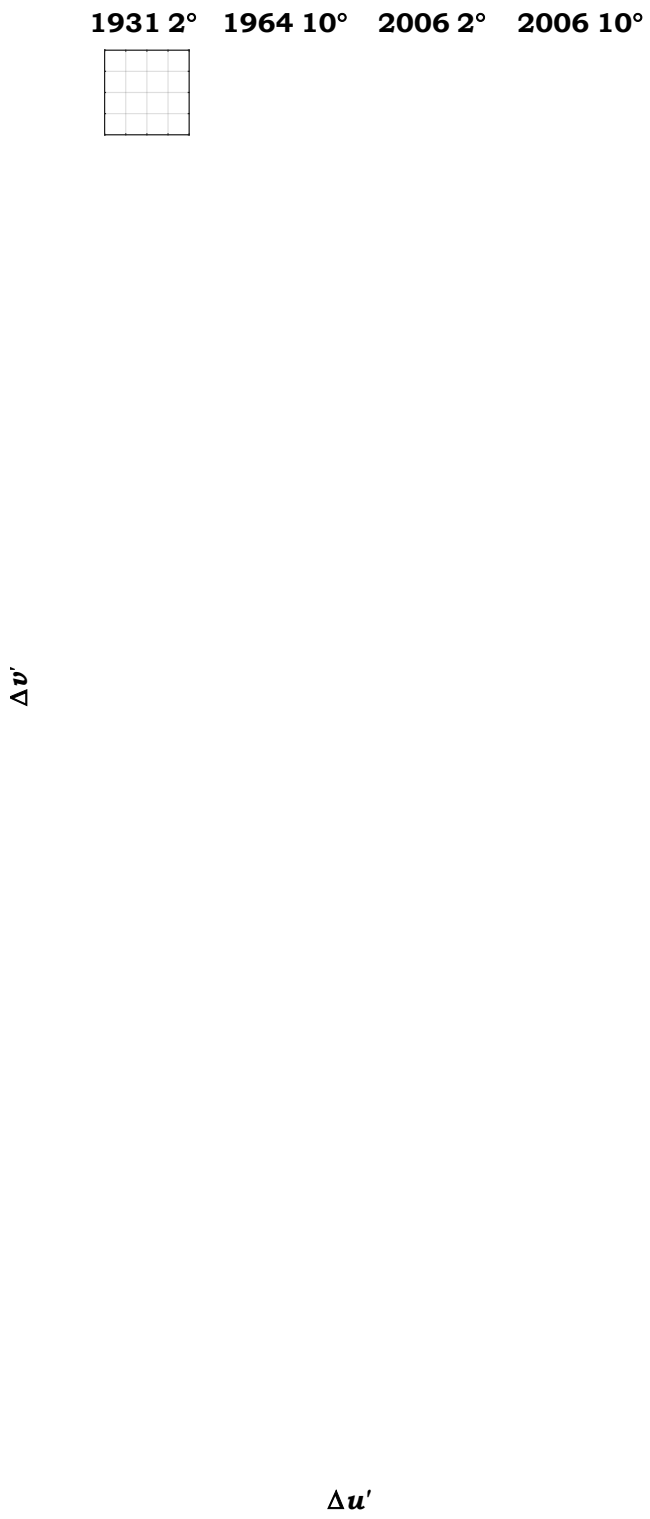

Figure 7-10 Chromaticities adjusted by observers, with relation to chromaticities of corresponding reference stimuli, plotted using four CMFs.

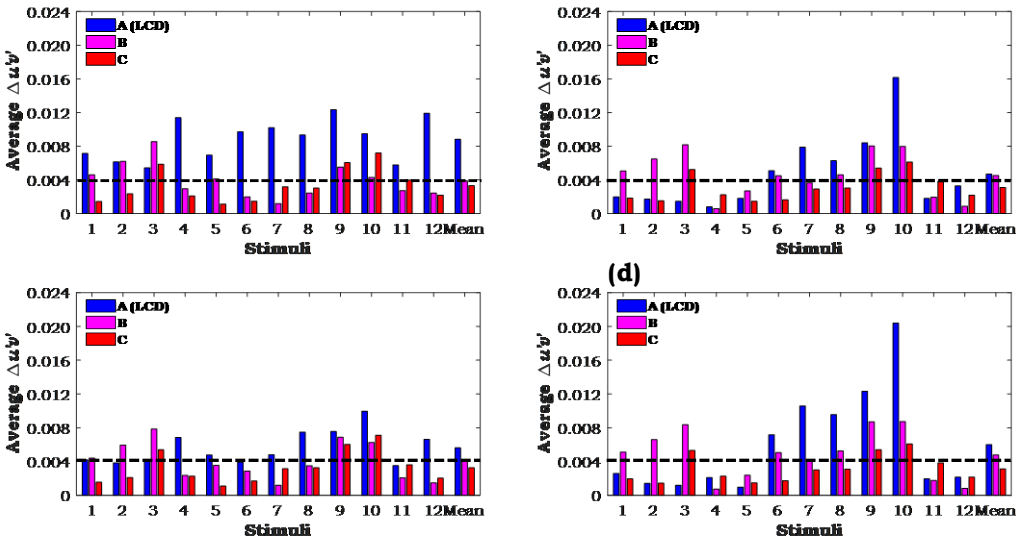

Figure 7-11 Average Δ*u'v'* between chromaticities of stimuli adjusted by eight observers using four displays and chromaticities of stimuli displayed on reference display calculated based on (a) CIE 1931 2° CMFs, (b) CIE 1964 10° CMFs, (c) CIE 2006 2° CMFs, and (d) CIE 2006 10° CMFs (Note: dashed-line labels 1 just-noticeable colour difference, JND. However, this was developed based on only the CIE 1931 CMFs and may not be applicable for other CMFs).

(d)

Figure 7-12 Area of 95%-confidence error ellipses for chromaticities of stimuli adjusted by eight observers using four displays calculated based on (a) CIE 1931 2° CMFs, (b) CIE 1964 10° CMFs, (c) CIE 2006 2° CMFs, and (d) CIE 2006 10° CMFs.

Table 7-1 Summary of average chromaticity distances and areas of 95%-confidence error ellipses of three test displays using four CMFs.

		Display A	Display B	Display C	Average
Chromaticity distances	CIE 1931 2°	0.00882	0.00361	0.00307	0.00517
	CIE 1964 10°	0.00436	0.00420	0.00288	0.00381
	CIE 2006 2°	0.00522	0.00373	0.00303	0.00399
	CIE 2006 10°	0.00557	0.00444	0.00291	0.00431
Areas of ellipses ($\times 10^3$)	CIE 1931 2°	0.397	0.117	0.064	0.397
	CIE 1964 10°	0.291	0.093	0.048	0.291
	CIE 2006 2°	0.338	0.103	0.057	0.338
	CIE 2006 10°	0.287	0.093	0.048	0.287

7.3.4 Correction of colour mismatches between LCD and OLED displays

According to the results adjusted by the observers on the test LCD, the chromaticities calculated using the CIE 1931 2° CMFs of all 12 colour stimuli on the LCD shifted toward *–u'+v'* direction in comparison to those of the stimuli on the OLED reference display. Therefore, a linear transformation from the chromaticities of reference stimuli may correct the shifts, and to a certain extent, reduce the degree of colour mismatch between the two displays characterized using the CIE 1931 2° CMFs. The transformation was applied to the tristimulus values of the stimuli $[X,Y,Z]_{reference}^{T}$ to ensure the constancy of luminance, as expressed in Equation (48). The transformed results are represented as the predicted tristimulus $[X,Y,Z]_{predictede}^{T}$ values of colours presented on the LCD with the same colour appearance as the reference stimuli. $M_{correction}$ denotes a 3 × 3 matrix, expressed in Equation (49) and calculated through the least-squares method described in Equation (50). The average tristimulus values of the colours adjusted by the observers for the 12 colour stimuli $[X_i,Y_i,Z_i]_{adjustment}^{T}$ (i = 1–12) were considered in the least-squares method. The coefficients in the calculated matrix $M_{correction}$ were scaled to ensure that the luminance of the stimuli remained constant after transformation. The matrix $M_{correction}$ calculated for the LCD is presented in Equation (51).

$$\begin{bmatrix} X \\ Y \\ Z \end{bmatrix}_{predicted} = M_{correction} \times \begin{bmatrix} X \\ Y \\ Z \end{bmatrix}_{reference} \tag{48}$$

$$M_{correction} = \begin{bmatrix} c_{xx} & c_{xy} & c_{xz} \\ c_{yx} & c_{yy} & c_{yz} \\ c_{zx} & c_{zy} & c_{zz} \end{bmatrix} \tag{49}$$

$$M_{correction} = \begin{bmatrix} X_1 & X_2 & X_3 & \cdots & X_{12} \\ Y_1 & Y_2 & Y_3 & \cdots & Y_{12} \\ Z_1 & Z_2 & Z_3 & \cdots & Z_{12} \end{bmatrix}_{adjustment} \times$$

$$\begin{bmatrix} X_1 & X_2 & X_3 & \cdots & X_{12} \\ Y_1 & Y_2 & Y_3 & \cdots & Y_{12} \\ Z_1 & Z_2 & Z_3 & \cdots & Z_{12} \end{bmatrix}^{-1}_{reference} \tag{50}$$

$$M_{ccorrection} = \begin{bmatrix} 0.9671 & 0.0017 & -0.0097 \\ -0.0216 & 1.0200 & 0.0016 \\ -0.0067 & -0.0414 & 0.9674 \end{bmatrix} \tag{51}$$

The shifts of the chromaticity coordinates from the 12 reference stimuli to the linearly transformed results are depicted in Figure 7-13. The chromaticity coordinates of the 12 colour stimuli corrected by the linear transformation and measured on the LCD were shifted along with the reference colours present in the origin. Accordingly, the distance between the average chromaticities matched by the observers and the reference can be compared with the distance between the transformed results and the reference. The performance improvement obtained after correction can be verified using CIE 1964 10° CMFs.

Those results indicated that the transformed values were representative of the observer adjustments, thereby indicating an appropriate performance of the matrix correction. The colour differences

between the observer adjustments and the corrected values ranged from 0.0012 to 0.0045, averaging at 0.0023, which is less than 1 unit of JND (= 0.004 in CIE 1976 *u'v'* diagram).

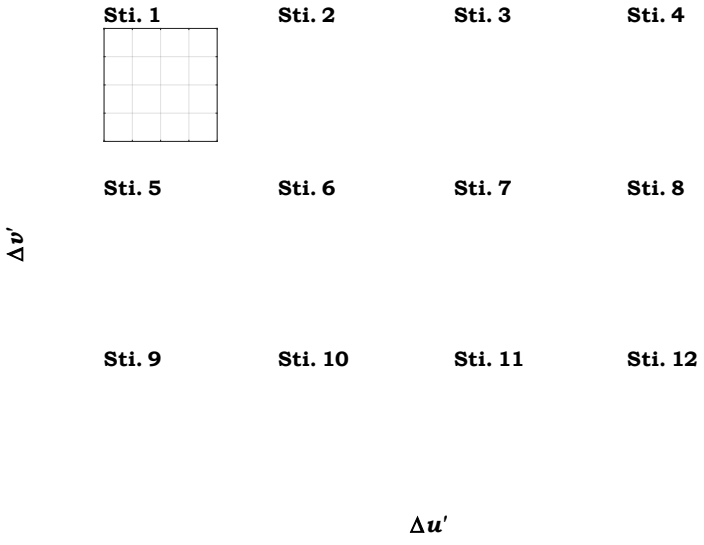

Figure 7-13 Distance between chromaticity coordinates of colours transformed with colours on reference display, compared with the distance between measured values and colours on reference display.

Applying the same method, the colour stimuli on the two OLED displays were corrected as well. The correction matrices are expressed in Equations (52) and (53). The shifts of the chromaticity coordinates from the 12 reference stimuli to the linearly transformed results are presented in Figure 7-14 and Figure 7-15. The results suggested that the linear transformation is also performed for correcting the colour mismatch between two OLED displays with various primaries, particularly for the blueish colours.

The colour differences between the observer adjustments and the corrected values ranged from 0.0012–0.0047 (average: 0.0023) for Display B, and 0.0006–0.0022 (average: 0.0014) for Display C. For all three displays, the average distances were less than 1 unit of JND (0.004 in CIE 1976 *u'v'* diagram), which indicates suitable performance of the correction.

$$M_{correction,\,2} = \begin{bmatrix} 1.1245 & -0.0902 & -0.0327 \\ 0.0495 & 0.9705 & -0.0201 \\ 0.0171 & -0.0323 & 0.9962 \end{bmatrix} \quad (52)$$

$$M_{correction,\,3} = \begin{bmatrix} 1.0307 & -0.0234 & -0.0132 \\ -0.0025 & 1.0151 & -0.0126 \\ -0.0051 & -0.0092 & 1.0150 \end{bmatrix} \quad (53)$$

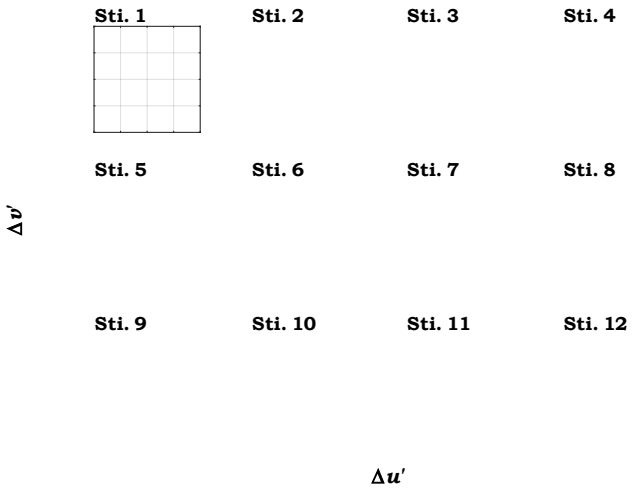

Figure 7-14 Distance between chromaticity coordinates of colours transformed with colours on reference display, compared with the distance between measured values on Display B and colours on reference display.

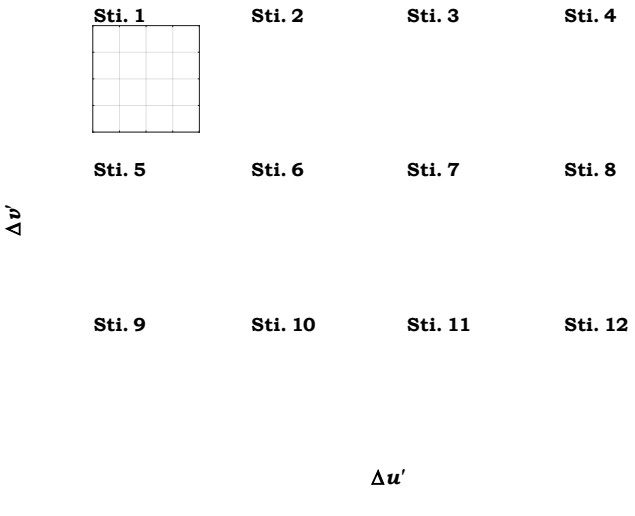

Figure 7-15 Distance between chromaticity coordinates of colours transformed with colours on reference display, compared with the distance between measured values on Display C and colours on reference display

Although the linear transformation can be used to correct the colour mismatch between an LCD and an OLED display, or OLED displays with various primaries, its use in practical production would be challenging because the matrix is device dependency. Regardless, the results of the colour matching experiments still provided a hypothesis idea on the correction of colour mismatch.

7.4 Discussion

7.4.1 Performance of Four CMFs

The performances of the four CMFs were comparatively analysed based on the chromaticities distance between the average adjusted chromaticities and chromaticities of reference stimuli, including the areas of the 95%-confidence error ellipses fitted using the adjusted chromaticities, as depicted in Figure 7-11 and Figure 7-12 and summarized in Table 7-1. The degree of colour mismatch obtained with various CMFs was evaluated according to the chromaticity distance, wherein a smaller distance implied a low level of colour mismatch or higher accuracy. The degree of observer metamerism was evaluated based on the ellipses areas, wherein a smaller area indicated a low level of observer metamerism.

Among the four CMFs, the CIE 1964 10° CMFs produced the smallest chromaticity distance, followed by the CIE 2006 2°, CIE 2006 10°, and CIE 1931 2° CMFs. However, for the five blueish stimuli (Stimuli 6 to 10) adjusted using the LCD, the distances calculated using the CIE 1964 10° CMFs were significantly larger than that evaluated using the CIE 2006 2° CMFs. Specifically, the distance for Stimuli 10 was 0.0162 calculated using the CIE 1964 10° CMFs, which is 1.6 times of the distance calculated using the CIE 2006 2° CMFs. Notably, the quantitative comparison between the two distances serves as a reference to illustrate their performance, which could not display mathematical significance owing to the varying scales of CMFs. In addition, the distances between the 12 stimuli ranged from 0.0008–0.0162 for the LCD when calculated using the CIE

1964 10° CMFs, thereby indicating a large degree of stimuli dependency on the performance of the CMFs. In case of using the CIE 2006 2° CMFs to calculate the chromaticities distances for the LCD, the average distance was marginally larger than that calculated using the CIE 1964 10° CMFs (0.00522 *vs* 0.00436), and the distances between the 12 stimuli fluctuated slightly. Although the CIE 1964 10° CMFs produced the smallest average distance, the CIE 2006 2° CMFs were considered to provide the best performance in terms of display accuracy.

In terms of ellipses areas, the CIE 1964 10° CMFs exhibited the smallest values, followed by the CIE 2006 10° and 2006 2° CMFs, and the CIE 1931 2° produced the largest values. Therefore, using the CIE 1931 2° CMFs would cause serious observer metamerism.

7.4.2 Comparison with the experiments in Study 2

Compared with the experiments in Study 2, this study adopted new displays with varying SPDs of primaries and stimuli with more saturated colours. The chromaticities of the LCD used in the current study compared with that used in Study 2 are plotted in Figure 7-16 (a). The SPDs of the primaries of the two displays were compared in Figure 7-16 (b). The stimuli selected for the current study and Study 2 are presented in Figure 7-17.

The results of Study 2 suggested that the usage of CIE 1931 2° CMFs in characterizing colour matching between LCDs and OLED displays would cause significant degrees of colour mismatch, regardless of the size of the FOV (4.77° and 20.2°). This finding was reiterated by the results of the current study as well, wherein the distances between the chromaticities of reference stimuli and the average chromaticities adjusted by the observers on the LCD were larger than 0.004 (1 JND) for all test stimuli. Moreover, the stimuli appearing neutral on the LCD appeared yellowish green on the OLED display if the CIE 1931 2° CMFs was used for characterization. This is concluded from the shifts of the average chromaticities adjusted by the observers in the $-u'+v'$-

direction compared with the chromaticities of reference stimuli, which were observed in the current study as well. However, the degree of chromaticity shifts was more concerning in this case, especially for the blueish stimuli. Specifically, the average shift distance in the current study was 0.00822 in comparison with that of 0.00662 in Study 2. The colours presented on various OLED displays were considered with the same appearance as each other, because the average chromaticities distances between them were less than 0.004 units of $\Delta u'v'$, which was similar to the results in Study 2. Upon comparing the performance of the four CMFs for characterizing the colour matches and observer metamerism in Study 2, the CIE 1931 2° CMFs delivered the most inferior performance among the four CMFs. This result was consistent with the present findings.

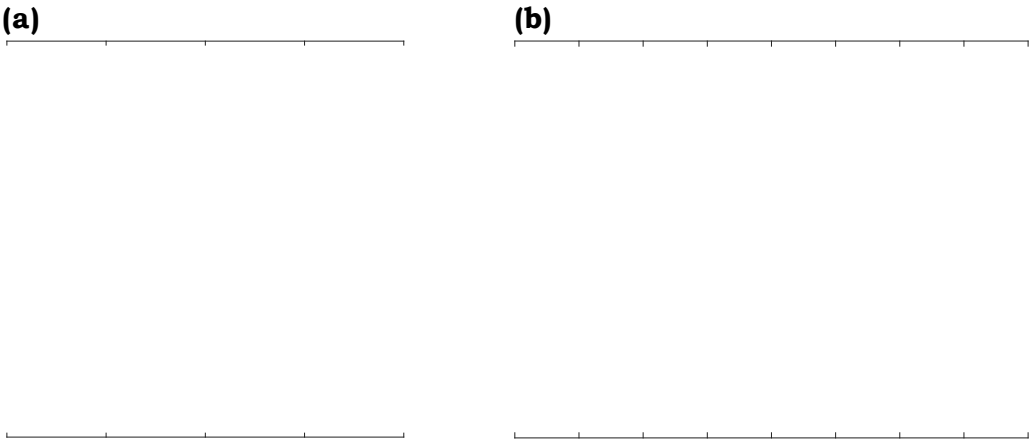

Figure 7-16 (a) Colour gamuts and white points of two LCDs used in previous studies and current study derived using CIE 1931 CMFs, including standard sRGB and P3 colour gamuts. (b) SPDs of primaries of two LCDs used in previous studies and current study.

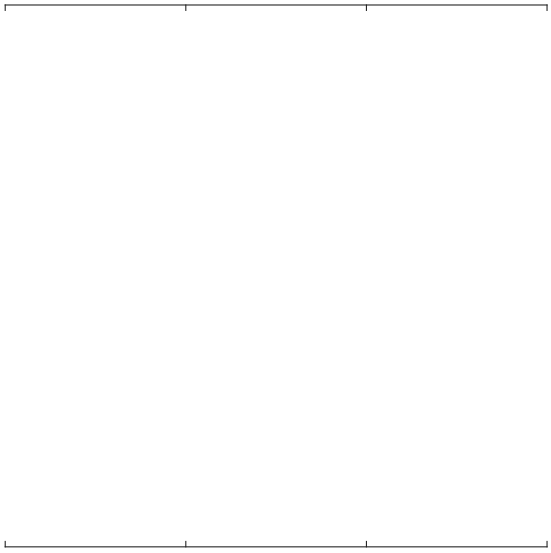

Figure 7-17 Chromaticity coordinates of colour stimuli characterized in CIE 1976 *u'v'* chromaticity diagram, adopted in previous studies and current study.

7.5 Conclusions

This study conducted a colour matching experiment between an OLED display and an LCD, or between different OLED displays. The data collected from the experiment were used to correct the colour mismatch between LCD and OLED displays. A new experimental apparatus was constructed to present the displays to the observers with an FOV ≈ 20.2°. In particular, this study adopted a greater number of colour stimuli covering a larger area of the CIE chromaticity diagram. In this experiment, eight human observers performed the colour matching of 12 colour stimuli using three smartphone displays (i.e., one LCD and three OLED displays) and a reference OLED smartphone display.

The results revealed large differences between the LCD and the reference OLED display, particularly for the bluish stimuli. This suggests the four standard CMFs resulting in the most

inferior performance for characterizing the colour matches between the LCD and the reference OLED displays with various primaries differing in either shapes or peak wavelength of SPDs. In case of using the CIE 1931 2° CMFs for characterizing the colour matches, the chromaticities of the stimuli produced by the LCD varied significantly from those produced by the OLED displays, with the chromaticities shifting toward the *–u'+v'*-direction in the CIE 1976 *u'v'* chromaticity diagram, which is consistent with the results of studies in Chapters 4 and 5.

Upon comparing the performances of the four CMFs, the degree of colour mismatch was represented based on the chromaticity distances between the stimuli presented on the reference OLED display and the average adjustments enacted by the observers on the three test displays. Among the four CMFs, the CIE 1964 10° CMFs produced the smallest average distance, and the variation in its results for the 12 colour stimuli was larger than those characterized by CIE 2006 2° CMFs. In addition, the characterization of the CIE 2006 2° CMFs produced the smallest distances at the bluish colour stimuli. Thus, the CIE 2006 2° CMFs still delivered the best performance in terms of the accuracy of characterization. The performance of the four standard CMFs on the characterization of observer metamerism was similar to the results in the studies described in Chapters 4 and 5, wherein the two 10° CMFs exhibited the best performance. Overall, the worst performance was resulted from the CIE 1931 2° CMFs.

According to the results of the colour matching experiment between the LCD and reference OLED displays, all the chromaticities calculated using the CIE 1931 2° CMFs of 12 colour stimuli on the LCD matched by the observers shifted toward the *–u'+v'*-direction compared with those on the reference OLED display. Furthermore, a linear transformation on the reference chromaticities was explored to reduce the colour mismatch for all the colour stimuli, and to a certain extent, correct the colour mismatch between the two displays characterized by the CIE 1931 2° CMFs. Although

the transformation results produced an appropriate performance after correction, its practical application would be challenging because the matrix is device dependent. Nonetheless, the results of the colour matching experiments provide a hypothetical idea on the correction of colour mismatch.

Chapter 8 Conclusions

This dissertation conducted three studies to explore the procedure of display calibration and its applications on modern electronic displays, particularly OLED displays. In particular, display calibration aims to present accurate colour on the display to reproduce the perception of colours of real-world objects or that viewed on another display. In the procedure, the digital count values used on the display projecting the three primaries were characterized according to the CIE colorimetry system, e.g., colour space of tristimulus values XYZ, using the CIE standard CMFs. Thereafter, the values were specified into a device-independent standard RGB colour space. Following this procedure, the displays were calibrated to produce colours according to standard RGB colour spaces.

In case of application to modern displays such as LCDs and OLED displays, the conventional models of the display characterization created assuming channel dependency and constant chromaticity were deemed as inapplicable on those displays. This is because the channel independence was invalid on the newly developed displays with the issues arising from the crosstalk effect. If the device was accurately calibrated, the appearance of the colours with the same values in the standard RGB colour space varied with the displays, as reported by the observers. This was caused by the limitations of the CIE colorimetry system regarding the characterization of the human visual system.

In the first study, new models of colour characterization were created to correct the influences of the “crosstalk effect” observed on OLED displays. This model required the measurement of only 64 stimuli, which is a significant improvement compared with the other models used for characterizing the channel-dependent displays. The predictions of the models were verified to ensure a high accuracy compared with the prediction results through the conventional GOG model

The average colour differences in the CIELAB colour space of the test stimuli ranged from 0.61 to 1.46 units for the nine test OLED displays, which were eight to ten times less than the colour differences evaluated from the GOG model.

The second study contains two parts of colour matching experiments performed with a small FOV (≈ 4.77°) and large FOV (≈ 20.2°). Various studies reported the problem of colour mismatch between colour stimuli exhibiting equal values in the CIE colorimetry system but presented on two distinctly calibrated displays. Thus, stimuli with the same chromaticities but distinct spectral compositions generated by displays containing various primaries created a dissimilar colour appearance. Based on this phenomenon, the effectiveness of the CIE system in the display characterization and specification remains unclarified. These experiments were performed to explore the performance of the CIE standard CMFs on the characterizations of displays with various primaries. In this study, 50 and 53 human observers performed the colour-matching tasks for six colour stimuli with a FOV of 4.77° and 20.2° between the same set of four test displays (i.e., one LCD and three OLED) and a reference OLED display. In all cases, the four CMFs exhibited the worst performance in characterizing the colour matches between the LCD and the reference OLED displays, regardless of the range of FOV. Generally, the LCD produced the highest degree of observer metamerism, and these results suggested the significance of the colour primaries, in terms of the peak wavelengths and spectral shapes, with respect to the perceived colour matches and observer metamerism. In case of using the CIE 1931 2° CMFs for characterizing the colours between LCD and OLED displays, the chromaticities shifted toward the $-u'+v'$-direction in the CIE 1976 $u'v'$ chromaticity diagram for those adjusted by the observers using the LCD. This indicated that a stimulus appearing neutral on an LCD may appear yellowish green on an OLED display, whereas a stimulus appearing neutral on an OLED display may appear

pinkish on an LCD. Among the four CMFs, the CIE 2006 2º CMFs delivered the best performance in all cases, which does not conform to the recommendation of adopting 10° for stimuli with a FOV > 4°.

In the third study, a method was proposed for correcting the colour mismatch between LCD and OLED displays. In the experiment, a greater number of colour stimuli covering a large area in the chromaticity diagram were selected. All observers completed the tasks of adjusting the chromaticities on LCD or OLED displays to match the colour appearances on a reference OLED display. The experimental results were highly consistent with the results of Study 2, which suggested the validity of the results under the true conditions of using smartphones. Specifically, the larger chromaticities distance between the chromaticities of reference stimuli and adjusted by observers in the chromaticity diagram were observed herein. This indicated that the degree of colour mismatch between the LCD and OLED displays was more concerning when characterized using the CIE 1931 2° CMFs under true conditions.

In summary, all the studies in this dissertation helps us to further understanding the colour matching mechanisms and the characterization of the colour matching mechanisms in the human visual system, which can help to develop better colorimetric models and tools for color specifications and calibrations. On the other hand, all the studies bring practical impacts to the imaging industry, by providing scientific evidence for promoting the importance of the display calibrations and specifications and also practical solutions for improving display colour specification and accuracy.

Reference

[1] I. Newton, “A letter of Mr. Isaac Newton,” *Philosophical transactions of the Royal Society of London*, vol. 6, no. 80, pp.3075-3087, Feb. 1672.

[2] D. R. Hilbert, *Color and color perception: A study in anthropocentric realism*. Chicago: Csli Press, 1987. p.1.

[3] I. Newton, *Óptica*. Sao Paulo: Edusp, 1704.

[4] T. Young, “II. The Bakerian Lecture. On the theory of light and colours,” *Philosophical transactions of the Royal Society of London*, vol.1, no.92, pp.12-48, Jan. 1802.

[5] W. Peddie, “Helmholtz’s Treatise on Physiological Optics,” *Nature*, vol.116, pp.88-89, Jul. 1925.

[6] J. C. Maxwell, “XVIII—Experiments on Colour, as Perceived by the Eye, with Remarks on Colour-Blindness,” *Earth and Environmental Science Transactions of the Royal Society of Edinburgh*, vol.21, no.2, pp.275-298, 1857.

[7] E. Hering, *Outlines of a Theory of the Light Sense*. Massachusetts: Harvard University Press, 1964.

[8] G. Buchsbaum and A. Gottschalk, “Trichromacy, Opponent Colours Coding and Optimum Colour Information Transmission in the Retina,” *Proceedings of the Royal society of London. Series B. Biological Sciences*, vol.220, no.1218, pp.89-113, Nov. 1983.

[9] E. Schrödinger and Q. Zaidi, “On The Relationship of Four-Color Theory to Three-Color Theory,” *Color Research & Application*, vol.19, no.1, pp. 37-47, Feb. 1994.

[10] L. M. Hurvich, and D. Jameson, “An Opponent-Process Theory of Color Vision,” *Psychological Review*, vol.64, no.6, pp.384-404, 1957.

[11] D. B. Judd, *Response functions for types of vision according to the Müller theory*, Washington, D.C.: US Government Printing Office, 1949.

[12] D. Jameson and L.M. Hurvich, "Some Quantitative Aspects of an Opponent-Colors Theory. I. Chromatic Responses and Spectral Saturation," *Journal of the Optical Society of America*, vol.45, pp.546-552, 1955.

[13] T. Tomita, A. Kaneko, M. Murakami, and E. L. Pautler, "Spectral Response Curves of Single Cones in the Carp," *Vision Research*, vol. 7, no.7-8, pp.519-531.1967.

[14] R. L. De Valois, C. J. Smith, S. T. Kitai, and A. J. Karoly, "Response of single cells in monkey lateral geniculate nucleus to monochromatic light," *Science*, vol.127, no.3292, pp.238-239, 1958.

[15] I. Obodovskiy, (2019). *Radiation: Fundamentals, Applications, Risks, and Safety*. Amsterdam: Elsevier, 2019.

[16] J. M. Artigas, A. Felipe, A. Navea, A. Fandino, and C. Artigas, "Spectral Transmission of the Human Crystalline Lens in Adult and Elderly Persons: Color and Total Transmission of Visible Light," *Investigative Ophthalmology & Visual Science*, vol.53, no.7, pp.4076-4084, 2012.

[17] T. Berendschot, W. Broekmans, I. Klöpping-Ketelaars, A. Kardinaal, G. Van Poppel, and D. Van Norren, "Lens Aging in Relation to Nutritional Determinants and Possible Risk Factors for Age-Related Cataract. *Archives of Ophthalmology*, vol.120. no.12, pp.1732-1737, 2002.

[18] D. V. Norren and J. J. Vos, "Spectral Transmission of the Human Ocular Media," *Vision Research*, vol.14, no.11, pp.1237-1244, 1974.

[19] B. H. Crawford, "The Scotopic Visibility Function," *Proceedings of the Physical Society. Section B*, vol.62, no.5, pp.321-334. 1949.

[20] J. Pokorny, V. C. Smith, and M. Lutze, “Aging of the Human Lens,” *Applied Optics*, vol.26, no.8, pp.1437-1440, 1987.

[21] S. Prasad, S. L.Galetta, “Anatomy and Physiology of the Afferent Visual System,” in *Handbook of Clinical Neurology*, P. Vinken and G. Bruyn, Ed. Amsterdam: Elsevier, 2011, ch. 1, pp.3-19.

[22] J. Daintith, *Biographical Encyclopedia of Scientists—2 Volume Set*. Florida: CRC Press, 1994.

[23] O. N. Rood, “On a Photometric Method which is Independent of Color,” *The London, Edinburgh, and Dublin Philosophical Magazine and Journal of Science*, vol.36, no.221, pp.380-383, 1893.

[24] H. Wassle and B. B. Boycott, “Functional Architecture of the Mammalian Retina,” *Physiological Reviews*, vol.71, no.2, pp.447-480, 1991.

[25] P. K. Brown and G. Wald, “Visual Pigments in Single Rods and Cones of the Human Retina. Science,” vol.144, no.3614, pp.45-52, 1964.

[26] D. M. Berson, F. A. Dunn, and M. Takao, “Phototransduction by Retinal Ganglion Cells that Set the Circadian Clock,” Science, vol.295, no.5557, pp.1070-1073, 2002.

[27] R. J. Lucas, R. H. Douglas, and R. G. Foster, “Characterization of an Ocular Photopigment Capable of Driving Pupillary Constriction in Mice,” *Nature Neuroscience*, vol.4, no.6, pp.621-626, 2001.

[28] D. Cao, A. Chang, and S. Gai, “Evidence for an Impact of Melanopsin Activation on Unique White Perception,” *Journal of the Optical Society of America A*, vol.35, no.4, pp.B287-B291, 2018.

[29] A. J. Zele, P. Adhikari, D. Cao, and B. Feigl, “Melanopsin Driven Enhancement of Cone-mediated Visual Processing,” *Vision Research*, vol.160, pp.72-81, 2019.

[30] J. A. Enezi, V. Revell, T. Brown, J. Wynne, L. Schlangen, and R. Lucas, “A ‘Melanopic’ Spectral Efficiency Function Predicts the Sensitivity of Melanopsin Photoreceptors to Polychromatic Lights,” *Journal of Biological Rhythms*, vol.26, no.4, pp.314-323, 2011.

[31] G. Wyszecki and W. S. Stiles, *Color Science: Concepts and Methods, Quantitative Data and Formulae, 2nd Edition*. New Jersey: Wiley, 1982.

[32] D. H. Krantz, “Color Measurement and Color Theory: I. Representation Theorem for Grassmann Structures,” *Journal of Mathematical Psychology*, vol.12, no.3, pp.283-303, 1975.

[33] C. Oleari and P. Maura, “Grassmann’s Laws and Individual Color-Matching Functions for Non-Spectral Primaries Evaluated by Maximum Saturation Technique in Foveal Vision,” *Color Research & Application*, vol.33, no.4, pp.271-281, 2008.

[34] P. W. Trezona, “Additivity of Colour Equations,” *Proceedings of the Physical Society. Section B*, vol.66, no.7, pp.548-556, 1953.

[35] P. W. Trezona, “Additivity of Colour Equations: II,” *Proceedings of the Physical Society. Section B*, vol.67, no.7, pp.513-522, 1954.

[36] W. A. Thornton, “Toward a more Accurate and Extensible Colorimetry. Part I. Introduction. The Visual Colorimeter-Spectroradiometer. Experimental Results,” *Color Research & Application*, vol.17, no.2, pp.79-122, 1992.

[37] W. A. Thornton, “Toward a more Accurate and Extensible Colorimetry. Part II. Discussion. *Color Research & Application*, vol.17, no.3, pp.162-186, 1992.

[38] W. A. Thornton, “Toward a more Accurate and Extensible Colorimetry. Part III. Discussion (Continued),” *Color Research & Application*, vol.17, no.4, pp.240-262, 1992.

[39] J. Li, P. Hanselaer, and K. A. Smet, “Impact of Color-Matching Primaries on Observer Matching: Part I–Accuracy,” *Leukos*, vol.18, no.2, pp.104-126, 2022.

[40] J. Li, P. Hanselaer, and K. A. Smet, “Impact of Color-Matching Primaries on Observer Matching: Part II–Observer Variability,” *Leukos*, vol.18, no.2, pp.127-144, 2022.

[41] International Commission on Illumination “Commission Internationale de l’Éclairage Proceedings, 1931,” Cambridge: Cambridge University Press, 1932.

[42] W. D. Wright, “A Re-Determination of the Trichromatic Coefficients of the Spectral Colours,” *Transactions of the Optical Society*, vol.30, no.4, pp.141-164, 1929.

[43] J. Guild, “The Colorimetric Properties of the Spectrum,” *Philosophical Transactions of the Royal Society of London. Series A, Containing Papers of a Mathematical or Physical Character*, vol.230. no.681-693, pp.149-187, 1931.

[44] J. Guild, “The Transformation of Trichromatic Mixture Data: Algebraic Methods,” *Transactions of the Optical Society*, vol.26, no.2, pp.95-108, 1924.

[45] International Commission on Illumination, “Commission Internationale de l’Éclairage Proceedings, 1924,” Cambridge: Cambridge University Press, 1926.

[46] W.W. Coblentz and W.B. Emerson, “The Relative Sensibility of the Average Eye to Light of Different Colors and some Practical Applications to Radiation Problems,” *Journal of the Franklin Institute*. vol.183, no.6, pp.771-772, 1917.

[47] E. P. T. Tyndall and K. S. Gibson, “Visibility of Radiant Energy Equation,” *Journal of the Optical Society of America*, vol.9, no.4, pp.403-403, 1924.

[48] W. Abney and E. R. Festing, “Colour Photometry – Part 1,” *Philosophical Transactions of the Royal Society of London*. vol.177, no.2, pp,423-456, 1886.

[49] W. S. Stiles and J. M. Burch, “NPL Colour-Matching Investigation: Final Report (1958),” *Optica Acta: International Journal of Optics*, vol.6, no.1, pp.1-26, 1959.

[50] N. I. Speranskaya, “Determination of Spectral Color Coordinates for Twenty-Seven Normal Observers,” *Optics and Spectroscopy*, vol.7, pp.424-428, 1959.

[51] T. Young, *A course of Lectures on Natural Philosophy and the Mechanical Arts*. London: Printed for J. Johnson.1807.

[52] J. Maxwell, “Experiments on Colour as perceived by the Eye, with Remarks on Colour-Blindness,” *Proceedings of the Royal Society of Edinburgh*, vol.3, pp.299-301, 1857.

[53] W. Peddie, “Helmholtz's Treatise on Physiological Optics,” *Nature*, vol.118, pp.74-76, 1926.

[54] K. R. Gegenfurtner and D. C. Kiper, “Color Vision,”. *Annual Review of Neuroscience*, vol.26, pp.181-206, 2003.

[55] International Commission on Illumination, “170-1: 2006: Fundamental Chromaticity Diagram with Physiological Axes–Part 1,” Vienna: Central Bureau of the International Commission on Illumination, 2006.

[56] A. Stockman and L. T. Sharpe, “The Spectral Sensitivities of the Middle-and Long-Wavelength-Sensitive Cones Derived from Measurements in Observers of Known Genotype,” *Vision Research*, vol.40, no.13, pp.1711-1737, 2000.

[57] International Commission on Illumination, “170-2: 2015: Fundamental Chromaticity Diagram with Physiological Axes – Part 2,” Vienna: Central Bureau of the International Commission on Illumination, 2015.

[58] B. B. Lee, P. R. Martin, and A. Valberg, “The Physiological Basis of Heterochromatic Flicker Photometry Demonstrated in the Ganglion Cells of the Macaque Retina,” *The Journal of Physiology*, vol.404, no.1, pp.323-347, 1988.

[59] J. P. C. Southall, *Helmholtz’s Treatise on Physiological Optics. Vol. 2: The Sensation of Vision*. New York: Dover Publication, 1962.

[60] K. K. Niall, *Erwin Schrödinger's Color Theory: Translated with Modern Commentary Edited by Keith K. Niall*. New York: Springer International Publishing, 2019.

[61] D. L. MacAdam, “Projective Transformations of ICI Color Specifications,” *Journal of the Optical Society of America*. vol.27, no.8, pp,294-299, 1937.

[62] D. L. MacAdam, “Specification of Small Chromaticity Differences,” *Journal of the Optical Society of America*. vol.33, no.1, pp.18-26, 1943.

[63] A. Robertson, “CIE Guidelines for Coordinated Research on Color-Difference Evaluation,” *Color Research & Application*, vol.3, no.3, pp.149-151, 1978.

[64] International Commission on Illumination, “CIE 015:2018 Colorimetry, 4th Edition,” Vienna: Central Bureau of the International Commission on Illumination, 2018.

[65] G. Wyszecki, “Proposal for a New Color-Difference Formula,” Journal of the Optical Society of America, vol.53, no.11, pp.1318-1319, 1963.

[66] M. R. Luo and B. Rigg, Chromaticity-Discrimination Ellipses for Surface Colours. *Color Research & Application*, vol.11, no.1, pp.25-42, 1986.

[67] P. C. Hung and R. S. Berns, “Determination of Constant Hue Loci for a CRT Gamut and their Predictions using Color Appearance Spaces,” *Color Research & Application*, vol.20, no.5, pp.285-295, 1995.

[68] G. Marcu, "Gamut Mapping in Munsell Constant Hue Sections," In *Proceedings of the 6th Color and Imaging Conference*, pp. 159-162, 1998.

[69] G. J. Braun, M. D. Fairchild, and F. Ebner, "Color Gamut Mapping in a Hue-Linearized CIELAB Color Space," In *Proceedings of the 6th Color and Imaging Conference*, pp. 163-168, 1998.

[70] R. G. Kuehni, "Color-Tolerance data and the Tentative CIE 1976 L* a* b* Formula," *The Journal of the Optical Society of America*, vol.66, no.5, pp.497-500, 1976.

[71] R. G. Kuehni and R. T. Marcus, "An Experiment in Visual Scaling of Small Color Differences," *Color Research & Application*, vol.4, no.2, pp.83-91, 1979.

[72] F.J.J. Clarke, R. McDonald, B. Rigg, "Modification to JPC79 Color-Difference Formula," Journal of the Society of Dyers and Colourists, vol.100, no.4, pp.128-132, 1984.

[73] International Commission on Illumination, "CIE 116-1995 Industrial Colour-Difference Evaluation," Vienna: Central Bureau of the International Commission on Illumination, 1995.

[74] International Commission on Illumination, "CIE 142-2001, Improvement to Industrial Colour-Difference Evaluation," Vienna: Central Bureau of the International Commission on Illumination, 2001.

[75] R. L. Alfvin and M. D. Fairchild, "Observer Variability in Metameric Color Matches using Color Reproduction Media," *Color Research & Application*, vol.22, no.3, pp.174-188, 1997.

[76] International Commission on Illumination, "CIE S 017/E:2011 ILV: International Lighting Vocabulary," Vienna: Central Bureau of the International Commission on Illumination, 1987.

[77] I. Pobboravsky, "Effect of Small Color Differences in Color Vision on the Matching of Soft and Hard Proofs," in *Proceedings of the Technical Association of the Graphic Arts 1988*, pp. 62-79.1988.

[78] W. Ambach, M. Blumthaler, T. Schöpf, E. Ambach, F. Katzgraber, F. Daxecker, and A. Daxer, "Spectral Transmission of the Optical Media of the Human Eye with Respect to Keratitis and Cataract Formation," *Documenta Ophthalmologica*, vol.88, no.2, pp.165-173, 1994.

[79] B. R. Hammond, B. R. Wooten, J. E. Náñez, and A. J. Wenzel, "Smoking and Lens Optical Density," *Ophthalmic and Physiological Optics*, vol.19, no.4, pp.300-305, 1999.

[80] M. Lutze and G. H. Bresnick, "Lenses of Diabetic Patients Yellow at an Accelerated Rate Similar to Older Normals," *Investigative Ophthalmology and Visual Science*, vol.32, no.1, pp.194-199. 1991.

[81] O. Howells, F. Eperjesi, and H. Bartlett, "Macular Pigment Optical Density in Young Adults of South Asian Origin," *Investigative Ophthalmology and Visual Science*, vol.54, no.4, pp.2711-2719, 2013.

[82] I. Alessandro, M. Marco, T. G. Kevin, J. J. Elizabeth, A. T. William, K. Emily, L. H. Tarsha, H. Tamara, S. Suzanne, C. J. Karen, and B. K. Stephen, "Macular Pigment Optical Density in the Elderly: Findings in a Large Biracial Midsouth Population Sample," *Investigative Ophthalmology and Visual Science*, vol.48, no.4, pp.1458-1465, 2007.

[83] T. A. Ciulla, J. Curran-Celantano, D. A. Cooper, B. R. Hammond Jr, R. P. Danis, L. M. Pratt, K. A. Riccardi, and T. G. Filloon, "Macular Pigment Optical Density in a Midwestern Sample," *Ophthalmology*, vol.108, no.4, pp.730-737, 2001.

[84] R. A. Bone, J. T. Landrum, L. H. Guerra, and C. A. Ruiz, "Lutein and Zeaxanthin Dietary Supplements Raise Macular Pigment Density and Serum Concentrations of these Carotenoids in Humans," *The Journal of Nutrition*, vol,133, no.4, pp.992-998, 2003.

[85] J. Nolan, O. O'Donovan, H. Kavanagh, J. Stack, M. Harrison, A. Muldoon, and S. Beatty, "Macular Pigment and Percentage of Body Fat," *Investigative Ophthalmology and Visual Science*, vol.45, no.11, pp.3940-3950, 2004.

[86] P. B. M. Thomas, M. A. Formankiewicz, and J. D. Mollon, "The Effect of Photopigment Optical Density on the Color Vision of the Anomalous Trichromat," *Vision Research*, vol.51, no.20, pp.2224-2233, 2011.

[87] A. Sarkar, "Identification and Assignment of Colorimetric Observer Categories and their Applications in Color and Vision Sciences," Ph. D. dissertation, University of Nantes, Nantes, 2011.

[88] Y. Asano, "Individual Colorimetric Observers for Personalized Color Imaging," Ph. D. Dissertation, Rochester Institute of Technology, 2015.

[89] G. Shiers, "Ferdinand Braun and the Cathode Ray Tube," *Scientific American*, vol.230, no.3, pp.92-101, 1974.

[90] N. Holonyak, and S. F. Bevacqua. "Coherent (Visible) Light Emission from Ga(as1-xpx) Junctions," *Applied Physics Letters*, vol.1, no.1, pp.82-83, 1962.

[91] L. E. Tannas, *Flat-Panel Displays and CRTs*. Berlin: Springer Science and Business Media, 2012.

[92] J. A. Castellano, *Handbook of Display Technology*. Cambridge: Academic Press, 2012.

[93] H. Kawamoto, "The History of Liquid-Crystal Display and its Industry," In *Proceedings of the 2012 Third IEEE History of Electro-Technology Conference*. pp. 1-6, 2012.

[94] G. Hong, X. Gan, C. Leonhardt, Z. Zhang, J. Seibert, J. M. Busch, and S. Bräse, "A Brief History of OLEDs-Emitter Development and Industry Milestones," *Advanced Materials*, vol.33, no.9, pp.2005630, 2021.

[95] W. W. Farley and J.C. Gutmann, “Technical Report HFL-80-2/ONR-80, Digital Image Processing Systems and an Approach to the Display of Colors of Specified Chrominance,” Blacksburg: Virginia Polytechnic Institute and State University, 1980.

[96] D. L. Post and C. S. Calhoun, “An Evaluation of Methods for Producing Desired Colors on CRT Monitors,” *Color Research & Application*, vol.14. no.4, pp.172-186, 1989.

[97] W. B. Cowan and N. L. Rowell, “On the Gun Independence and Phosphor Constancy of Colour Video Monitors,” In *Proceedings of the 1986 AIC Interim Meeting on Color in Computer Generated Displays*, pp.s34-s38, 1986.

[98] W. B. Cowan, “An Inexpensive Scheme for Calibration of a Colour Monitor in terms of CIE Standard Coordinates,” *ACM SIGGRAPH Computer Graphics*, vol.17, no.3, pp.315-321, 1983.

[99] R. S. Berns, R. J. Motta, and M. E. Gorzynski, “CRT colorimetry. part I: Theory and Practice,” *Color Research & Application*, vol.18, no.5, pp.299-314. 1993.

[100] R. S. Berns, R. J. Motta, and M. E. Gorzynski, “CRT colorimetry. part II: Metrology,” Color *Research & Application*, vol.18, no.5, pp.315-325, 1993.

[101] R. S. Berns, “Methods for Characterizing CRT Displays,” *Displays*, vol.16, no.4, pp.173-182, 1996.

[102] G. Sharma, “LCDs Versus CRTs: Color-Calibration and Gamut Considerations,” in *Proceedings of the Institute of Electrical and Electronics Engineers*, vol.90, no.4, pp.605-622, 2002.

[103] D. H. Brainard, D. G. Pelli, and T. Robson, *Display Characterization*. New York: Wiley, 2002.

[104] Y. Kwak and L. MacDonald, “Characterization of a Desktop LCD Projector,” *Displays*, vol.21, no.5, pp.179-194, 2000.

[105] N. Katoh, T. Deguchi, and R. Berns, “An Accurate Characterization of CRT Monitor (I): Verification of Past Studies and Clarifications of Gamma,” *Optical Review*. vol.8, no.5, pp.305-314, 2001.

[106] International Electrotechnical Commission, “Colour Measurement and Management in Multimedia Systems and Equipment. Part 3 Equipment using Cathode Ray Tubes,” Geneva: International Electrotechnical Commission , 1998.

[107] L. D. Silverstein and T. G. Fiske, “Colorimetric and Photometric Modeling of Liquid Crystal Displays,” In *Proceedings of the 1st Color and Imaging Conference*, pp. 149-156, 1993.

[108] Y. Kwak, C.Li, and L. MacDonald, “Controling Color of Liquid-Crystal Displays,” *Journal of the Society for Information Display*, vol.11, no.2, pp.341-348, 2003.

[109] Y. Yoshida and Y. Yamamoto, “Color calibration of LCDs,” In *Proceedings of the 10th Color and Imaging Conference*, pp.305-311, 2002.

[110] N. Katoh, T. Deguchi, and R. S. Berns, “An Accurate Characterization of CRT Monitor (II): Proposal for an Extension to CIE Method and its Verification,” *Optical Review*, vol.8, no.5, pp.397-408, 2001.

[111] N. Tamura, N. Tsumura, and Y. Miyake, “Masking Model for Accurate Colorimetric Characterization of LCD,” *Journal of the Society for Information Display*, vol.11, no.2, pp.333-339, 2003.

[112] S. Wen and R. Wu, “Two-Primary Crosstalk Model for Characterizing Liquid Crystal Displays,” *Color Research & Application*, vol.31, no.2, pp.102-108, 2006.

[113] P. Colantoni and J. B. Thomas, “A Color Management Process for Real Time Color Reconstruction of Multispectral Images,” In *Proceedings of the Image Analysis: 16th Scandinavian Conference*, pp 128-137, 2009.

[114] J. F. Stauder, P. F. Colatoni, and L. F. Blonde, “Device and Method for Characterizing a Colour Device,” European Patent WO2006094914, 2006.

[115] J. Stauder, J. Thollot, P. Colantoni, and A. Tremeau, “Device, System and Method for Characterizing a Colour Device,” European Patent WO2007116077, 2007.

[116] B. Bastani, B. Cressman, and B. Funt, “Calibrated Color Mapping between LCD and CRT Displays: A Case Study,” *Color Research & Application*, vol.30, no.6, pp.438-447, 2005.

[117] X. Zhang and H. Xu, “Piecewise Partition Model for Accurate Colorimetric Characterization of Liquid Crystal Displays,” *Acta Optica Sinica*, vol.27, no.9, pp.1719-1724, 2007.

[118] R. Safaee-Rad and M. Aleksic, “R/G/B Color Crosstalk Characterization and Calibration for LCD Displays,” In *Proceedings of the Color Imaging XVI: Displaying, Processing, Hardcopy, and Applications*, pp. 24-35, 2011.

[119] R. Gong, H. Xu, X. Zhang, and M. R. Luo, “Sub-Space Compensation Model for Accurate Colorimetric Characterization of Liquid Crystal Displays,” *Acta Optica Sinica*, vol.31, no.4, pp.289-294, 2011.

[120] R. Gong, H. Xu, and Q. Tong, “Colorimetric Characterization Models based on Colorimetric Characteristics Evaluation for Active Matrix Organic Light Emitting Diode Panels,” *Applied Optics*, vol.51, no.30, pp.7255-7261, 2012.

[121] P. Sun and M. R. Luo, “Color Characterization Models for OLED Displays,” *SID Symposium Digest of Technical Papers*, vol.44, pp.1453-1456, 2013.

[122] J. Q. Zhang, F. Cai, Z. Liu, G. Y. Wu, and M. Zhu, "A Composite Model for Accurate Colorimetric Characterization of Liquid Crystal Displays," *Journal of the Society for Information Display*, vol.24, no.10, pp.600-610, 2016.

[123] D. Tian, L. Xu, and M. R. Luo, "The Characterization of HDR OLED Display," *SID Symposium Digest of Technical Papers*, vol.10, pp.326-1-326-6, 2019.

[124] S. Wen and R. Wu, "Two-Primary Crosstalk Model for Characterizing Liquid Crystal Displays," *Color Research & Application*, vol.31, no.2, pp.102-108, 2006.

[125] X. F. Feng and S. J. Daly. "Improving Color Characteristics of LCD," In *Proceedings of the Color Imaging X: Processing, Hardcopy, and Applications*, pp. 328-335, 2005.

[126] N. Tamura, N. Tsumura, and Y. Miyake, "Masking Model for Accurate Colorimetric Characterization of LCD," Journal of the Society for Information Display, vol.11, no.2, pp.333-339, 2003.

[127] P. C. Hung, "Colorimetric Calibration in Electronic Imaging Devices using a Look-Up-Table Model and Interpolations," *Journal of Electronic Imaging*, vol.2, no.1, pp.53-61, 1993.

[128] T. Rao, X. Ma, and X. Wang, "3D-LUT Based Ultra-Low Latency 4K Color Calibration System on FPGA," *SID Symposium Digest of Technical Papers*, vol.52, no.S2, pp.391-394, 2021.

[129] J. Wu, M. Wei, Y. Fu, and C. Cui, "Color Mismatch and Observer Metamerism between Conventional Liquid Crystal Displays and Organic Light Emitting Diode Displays," *Optics Express*, vol.29, no.8, pp.12292-12306, 2021.

[130] G. Hong, M. R. Luo, and P. A. Rhodes, "A study of digital camera colorimetric characterization based on polynomial modeling," *Color Research & Application*, vol.26, no.1, pp.76-84. 2001.

[131] M. Anderson, R. Motta, S. Chandrasekar, and M. Stokes, M. “Proposal for a Standard Default Color Space for the Internet-sRGB,” In *Proceedings of the 4th Color and Imaging Conference*, pp.238-245, 1996.

[132] International Telecommunication Union. “Recommendation ITU-R BT.709-5: Parameter Values for the HDTV Standards for Production and International Programme Exchange,” Geneva: International Telecommunication Union Radiocommunication Sector, 2002.

[133] S. S. Stevens, “To Honor Fechner and Repeal His Law: A Power Function, not a Log Function, Describes the Operating Characteristic of a Sensory System,” *Science*, vol.133, no.3446, pp.80-86, 1961.

[134] Digital Cinema Initiatives Limited Liability Company. “Digital Cinema Initiative Distribution Master (DCDM), Version 1.0,” California: Digital Cinema Initiatives Limited Liability Company, 2005.

[135] Society of Motion Picture and Television Engineers, “RP 431-2:2011–SMPTE Recommended Practice–D-Cinema Quality-Reference Projector and Environment,” New York: Society of Motion Picture and Television Engineers, 2011.

[136] Apple Technology Company, “Apple Developer Documentation,” California: Apple Technology Company, 2022.

[137] E. Nakasu, “Super Hi-Vision on the Horizon: A future TV System that Conveys an Enhanced Sense of Reality and Presence,” IEEE Consumer Electronics Magazine, vol.1, no.2, p.36-42, 2012.

[138] International Telecommunication Union, “BT.2020: Parameter Values for Ultra-High Definition Television Systems for Production and International Programme Exchange,” Geneva: International Telecommunication Union Radiocommunication Sector, 2014.

[139] S. Komura, K. Okuda, K. Onoda, H. Kijima, “Seventeen-inch Laser Backlight in-Plane Switching Liquid Crystal Display with 8K, 120-Hz Driving, and BT.2020 Color Gamut,” *Journal of the Society for Information Display*, vol.29, no.1, pp.17-28, 2021.

[140] J. Fang and Y. J. Kim, “A Matrix-Based Method of Color Correction for Metamerism Failure between LCD and OLED,” *SID Symposium Digest of Technical Papers*, vol.49, no.1, pp.1044-1047, 2018.

[141] B. Bodner, N. Robinson, R. Atkins, and S. Daly, “Correcting Metameric Failure of Wide Color Gamut Displays,” *SID Symposium Digest of Technical Papers*, vol.49, no.1, pp.1040-1043, 2018.

[142] B. Oicherman, M. R. Luo, B. Rigg, and A. R. Robertson, “Adaptation and Colour Matching of Display and Surface Colours,” *Color Research & Application*, vol.34, no.3, pp.182-193, 2009.

[143] A. Sarkar, L. Blondé, P. L. Callet, F. Autrusseau, P. Morvan, and J. Stauder, “A Color Matching Experiment using two Displays: Design Considerations and Pilot Test Results,” In *Proceedings of the 5th Conference on Colour in Graphics, Imaging, and Vision*, pp. 414-422, 2010.

[144] Y. Hu, M. Wei, and M. R. Luo, “Observer Metamerism to Display White Point using Different Primary Sets,” *Optics Express*, vol.28, no.14, pp.20305-20323, 2020.

[145] D. I. MacLeod and R. M. Boynton, “Chromaticity Diagram Showing Cone Excitation by Stimuli of Equal Luminance,” *Journal of the Optical Society of America*, vol.69, no.8, pp.1183-1186, 1979.

[146] M. Wei and S. Chen, “Effects of Adapting Luminance and CCT on Appearance of White and Degree of Chromatic Adaptation,” *Optics Express*, vol.27, no.6, pp.9276-9286, 2019.

[147] W. J. Joo, J. Kyoung, M. Esfandyarpour, S. H. Lee, H. Koo, S. Song, and M. L. Brongersma, "Metasurface-Driven OLED Displays beyond 10,000 Pixels per inch," Science, vol.370, no.6515, pp.459-463, 2020.

[148] Y.Park, M. J. Murdoch, and M. D. Fairchild, "Observer Metamerism: Why do [Mis]matches of Neutral appear Pinkish or Greenish?," In *Proceedings of the 28th Color and Imaging Conference*, pp.7-12, 2020.

[149] International Commission on Illumination, "Colorimetry, 4th Edition in CIE 15:2018," Vienna: International Commission on Illumination, 2018.

[150] Y. Asano, M. D. Fairchild, L. Blondé, and P. Morvan, "Color Matching Experiment for Highlighting Interobserver Variability," *Color Research & Application*, vol.41, no.5, pp.530-539, 2012.

[151] M. Huang, G. Cui, Y. Liu, and H. Liu, "Analysis of Observers Metamerism Differences for Different Retinal Cone Visual Responses," *Spectroscopy and Spectral Analysis*, vol.35 no.10, pp.2802-2809, 2015.

[152] Hu, X., & Houser, K. W. (2006). Large-Field Color Matching Functions. Color Research & Application, 31(1), 18-29.

[153] K. W. Houser and X. Hu, "Visually Matching Daylight Fluorescent Lamplight with Two Primary Sets," *Color Research & Application*, vol.29, no.6, pp.428-437, 2004.

[154] C. Y. Bai and C. Ou, "Observer Variability Study and Method to Implement Observer Categories for Novel Light Source Projection System," *Color Research & Application*, vol.46, no.5, pp.1019-1033, 2021.

[155] Y. J. Seo, E. Lee, Y. Yi, B. Choi, and S. Jo, “Color Correction Model based on Spectral Distribution for solving Metameric Failure in Wide Color Gamut Displays,” *SID Symposium Digest of Technical Papers*, vol.52, pp.454-457, 2021.

[156] D. C. Rich and J. Jalijali, “Effects of Observer Metamerism in the Determination of Human Color-Matching Functions,” *Color Research & Application*, vol.20, no.1, pp.29-35, 1995.

[157] H. Xie, S. P. Farnand, and M. J. Murdoch, “Observer Metamerism in Commercial Displays,” *Journal of the Optical Society of America A*, vol.37, no.4, pp.A61-A69, 2020.

[158] B. Oicherman, M. R. Luo, B. Rigg, and A. R. Robertson, “Effect of Observer Metamerism on Colour Matching of Display and Surface Colours,” *Color Research & Application*, vol.33, no.5, pp.346-359, 2008.